AD-A058 883 RHODE ISLAND UNIV KINGSTON DEPT OF OCEAN ENGINEERING F/G 11/6
CHARACTERIZATION OF CORROSION FILMS ON LEAD BY INFRARED REFLECT--ETC(U)
AUG 78 A GOLDFARB, C BROWN, R HEIDERSBACH N00014-76-C-0889

UNCLASSIFIED TR-5 NL

1 OF 2
ADA
058883

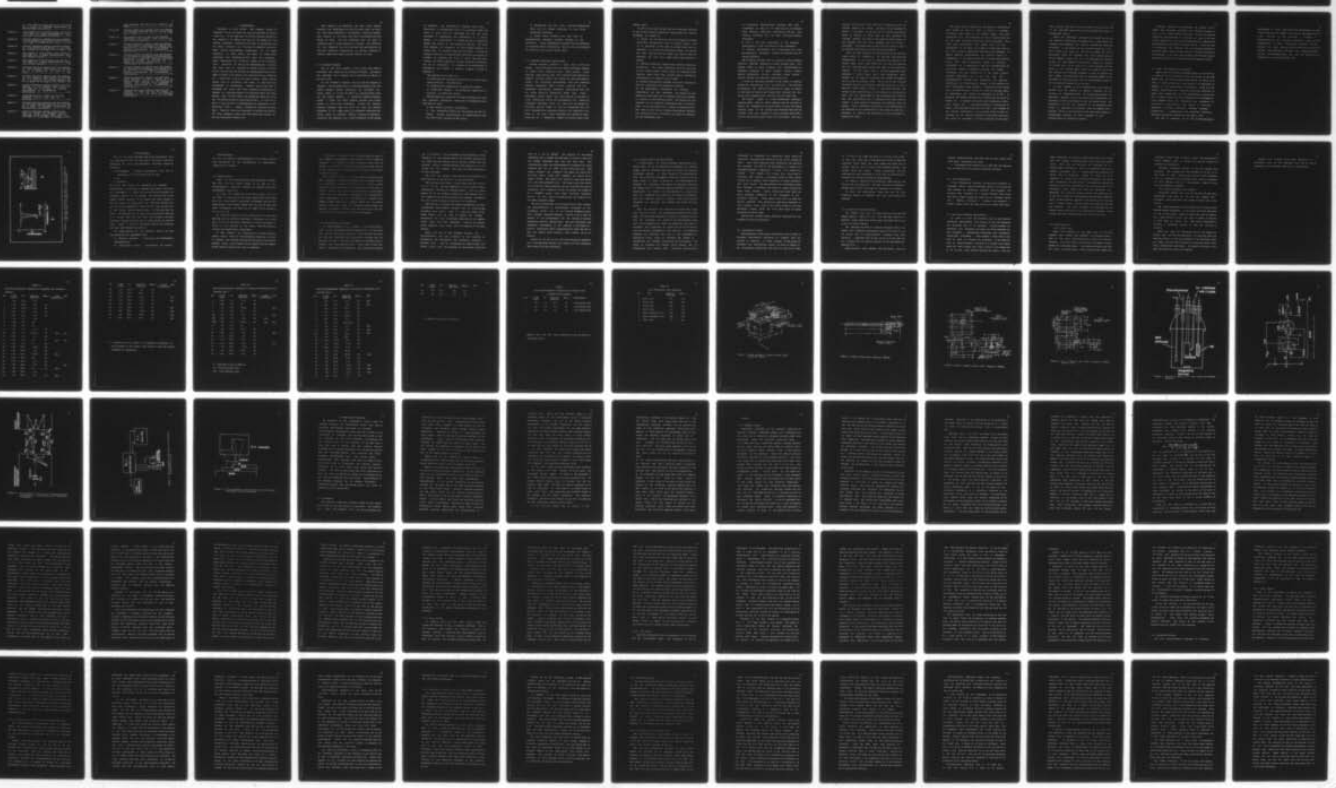

LEVEL II

12

CHARACTERIZATION OF CORROSION FILMS ON LEAD BY INFRARED REFLECTION SPECTROSCOPY

TECHNICAL REPORT NUMBER 5

14 TR-5

15 CONTRACT NUMBER: N00014-76-C-0889

SUBMITTED TO:

DEPARTMENT OF THE NAVY
OFFICE OF NAVAL RESEARCH
METALLURGY PROGRAM - CODE 471

PREPARED BY:

10 Arnold N. GOLDFARB, C. / BROWN [redacted] R. / HEIDERSBACH
DEPARTMENT OF OCEAN ENGINEERING
UNIVERSITY OF RHODE ISLAND
KINGSTON, RHODE ISLAND 02881

11 AUGUST 1978

12 190 p.

9 / Master's thesis,

CHARACTERIZATION OF CORROSION FILMS ON LEAD BY INFRARED REFLECTION SPECTROSCOPY

TECHNICAL REPORT NUMBER 5

CONTRACT NUMBER: N00014-76-c-0889

SUBMITTED TO:

DEPARTMENT OF THE NAVY
OFFICE OF NAVAL RESEARCH
METALLURGY PROGRAM - CODE 471

PREPARED BY:

A. GOLDFARB, C. BROWN AND R. HEIDERSBACH
DEPARTMENT OF OCEAN ENGINEERING
UNIVERSITY OF RHODE ISLAND
KINGSTON, RHODE ISLAND 02881

AUGUST 1978

SECURITY CLASSIFICATION OF THIS PAGE (When Data Entered)

REPORT DOCUMENTATION PAGE		READ INSTRUCTIONS BEFORE COMPLETING FORM
1. REPORT NUMBER Technical report number 5	2. GOVT ACCESSION NO.	3. RECIPIENT'S CATALOG NUMBER
4. TITLE (and Subtitle) Characterization of Corrosion Films on Lead by Infrared Reflection Spectroscopy		5. TYPE OF REPORT & PERIOD COVERED Technical report 1978 6. PERFORMING ORG. REPORT NUMBER
7. AUTHOR(s) A. Goldfarb, C. Brown and R. Heidersbach		8. CONTRACT OR GRANT NUMBER(s) N00014-76-c-0889
9. PERFORMING ORGANIZATION NAME AND ADDRESS Department of Ocean Engineering University of Rhode Island Kingston, Rhode Island 02881		10. PROGRAM ELEMENT, PROJECT, TASK AREA & WORK UNIT NUMBERS
11. CONTROLLING OFFICE NAME AND ADDRESS Office of Naval Research Department of the Navy Arlington, Virginia 22217		12. REPORT DATE August 1978 13. NUMBER OF PAGES 188
14. MONITORING AGENCY NAME & ADDRESS(if different from Controlling Office)		15. SECURITY CLASS. (of this report) unclassified 15a. DECLASSIFICATION/DOWNGRADING SCHEDULE

16. DISTRIBUTION STATEMENT (of this Report)

This document has been approved for public release and sale; its distribution is unlimited.

17. DISTRIBUTION STATEMENT (of the abstract entered in Block 20, if different from Report)

18. SUPPLEMENTARY NOTES

19. KEY WORDS (Continue on reverse side if necessary and identify by block number)

Lead; lead oxide; infrared spectra; corrosion products; oxidation; passive films; surface films

20. ABSTRACT (Continue on reverse side if necessary and identify by block number)

This report contains the manuscript of a thesis by A. Goldfarb, M.S. candidate in Ocean Engineering at the University of Rhode Island.

Electrochemical exposures of lead samples in aqueous carbonate, phosphate, sulfate and chloride solutions were made at various pH and potential values. The resulting surface films were investigated by infrared reflection spectroscopy in order to identify the surface species; to show the applicability of the reflection technique to corrosion research.

DD FORM 1 JAN 73 1473 EDITION OF 1 NOV 65 IS OBSOLETE

SECURITY CLASSIFICATION OF THIS PAGE (When Data Entered)

20. Abstract (cont.)

The experimental results were compared to the appropriate theoretical Pourbaix diagram. The experimental results did not always confirm the theoretical prediction mainly due to the lack of the kinetic effect in the Pourbaix diagram calculation.

Thicknesses of passive films formed on lead in sulfate solutions were measured. From this the sensitivity of infrared reflection spectroscopy for detecting this type of films was found to be better than 200 Angstroms.

Infrared reflection spectra were compared to the appropriate transmission spectra and explanations for bands' shift, angle of incidence dependence, and number of reflections are given.

Preliminary experiments of high temperature Armco iron exposures are also presented.

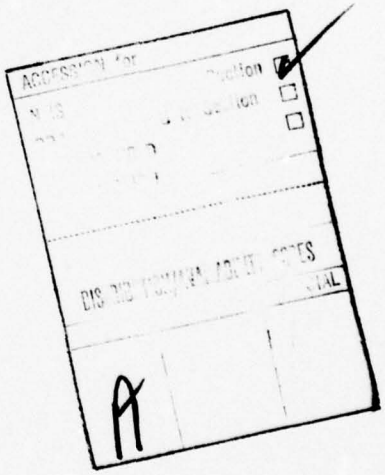

CHARACTERIZATION OF CORROSION FILMS ON LEAD BY INFRARED REFLECTION SPECTROSCOPY

BY

ARNON GOLDFARB

A THESIS SUBMITTED IN PARTIAL FULFILLMENT OF THE REQUIREMENTS FOR THE DEGREE OF

MASTER OF SCIENCE

IN

OCEAN ENGINEERING

UNIVERSITY OF RHODE ISLAND

1978

TABLE OF CONTENTS

LIST OF TABLES

LIST OF FIGURES

1. INTRODUCTION

Corrosion is very costly. The expenses caused by corrosion in the U.S alone run into the billions of dollars a year (1). At the same time the entire industry depends on the stability of metals, and they in turn depend on a few hundred angstroms, sometimes even less, of protective film for their stability (2). "The loss of chemical reactivity under certain envircnmental conditions" (1), is termed passivity. In other words, the metal is stable under conditions that thermodynamically favor its corrosion. Other definitions for passivity appear in the literature (3-5). Passivity of metals was discovered over a century ago, when iron was observed to corrode rapidly in dilute nitric acid but did not corrode in concentrated nitric acid. Then, as today, this behavior was explained by the formation of a protective film on the metal surface. These surface layers vary in thickness from metal to metal and from environment to environment. Surface layers less than 10 angstroms (6) thick have been reported to passivate the surface of stainless steels, but naturally there are other metals, such as lead, where the protective films that form can be several orders of magnitude thicker. In view of all this it will be hard to overemphasize the importance of the protective films - oxides, carbonates, sulfates and many more. Theories have been developed to explain and predict the film formation, among them the "Oxide film theory" (3) and the "Adsorption theory" (4).

Much research on passivity was done since Faraday observed the passivation of iron in nitric acid, but there are still many questions to be answered. Passivity affects many aspects of our life, from cars to buildings and from energy to food. Any new technique that can help in answering some of these questions is welcome. The objective for this research is to try and show the applicability of infrared reflection spectroscopy to surface analysis of passive films while doing original research on lead.

1.1. Pourbaix Diagrams

One of the most powerful tools to deal with surface reactions and films are the Pourbaix diagrams. The method was developed by M. Pourbaix and is explained in detail in his atlas (7).

In the Pourbaix diagrams one can find the regions of immunity - the unreacted metal is thermodynamically the most stable chemical specie, passivity, and corrosion - the region where an ion of the metal or a nonprotective oxide are the stable species. A simplified Pourbaix diagram, Figure 1, shows the three general regions for a given system - in this case lead-water. Unlike the detailed Pourbaix diagrams this one does not show the species predicted to be stable under the different conditions but rather gives an overview, showing regions of corrosion, passivity, and immunity, for a quick reference to the system

of interest. The potential-pH diagrams store huge quantities of thermodynamic data in a relatively simple way which is quite easy to understand and has the great advantage of summarizing the information in a graphic manner. In constructing a diagram one has to define the system and within it the species of interest. The Gibbs free energies of formation of the different species, or enough data to calculate them, must be known. A series of chemical reactions, in equilibrium, involving the species of interest is selected and from it using the Vant-hoff, Faraday and Nernst equations a linear relation of potential and pH is calculated. An example of the methodology of calculating and drawing a Pourbaix diagram is given in Appendix 1.

The diagrams can be used for:

a) Predicting the spontanous direction of reaction under given potential - pH conditions.

b) Estimating the composition of corrosion products.

c) Predicting changes - pH, potential, composition of solution - to reduce the attack.

Thermodynamically calculated Pourbaix diagrams have some very important limitations which must be remembered every time they are used:

1) They contain no kinetic information.

2) The information exists for pure metals and not for alloys. Present understanding of thermodynamics does not allow their calculation for alloys.

3) Assumptions are made about solution compositions which are not always applicable to real world engineering problems.

In recent years attempts have been made to experimentally determine Pourbaix diagrams in the laboratory. These experimental diagrams have the advantage of providing kinetic information; they can also be developed for alloys as well as pure metals (8,9).

1.2. Infrared Reflection Spectroscopy

Surface analysis advanced a great deal in the last decade. Many techniques that were barely developed emerged to become major analytical tools. These include : Auger Electron Spectroscopy (AES) (10), Electron Spectroscopy for Chemical Analysis (ESCA) (11), Second Ion Mass Spectrometry (SIMS), Ion Scattering Spectroscopy (ISS) (12), Scanning Electron Microscopy (SEM) (13,14), electron and ion microprobe spectroscopy, Mossbauer spectroscopy (15), and low energy electron diffraction (LEED) (16). These techniques joined those that were already in use such as X-ray diffraction (13,14) and ellipsometry (17). Among the techniques mentioned there are some that are capable of detecting surface films as thin as 5 angstroms (12), and give information on oxidation states or the identity of the atoms in the film. Other techniques are capable of depth profiling by a sequential removal of surface layer after

surface layer.

In view of all this one must ask the inevitable question of why we need infrared reflection spectroscopy as a surface technique. The answer is:

1) Unlike all the electron and ion techniques infrared reflection spectroscopy does not require vacuum. This is an advantage in the case of surface films that are sensitive to and can be altered by vacuum. An example for this type of films are films that contain water of hydration and will lose these waters when exposed to vacuum.

2) Infrared reflection spectroscopy provides structural information. The other techniques which are sensitive to thin surface layers provide atomic or oxidation state identity (SIMS, ESCA, AES), provide kinetic information (ellipsometry) or require vacuum (LEED).

3) Infrared spectroscopy provides structural information both for crystalline and amorphous materials.

4) The experimental instruments for infrared spectroscopy are well developed, and almost any good commercial instrument can be adjusted with minor changes to operate in the reflection mode. The things that are required are two reflection attachments and a polarizer, these can be purchased from a variety of manufacturers. The overall price for an infrared spectrometer equipped for reflection work is 50-10% of the price for electron and ion instruments (12).

5) Preliminary investigations indicate that film thicknesses as thin as 10 angstroms can be analyzed using infrared reflection spectroscopy (18,19). This compares favorably with the most sensitive electron techniques.

6) One of the main advantages of the infrared spectroscopy is that its theory is fully developed.

7) Infrared spectroscopy can be considered as a truly non-destuctive technique, probing the surface with low energy radiation.

The technique has been used in research of the following subjects: adsorbed molecules on metal surfaces (20) , thin polymer films on metal surfaces (21), identification of oxidation compounds on metal surfaces (18,19), ceramic surface degradation (22,23), recording single crystal spectra (24,25), and corrosion inhibition (26).

A brief and intuitive approach to the theory of infrared reflection spectroscopy will be given here. For detailed mathematical and optical formulation the reader is refered to the works by Francis and Ellison (27), Greenler (28, 31), Poling (32), Tompkins (33), Harrick (34) and Lavin (35).

The problem refers to a thin, homogenous, isotropic, parallel-sided film on a metal surface, such as is shown in Figure 2a. Assuming the radiation falls at near the normal incident angle to the surface the reflected wave and the incident wave will combine to form a standing wave with a node of the electric field vector at the surface. With zero

electric field vector at the surface no interaction with the surface species can result, and thus its not possible to obtain a spectrum. In the case of a 10 micron wavelength, which is typical of those used in this research, the distance between the node of the electric field vector, at the surface, and the first maximum will be 25,000 angstroms, thus making the surface the best place to hide a few hundred angstroms of oxide film from detection.

With the same approach the polarization of the incident light should be considered. An incident wave polarized perpendicular to the plane of incidence will undergo a 180 degree phase shift upon reflection, and thus the incoming and the outgoing waves cancel each other at the reflecting surface. On the other hand a parallel polarized light undergoes a finite phase shift upon reflection, which depends on the angle of incidence, and becomes 180 degrees only at grazing incidence angle. The result of the parallel polarized light is an elliptical standing wave with a finite electric field vector normal to the metal surface. The change of the reflectivity, at the vicinity of an absorption band, and the phase shift of the polarized light indicate that the sensitivity, for a 5 angstrom thick film, will be highest at high angles of incidence, 85-88 degrees from the normal. From theoretical prediction on the sensitivity of the spectrum to the polarization of the light the need for a polarizer to enhance the sensitivity of the instrument is immediately clear.

The next thing to consider is the number of reflections that should be used in order to obtain a spectrum. Intuitivly there must be an optimum number since each reflection will add information to the travelling wave but at the same time will reduce the overall radiation. Thus after many reflections, even though there is more information in the wave, the signal to noise ratio will be too low to allow a significant spectrum to be recorded. In modern infrared spectrometers the detector noise is independent of the signal level and is usually the limiting factor (30). When considering single vs. multiple reflections it is necessary to take into consideration the relatively simple arrangement required for single reflection, and the possibility to use other surface analysis techniques, all at the same time. The instrumentation becomes more complicated for multiple reflections and simultaneous probing of the surface with other techniques is not possible. Calculations (29) showed that the deviation by a factor of 2 from the optimum number of reflections can reduce the reflectance by 20-30% . An equation and graphic definition of reflectance are given in Figure 2b. In general when using good reflectors, silver, gold, copper etc. , the optimum number of reflections is higher than when poor reflectors are used. This depends on the initial reflectivity of the metals which in turn is a function of the optical constants of the metal substrate, the angle of incidence, and the wavelength of the light.

This suggests that when using poor reflectors more than 70% of the available sensitivity can be achieved with only 1-2 reflections (30,31).

There are additional problems to be solved in the use and design of reflection instrumentation. Since almost all infrared spectrometers use thermal sources the resulting divergence of the sample and the reference beams is a fact. This causes the light to fall on the sample, not at one particular angle of incidence but over a space angle of 10-15 degrees; thus, not all the components of the beam travel the same number of reflections. There is a problem of losing part of the light due to rays "walking" off the edges of the mirrors (29). There is a limit on how close the mirrors can be brought together in order to provide the high number of reflections that is sometimes needed, since the image of their exit must fill the monochromator slits if all the energy available is to be used.

A major problem in the interpretation of the spectra derives from the changes in optical constants in the vicinity of absorption bands. In transmission spectra the absorption depends only on the extinction coefficient, but reflection spectra also depend on the refractive index. The combination of the two constants at an absorption band causes an asymetery of the bands. This can combine with a possible shift in the position of the bands with respect to transmission spectra, to cause problems in the interpretation of reflection spectra.

Infrared reflection spectroscopy has proved to be a useful and sensitive technique for surface analysis, in spite of the problems mentioned above. The use of infrared reflection spectroscopy is expected to grow in the near future mainly due to the recent availability of theoretical formulation and numerical solutions (27-32). These can help in predicting and choosing the best working conditions. Existing results show the sensitivity of infrared reflection spectroscopy to be, when used properly, 20-30 times greater than the sensitivity of transmission spectroscopy (32-34).

1.3. Lead - Applications and Research

Lead is one of the most important metals to our society. It does not have the glamour of the coin metals or the high demand and use of the construction metals, but where it is used it serves well, and in many cases it is impossible to replace it with other metals or materials. Among its most popular applications are: lead-acid batteries, additives to fuels (its consumption for this application is going down due to lead toxicity and lead pollution of the atmosphere), lead covered cables for electrical use, equipment for production, transportation, and storage of corrosive chemicals, corrosion resistence, solders, plumbing, architecture - ornamentation and vibration isolation, radiation protection, ammunition, and paints (36).

Lead use in batteries is by far the most consuming

application of lead. This makes the understanding of lead electrochemistry and surface reactions an important field of study. Research on lead compounds of interest in electrochemistry and corrosion prevention deals with the investigation of their crystalline structure (37-39), infrared and Raman spectra (40-42), kinetics of formation (43-46), thermodynamic stability (7), electrochemistry (47-53), photodecompcsition (54) and ion selectivity in diffusion thru corrosion layers (55).

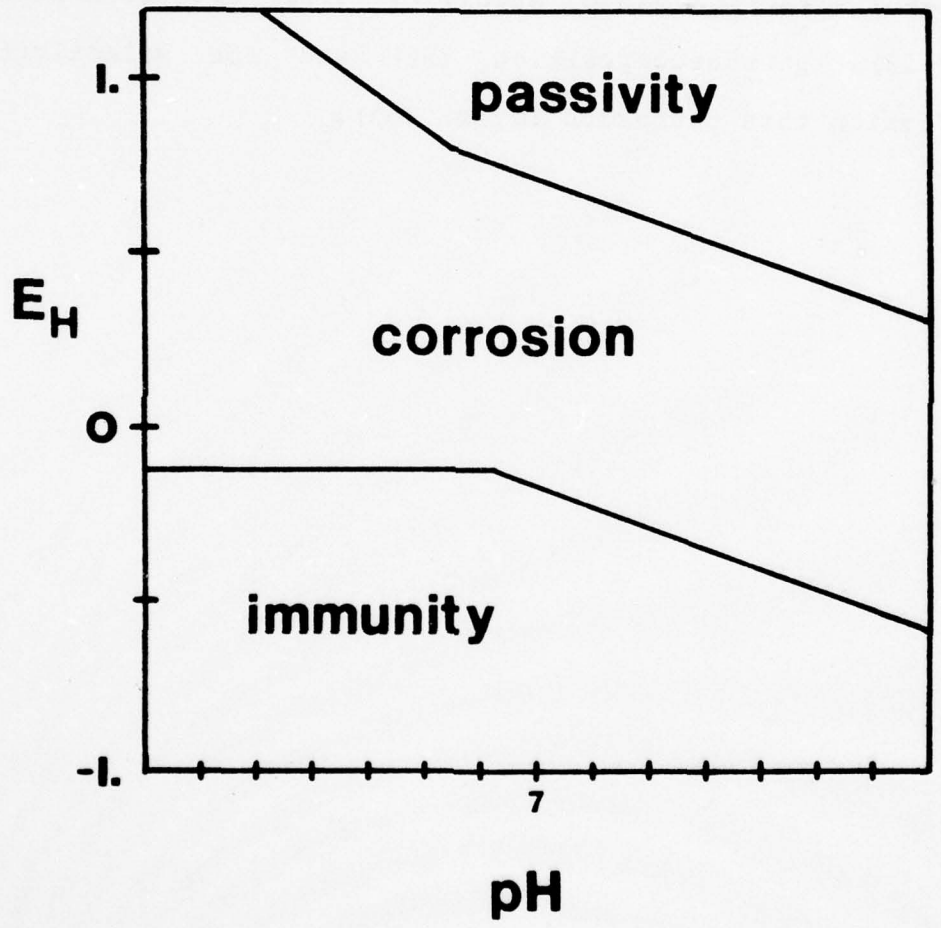

Figure 1. Simplified Pourbaix diagram of the system Lead-Water. M. Pourbaix, Atlas of Electrochemical Equilibria, Pergamon, N.Y (1966).

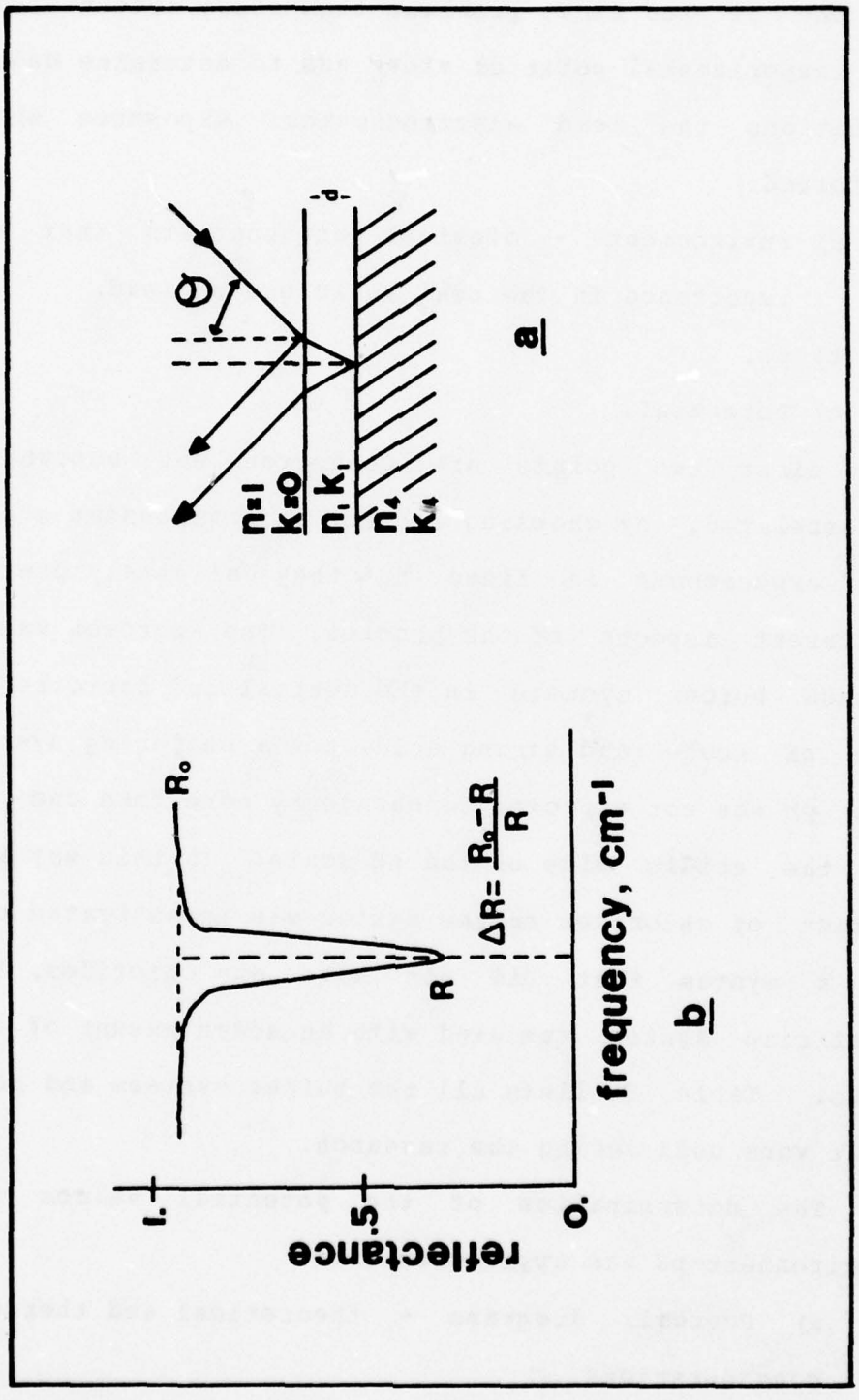

Figure 2. Specular reflection from metal. a) Film schematics and light path. b) Definition of reflectance.

2. EXPERIMENTAL

One of the first problems this study encountered, from the experimental point of view, was to determine under what conditions the lead electrochemical exposures should be performed:

a) Environment - chemical environments that are of importance in the real world use of lead.

b) pH.

c) Potential.

The first two points are connected and somewhat interrelated, by choosing a chemical environment a pH range for experiments is fixed, but they definitely present two different aspects of the problem. The approach was to use common buffer systems in the neutral and basic regions of the pH scale and strong acid, not a buffering system, but the pH was not expected to change by more than one pH unit, at the acidic side of the pH scale. In this way when the effect of chlorides on the system was investigated compared to a system that did not have any chlorides, the same buffering system was used with an added amount of chloride ions. Table I lists all the buffer systems and solutions that were used during the research.

The determination of the potential values for each environment-pH was approached from:

a) Pourbaix diagrams - theoretical and thermodynamic considerations.

b) Polarization curves - experimental and kinetic

considerations.

In this way both the thermodynamic and the kinetic aspects were considered for the determination of experimental conditions of interest.

2.1. Sample Holder

There are some unique features characterizing a sample, and thus also the sample holder to be used in the electrochemical exposures, intended for infrared reflection measurements. These are:

a) Size: The sample has to be fairly large, 2.8 X 5.7 cm. This is the size of the larger sample that can be used with the Wilks Model 9 reflection attachments used in this investigation. The smaller sample size that can be used with these attachments, but which was not used in this research, is 2.8 X 4.3 cm.

b) Flatness: The goal of this research was to work with specular and not diffuse reflectance. Therefore, the sample must be flat so that upon reflection it will be possible to direct a good portion of the light, with the mirrors, towards the monochromator compartment.

c) Safe removal: The sample has to be taken from the sample holder after the electrochemical exposure, in order to measure the infrared reflection spectrum of the surface species. Thus, a safe removal of the sample from the sample holder without altering the film is required.

d) Material: The sample holder material must be inert to all chemical environments used during the electrochemical exposures. It should not form a galvanic couple with the sample on contact in solution. The material should also be strong enough to be pressed against the edges of the sample to prevent leakage.

Many sample holders for electrochemical exposures have been described in the past (56-62), but none could fulfill the requirments mentioned in points a to c. Thus, a sample holder for this research had to be developed. It was made of TEFLON; Figures 3-6 show the various parts of the sample holder and any necessary information for construction. Other requirements in the development of a standard type sample holder would be: standard necks for all sample holders, different heads for different sample sizes, and special attachments between heads and necks as in the case of the tilt angle required for Raman measurements.

2.2. Electrochemical Exposures

An electrochemical cell, Figure 7, was filled with 1 liter of the appropriate buffer solution and 4 of the necks were sealed with rubber stoppers. The fifth neck was used for the gas dispersion unit, purging dry nitrogen into the solution in order to minimize the amount of dissolved carbon dioxide, and thus carbonate ions which tend to form very stable, insoluble lead carbonates. The solution was purged

for 1.5-2 hours. A few experiments were performed in which degassing of the solution before the nitrogen purging step was done, this was carried out by putting a beaker with the solution inside a vacuum desicator and pumping it to a low vacuum for 5-10 minutes. This step was found unnecessary and was abandoned.

The lead was greater than 99% pure as purchased from Alfa Products in the form of a 1.6 mm thick sheet.

While purging took place, a lead sample was cut to size, 2.8 X 5.7 cm, and was immersed in a hot, almost boiling, concentrated solution of ammonium acetate. This is a known method (1) for the chemical cleaning of lead surfaces due to the formation of the very soluble lead acetate. The sample was left in the cleaning solution for 10-15 minutes.

Some efforts to improve the surface preparation by using conventional metallurgical methods such as grinding and polishing were tried. Lead is a very soft metal so all these efforts did not seem to improve the surface preparation but only introduced impurities to the surface layer; thus, they were abandoned. Electron micrographs which emphasize this point will be discussed in the next chapter.

Toward the end of the nitrogen purging, the electrochemical cell was prepared for the exposure by introducing the thermometer and auxilliary electrode - platinum mesh - and by connecting the Luggin probe, via tubing filled with the solution, to the calomel electrode

cell in a 100 ml beaker. The purpose of the tubing connection was to hinder the diffusion of chloride ions from the calomel electrode cell into the main cell. Cell construction, parts and electrochemical procedures are quite standard and can be found in the literature (63). When sample cleaning was completed the sample was rinsed with distilled water, dried with KIMWIPES and placed in the sample holder. The sample had a metallic shine when placed into the electrochemical cell. The Luggin probe was placed 1-2 mm from the sample surface, and the solution was stirred constantly with a magnetic stirrer to prevent the formation of a Helmholz layer, which might introduce resistance errors. At this point the potentiostat was turned on and the sample exposure began.

The WL-1 potentiostat is an inhouse device that displays the characteristics of potentiostats described in the literature (5,63), i.e, it is a voltage feedback circuit that utilizes negative feedback. Figures 8 and 9 show the details of the potentiostat and the current to voltage conversion circuits, respectively. The main difference from commercial instruments is the addition of the Kepco Inc. bipolar operational power supply/amplifier model BOP 36-1.5 that can supply high currents, when needed, up to 1.5 amperes.

Tables II, III and IV list the electrochemical exposures that were performed during this research and the conditions under which they were performed.

2.3. Infrared Reflection Spectroscopy

A Perkin-Elmer 521 grating infrared spectrometer with Wilks model 9S and 9D reflection attachments and a Beckman 42-POL grating polarizer were used to measure the infrared reflection spectra. A block diagram of the spectrometer with the reflection attachments, polarizer position and the light paths is given in Figure 10. The spectrometer was prepared for recording the spectra by carefully balancing the beams, then the reference beam was adjusted for maximum reflectivity by working the spectrometer in a single beam mode and adjusting the mirrors in the model 9D attachment, with two aluminum mirrors as samples. When this step was satisfied the polarizer was mounted just before the main slits.

When the exposure was completed the sample was rinsed with distilled water and immediately mounted in the Wilks model 9S reflection attachment, against an aluminum mirror, then the attachment was placed in the spectrometer light path and adjustments for number of reflections and angle of incidence were performed by moving the M2 and M5 mirrors with the matching adjustments at M2' and M5'. A preliminary spectrum was recorded, and from it the adjustments in polarizing angle, angle of incidence and number of reflections for maximum sensitivity were determined. The angle of incidence was usually 65-70 degrees and 2-5 reflections were usually used. Polarizer settings were

determined by adjusting the polarizing angle while the instrument wavelength was centered on one of the absorption bands. Once best conditions were determined, the spectrum was recorded from 1800 to 250 wavenumbers at a speed of 25 wavenumbers/minute, suppression - 6, gain - 5-6, normal slit program - 1000 (double slit widths were also tried in recording some spectra), attenuator speed of 1100, source current of 0.8 amperes, scale expansion 1X (other expansions were also tried). The spectrometer was continously purged with nitrogen to minimize the amount of carbon dioxide and water vapor present. Carbon dioxide and water vapor can cause problems, especially if the instrument is not perfectly balanced. Their spectra will add to or mask the spectra recorded. This problem was especially important in this research since most of the oxides absorb in the long wavelength region, below 600 cm^{-1}, where there is strong absorption by water vapor.

Spectra were recorded under identical conditions for two extremes of light polarization.

2.4. Polarization Curves

Electrochemical polarization curves were run in order to determine experimental conditions of interest that are related to kinetics. A block diagram of the setup for recording the polarization curves is given in Figure 11. The polarization curves were run from +1 V SCE (1.24 V NHE)

to -1 V SCE (-.76 V NHE) and back to +1 V SCE (1.24 V NHE). In this way there was a reduction cycle first so when the oxidation cycle began the lead surface was clean with no surface species on it to alter the oxidation process. The current scale was linear. Sample preparation and cell configuration were identical to those used in potentiostatic exposures for infrared reflection measurements.

An Elscint potential scan generator, model ABA-26, was used to scan the potential. The scan rate was 40 mv/minute. Results were plotted cn an MFE 815 Plotmatic X-Y recorder.

At least one pclarization curve was run for each buffering system or solution that was used during this research.

2.5. Scanning Electron Microscopy

The samples were cut so they could fit into the SEM sample chamber - about 6 X 6 mm - then they were placed on a mounting block glued with silver paint and were left to dry in air for several hours.

The SEM work was done on a Hitachi Scanscope SSM-2, the camera was a Tektronix osciloscope camera C-27 with f1.4 to f16 optics and 1:1 magnification. Polaroid film #665 (positive - negative) with an ASA rating of 75 was used for all pictures with an aperture setting of f16 and photometer reading 75-85.

Magnifications were between 200X and 2000X. Very few

samples needed coating, and those that did were coated with 60-40 gold - palladium 8 mil wire.

A few samples were examined on an AMR 1000 SEM equipped with an EDAX 707A X-ray energy dispersive analyzer.

2.6. X-ray Diffraction

X-ray diffraction patterns of analytical reagents, to determine purity and for reference spectra, and of passive film samples of particular interest were recorded. The patterns were recorded on a General Electric 11GJ1 X-ray unit with a copper target and beam slit of 3 degrees, Soller slit - medium, filtration - 2 Nickel, time constant - 1 second, linear scale, and 2000 counts per second full scale.

2.7. Lead Film Thickness Measurements

In order to find the detection limit of the infrared reflection measurements with respect to the film thickness the thickness had to be measured. Several methods for measuring film thickness are known, two were available for this research - interference microscopy, and a Taylstep-1 stylus-type instrument - both require a sharp step in the film in order to measure its thickness. It was expected that an electrochemical exposure of a regular lead sample would not leave a sharp step, even if part of the sample was to be masked; thus, another approach was taken. Lead was

vapor deposited on gold on a microscope slide, and a sharp step was created by masking part of the gold with another slide. This step was measured for thickness by a Taylor-Hobson Taylstep-1, this is a commercial stylus-type profile instrument with a maximum vertical resolution of better than 10 angstroms. Figure 12 shows the film deposited on glass and a simplified diagram of the stylus type instrument and its output. The sample was exposed by making an electrical connection to the top front side of the microscope slide, where the film was deposited, and immersing the slide in solution leaving the connection out in the air to avoid any interference from galvanic coupling. After electrochemical exposure the sample was cut to size with a diamond cutter, and the infrared reflection spectrum was recorded. The film thickness was corrected for the density change from lead to the appropriate compound. Table V gives the lead exposures that were done in this way.

2.8. Iron Exposures

2.8.1. Armco iron:

Armco iron samples, of the same size as the lead samples, were ground with CARBIMET - SiC grinding paper - down to 600 grit, hand grinding was found to be the most accurate, and then down to 0.3 micron with Buehler alumina powder on a revolving table. The alumina polishing was done wet using distilled water. After polishing the sample was

carefully rinsed with distilled water and spectroscopic grade methanol, then it was put in a vacuum desicator to minimize air oxidation.

Infrared background spectra of the iron samples were recorded. The samples were then exposed in air for 0.5 to 480 hours at 230°c. Spectra were recorded using unexposed iron or aluminum in the reference beam, angle of incidence of 65-75 degrees and up to 7 reflections. Table VI lists the iron exposures conducted.

2.8.2. Vapor deposited iron samples:

Microscope slides were used as the base for the vapor deposition, they were cut to size and cleaned with detergent, distilled water and acetone and were left to dry in air.

The vapor deposition was performed with a Hitachi model HUS-4GB vacuum evaporator. A gold layer was first deposited on top of the glass. Figure 12 shows this type of sample, with lead instead of iron. This type of sample is similiar to that used by Pcling (19). This sample configuration provides a reflecting surface in case all the iron is oxidized.

After the gold was deposited, part of the sample was masked when the iron was deposited. In that way, when the mask was lifted, a step the thickness of the deposited layer was there and the film thickness was measured using a Karl Zeiss interference microscope. The samples were put in the same oven with the Armco Iron samples.

Spectra were recorded using gold deposited on a microscope slide in the reference beam and an angle of incidence of 70-75 degrees with up to 7 reflections.

TABLE I

Electrolyte Solutions Used in This Research

Solution	pH	ELECTROLYTE COMPOSITION
a	4.01	0.05M $KHC_8O_4H_4$
b	6.87	0.025M KH_2PO_4 + 0.025M Na_2HPO_4
c	10.00	50 ml 0.05M $NaHCO_3$ + 10.7 ml 0.1M NaOH
d	7.00	50 ml 0.1M KH_2PO_4 + 29.1 ml 0.1M NaOH
e	7.00	d + 0.1M KCl
f	10.00	c + 0.1M KCl
g	1.1	0.1M HCl
h	0.9	0.1M H_2SO_4
i	5.75	0.1M K_2SO_4
j	7.00	d + 0.1M K_2SO_4
k	10.00	c + 0.1M K_2SO_4
l	11.1	KOH + 0.1M K_2SO_4

Remark: All the chemicals were reagent grade.

TABLE II

Lead Electrochemical Exposures in Phosphate and Carbonate Buffers *

No.	E NHE volts	pH	Exposure Time hrs.	Temp. C	X-ray Diffraction	SEM
1	.28	4.0	1.5			
2	-.16	6.87	1.5	23		
3	-.16	6.93	4.5	25		
4	-.76	7.0	2.0	19		
5	-.64	7.0	2.0	18		
6	-.42	7.0	2.5			
7	-.16	7.0	16			
8	.48	7.0	21			
9	.67	7.0	2.0	18		
10	.99	7.0	1.0-2.0	19	yes	yes
11	1.08	7.0	3.5	20		
12	-.42	9.7	17	21	yes	yes
13	-.42	9.7	17	24		
14	-.56	10.0	2.75	18		
15	-.42	10.0	4.5	25		
16	-.42	10.0	17.75	24	yes	
17	-.42	10.0	24	25		
18	-.37	10.0	2.5	20		
19	-.28	10.0	4.0	18		yes
20	.02	10.0	23	25	yes	
21	.04	10.0	1.5			
22	.24	10.0	1.5	23	yes	

No.	E NHE volts	pH	Exposure Time hrs.	Temp. C	X-ray Diffraction	SEM
23	.24	10.0	5.5	22		
24	.24	10.0	18.5	23		
25	.51	10.0	6.0	22		yes
26	.75	10.0	2.25	19		yes
27	.75	10.0	5.5	22		
28	.83	10.0	1.0	19		yes
29	.83	10.0	3.25	18		yes
30	.89	10.0	17.25	20		yes
31	1.08	10.0	14.5	24		yes

* - Solutions b,c,d in Table I. An exposure in solution a is also included in this table, even though it does not contain carbonates or phosphates.

TABLE III

Lead Electrochemical Exposures in Solutions Containing 0.1M Chloride Ions *

No.	E NHE volts	pH	Exposure Time hrs.	Temp. C	X-ray Diffraction	SEM
1	1.18	1.1	1.0	22		
2	-.42	7.0	25	24		
3	-.11	7.0	16.25	24		yes
4	-.11	7.0	17	23		
5**	-.01	7.0	2.5	20		yes
6**	-.01	7.0	3.0	21	yes	
7***	-.01	7.0	18.45	20	yes	yes
8	.49	7.0	21			
9	.49	7.0	22.5	20		
10	1.08	7.0	3.0	24		yes
11	-.42	10.0	2.0	20		
12	-.42	10.0	17.5	23		
13	-.24	10.0	2.0	19		yes
14	.49	10.0	3.25	20		
15	.49	10.0	20.0	20		
16	1.08	10.0	4.5	22		

* - Solutions e,f,g in Table I.

** - 0.01M chloride icns.

*** - 0.5M chloride icns.

TABLE IV

Lead Electrochemical Exposures in Solutions Containing 0.1M Sulfate Ions *

No.	E NHE volts	pH	Exposure Time hrs.	Temp. C	SEM
1	.48	0.3	2.0	26	yes
2	-.40	0.9	2.0	21	yes
3	-.40	0.9	17.0	23	
4	-.23	0.9	2.5	23	
5	-.02	0.9	16.25	21	
6	-.02	0.9	3.0	21	
7	.80	0.9	.5-1.5-2.5	21	
8	.80	0.9	3.5	20	yes
9	.80	0.9	7.0	20	yes
10	.80	0.9	16.0	21	yes
11	.80	0.9	20.5	20	
12	-.62	5.75	3.0	24	
13	.24	5.75	1.75	20	
14	1.08	5.75	3.5	24	
15	.24	7.0	16.75		
16	.24	10.0	16.75	22	yes
17	.24	10.9	0.05	24	
18	.24	10.9	0.5	24	
19	-.67	11.1	3.75.	19	yes
20	.64	11.1	3.25	18	yes
21	.96	11.1	3.25	21	yes
22	.24	11.2	2.5	24	

No.	E NHE volts	pH	Exposure Time hrs.	Temp. C	SEM
23	.24	11.2	3.5	26	
24	.24	11.2	2.75	19	

* - Solutions h,i,j,k,l in Table I.

TABLE V

Lead Electrochemical Exposures for Passive Film Thickness Measurements.

No.	E NHE volts	pH	Exposure Time hrs.	Temp. C	Description
1	.80	0.9	0.5	21	0.06 micron lead
2	.80	0.9	0.25	20	0.05 micron lead
3	.80	0.9	2.0	21	0.34 micron lead

Remark: The lead was vapor deposited on top of gold on a microscope slide.

TABLE VI

High Temperature Iron Exposures

No.	Type	Exposure Time hrs.	Temp. C
1	Armco iron	405	230
2	Armco iron	405	230
3	Armco iron	288	230
4	Armco iron	0.5	230
5	Vapor deposited iron	480	230
6	Vapor deposited iron	480	230
7	Armco iron	50	250

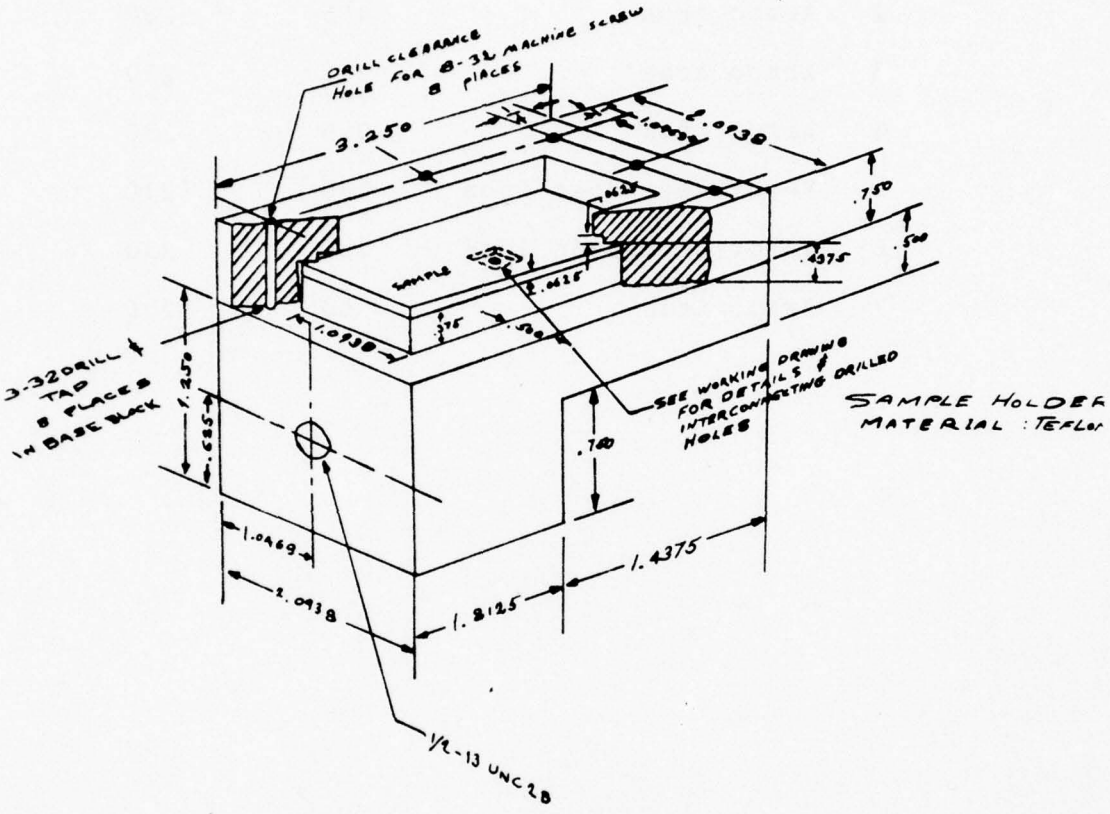

Figure 3. Cross section of sample holder "head".
Material: TEFLON.

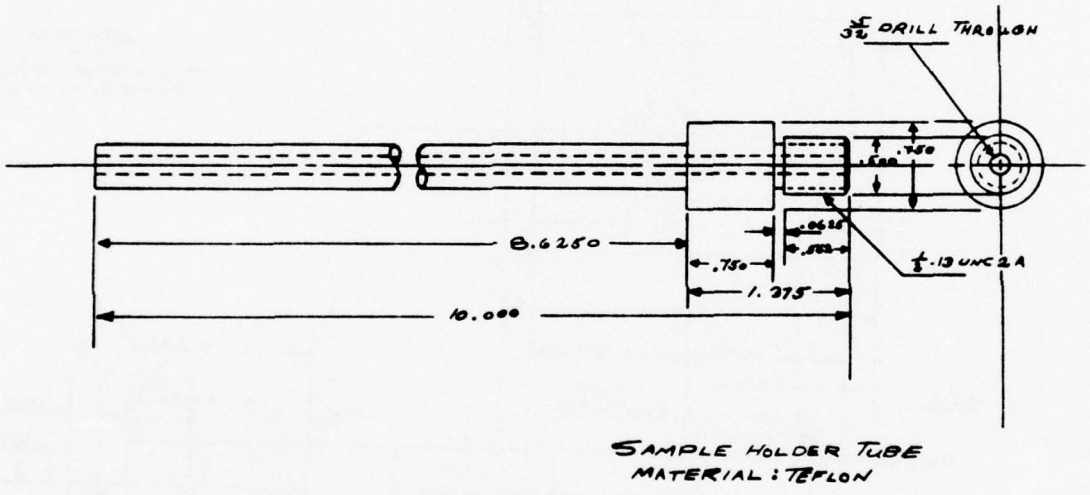

Figure 4. Sample holder tube. Material: TEFLON.

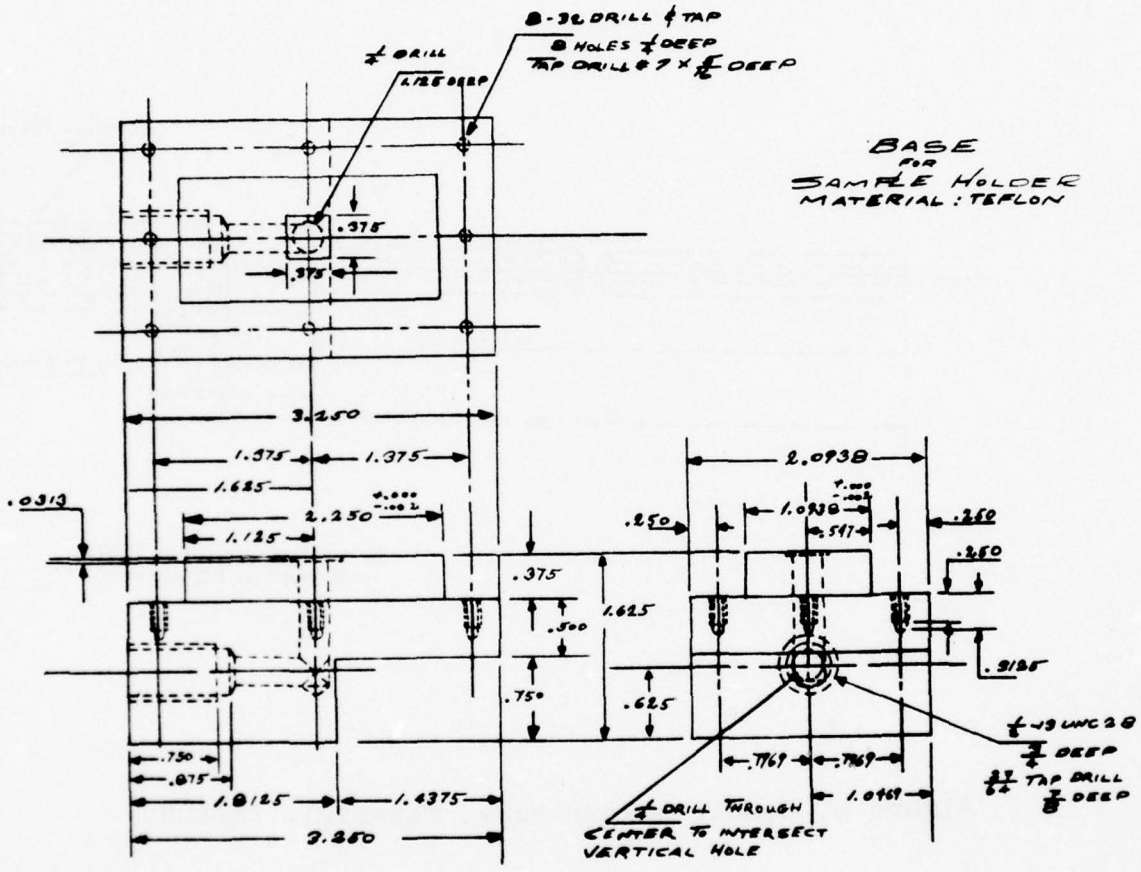

Figure 5. Base of sample holder "head". Material: TEFLON.

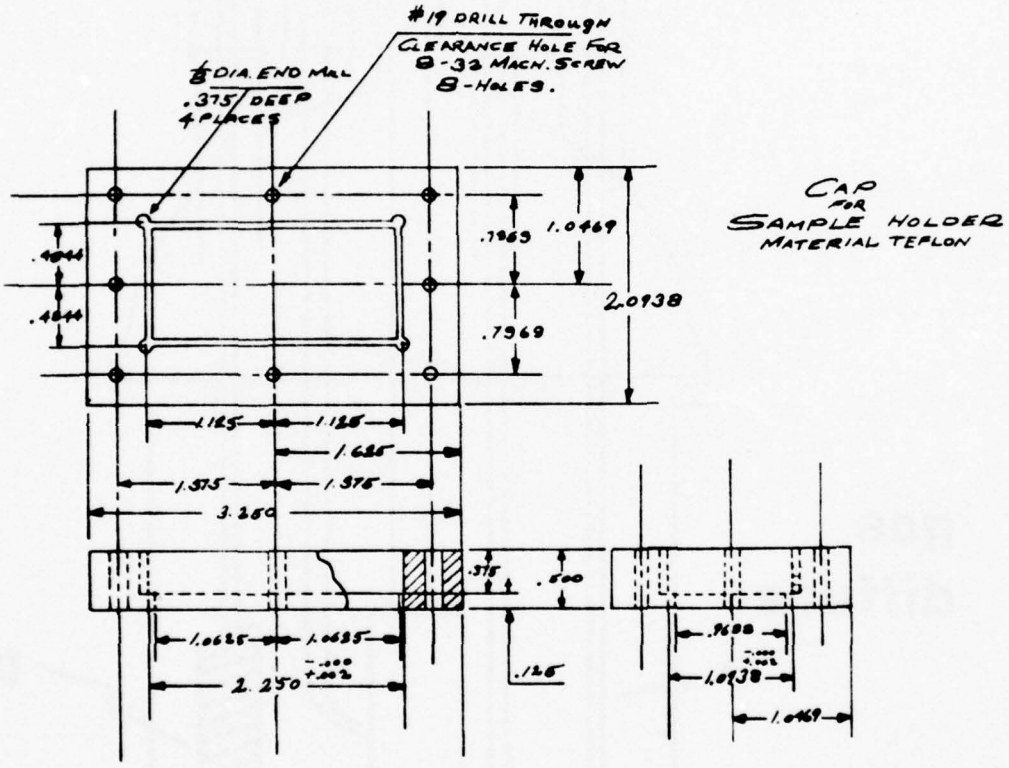

Figure 6. Cap of sample holder "head". Material: TEFLON, screws' - PVC.

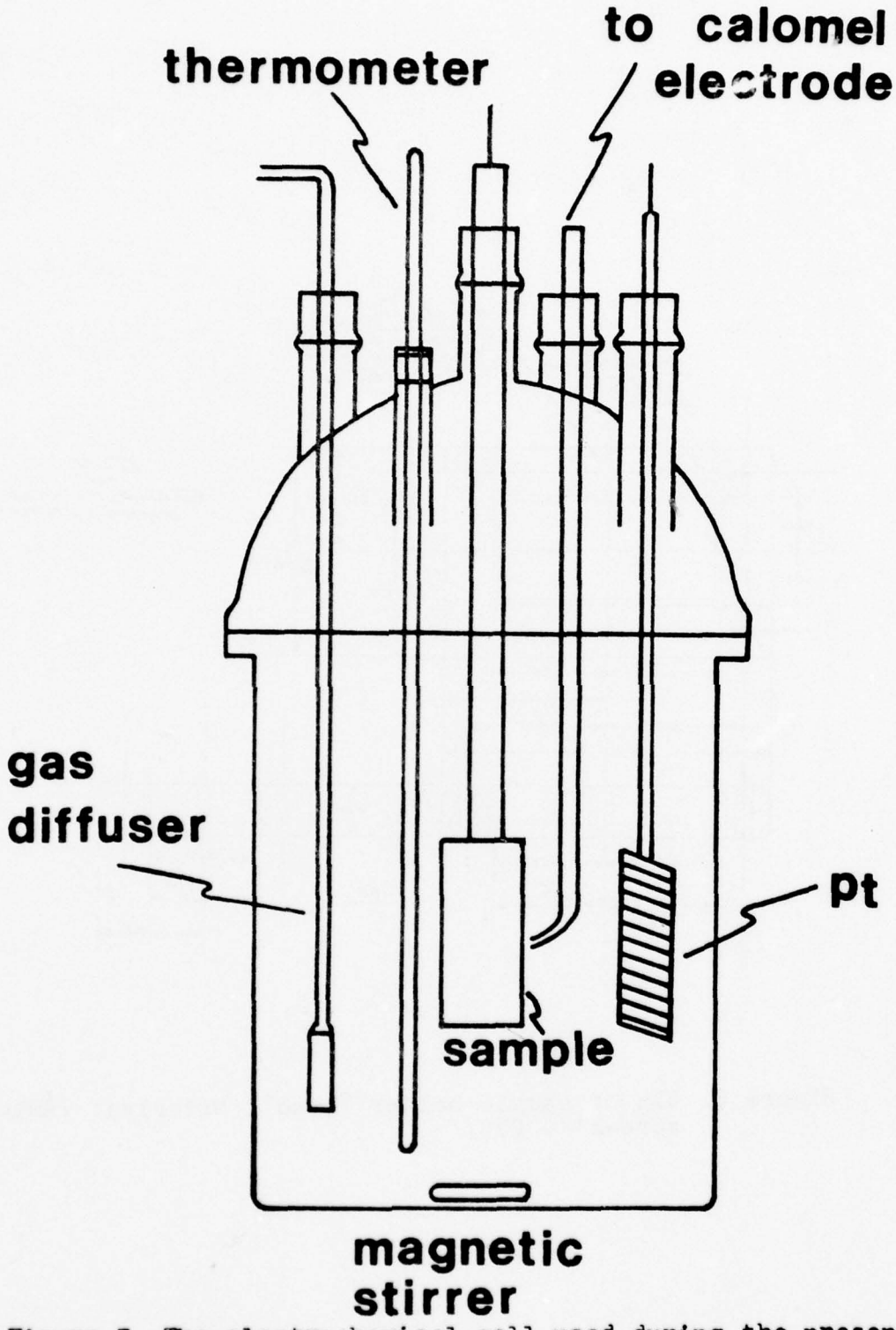

Figure 7. The electrochemical cell used during the present research.

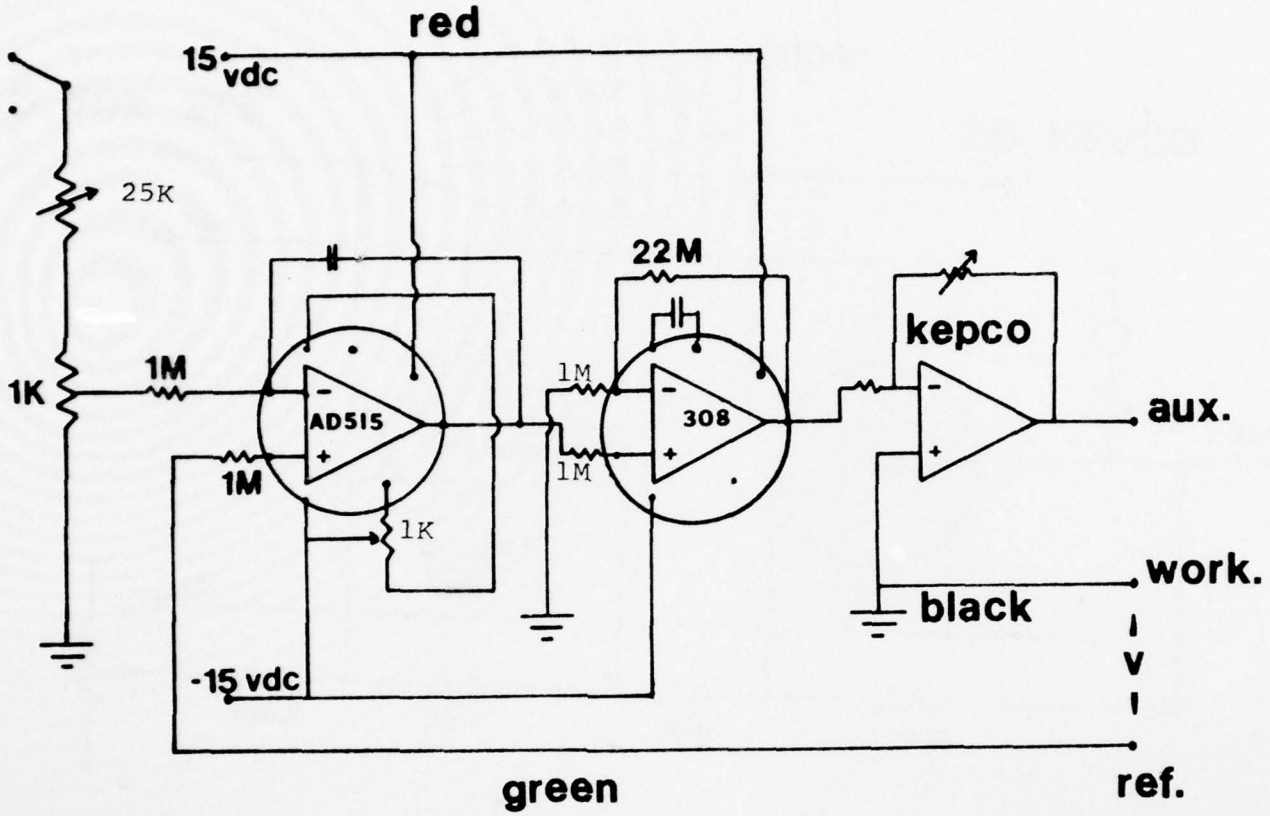

Figure 8. WL-1 potentiostat, main circuit.

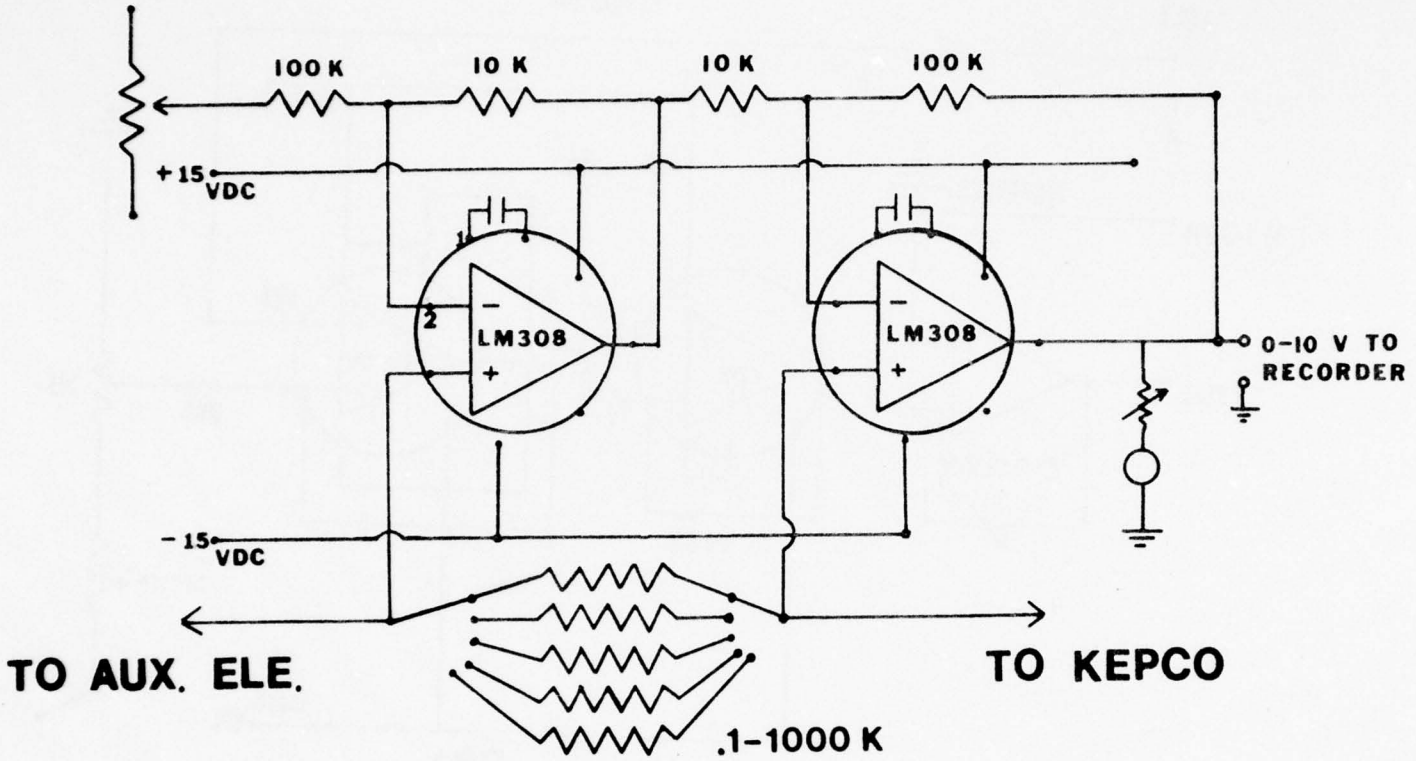

Figure 9. WL-1 potentiostat, current to voltage conversion circuit.

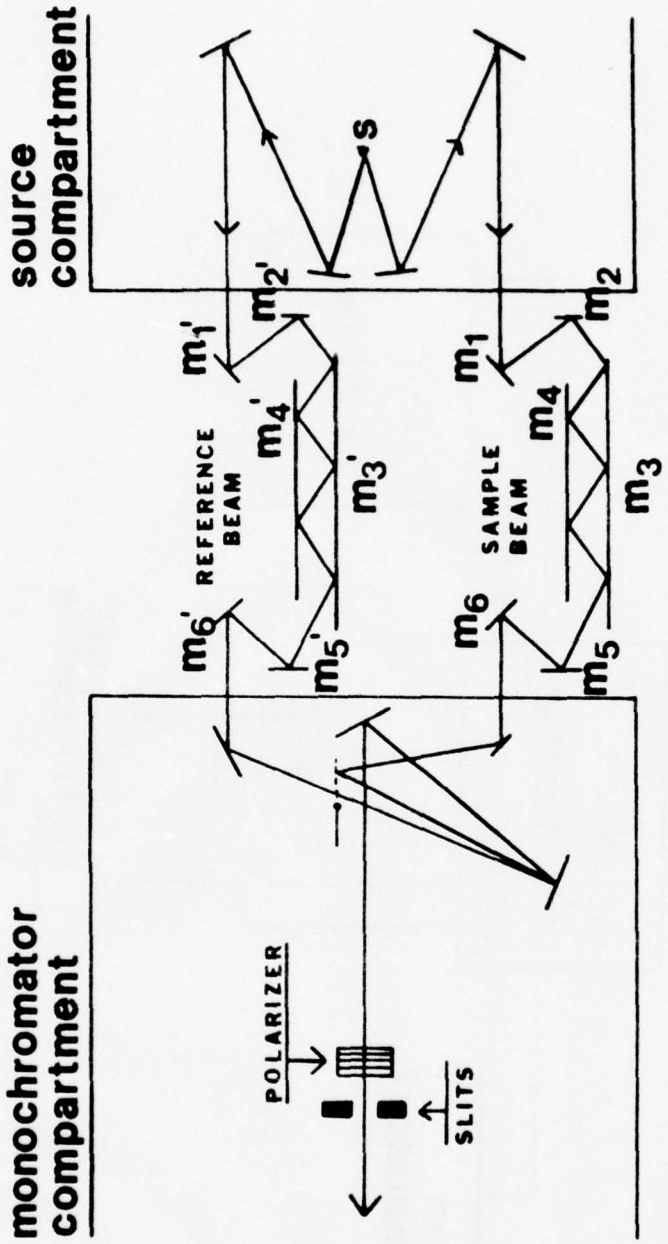

Figure 10. Block diagram of the P.E. 521 infrared grating spectrometer, equipped with Wilks' reflection attachments.

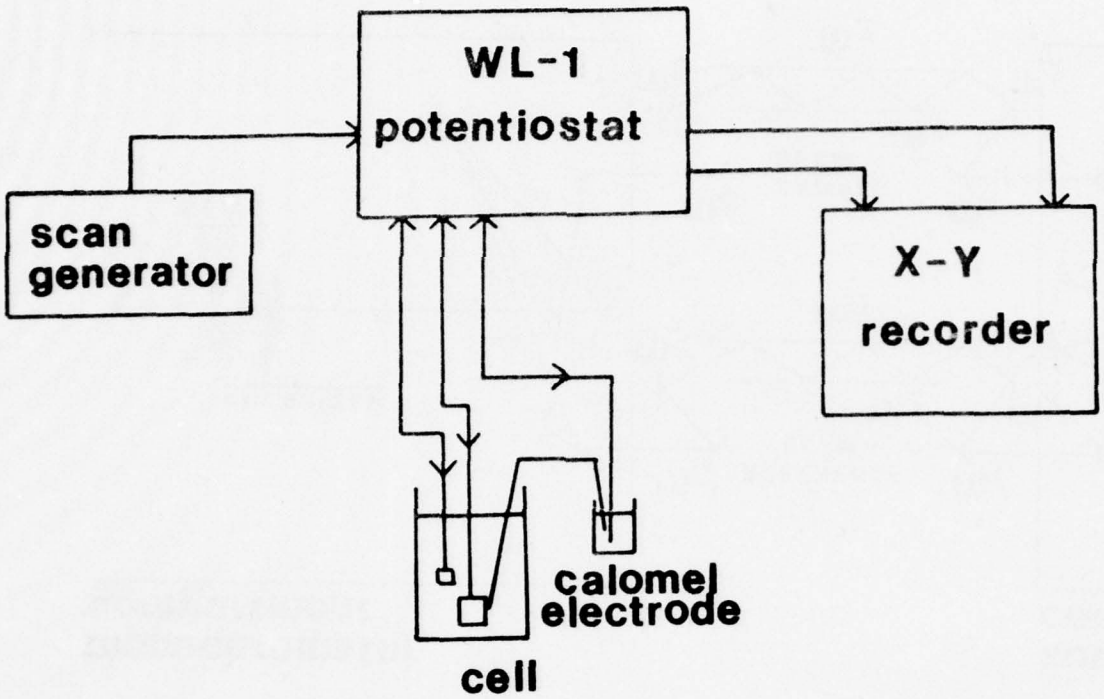

Figure 11. Block diagram of the setup for recording polarization curves.

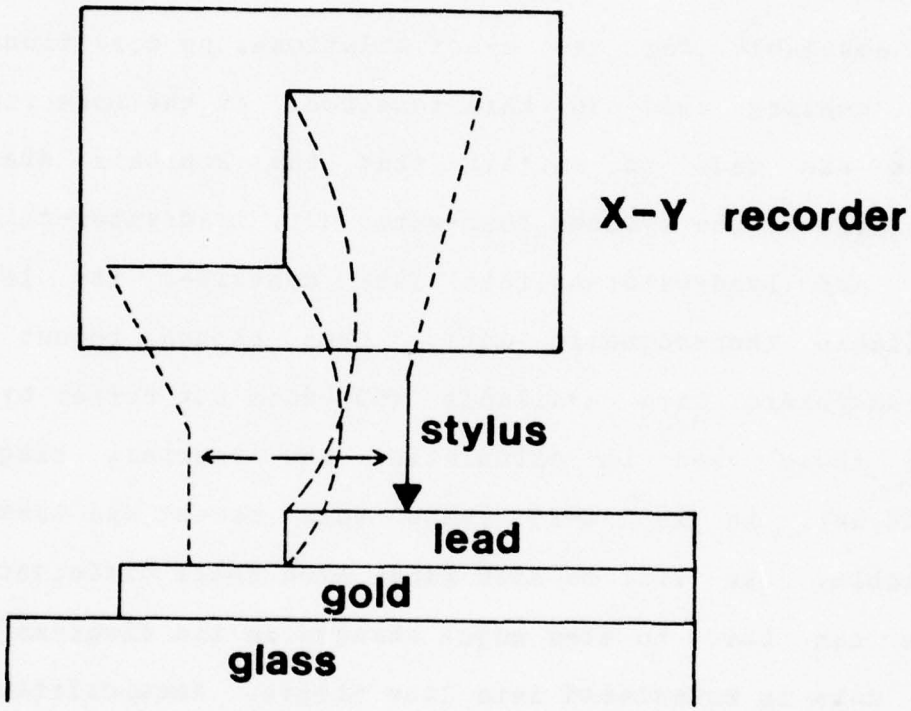

Figure 12. Vapor deposited films on glass, and the stylus instrument working principle.

3. RESULTS AND DISCUSSION

As discussed in the experimental section both the Pourbaix diagrams and polarization curves were used to determine experimental conditions of interest. Electrochemical polarization curves were run on lead in each environment of interest; this was necessary since no data was available for the exact solutions, pH conditions and lead quality used in this research. At the same time, a check was made to certain that the Pourbaix diagrams available on the systems lead-water (7), lead-water-chloride (64) and lead-water-sulfate (48) contained the latest available thermodynamic data. Even though recent thermodynamic data available (65) does not differ by much from those used in calculating the Pourbaix diagrams (7,48,64), it is 10-25 years more recent and thus more reliable. As will be seen later even small differences in data can lead to some major changes in the diagrams since the data is translated into line slopes. Recalculations of the Pourbaix diagrams for the systems lead-water, lead-water-chloride and lead-water-sulfate are given in appendices I-III respectively.

3.1. Lead-Water

The original, simplified Pourbaix diagram of this system (7), Figure 13, has the regions of lead metal - Pb, plumbous ion - Pb^{++}, lead monoxide - PbO - the stable monoxide was

calculated to be the tetragonal form, plumbo-plumbic oxide - Pb_3O_4 and lead dioxide - PbO_2. Recalculation of the diagram using newer data, appendix I, shows, Figure 14, that the tetragonal lead monoxide region extends towards higher potentials - compared to Figure 13 - thus squeezing the Pb_3O_4 region. Part of the Pb_3O_4 region was replaced by lead sesquioxide - Pb_2O_3, and the lead dioxide lower potential boundary was moved into what used to be Pb_3O_4 region. The new diagram has theoretical transitions in the neutral and basic regions of Pb to PbO to Pb_3O_4 to Pb_2O_3 ending with PbO_2 in the highest potential region.

Unlike most of the nonprecious metals, lead is thermodynamically stable within part of the water stability range, marked by lines a and b in Figures 13 and 14.

Figures 15-16 show the polarization curves that were run for pH=7 and pH=10 solutions respectively. In the oxidation cycle of the polarization curve at pH=7 solution there are four distinct waves. The lower wave corresponds, approximately, to the Pb/PbO transition in the Pourbaix diagram and the upper wave to the lower potential boundary of the lead dioxide region. Immediate correlation between the two middle waves and the Pourbaix diagram does not exist, this could be due to the buffer solution, phosphate, and/or a kinetic effect even though the potential scan was fairly slow, 40 mv/minute. Position and shape of waves in polarization curves depend upon: sweep rate, electrode material, solution composition and concentration of

reactants (5). There are five distinct waves in the oxidation cycle of the polarization curve in the pH=10 bicarbonate solution. The one at the lowest potential corresponds to the Pb/PbO transition, and the wave at .64 V SCE (.88 V NHE) corresponds to the lower potential boundary of the lead dioxide region in the Pourbaix diagram. The wave that runs off scale above the lead dioxide transition wave corresponds to the oxygen evolution line. From looking at the Pourbaix diagrams, Figures 13 and 14, it is clear why this line appears in the pH=10 solution and not in the pH=7 solution. The small waves between the Pb/PbO transition wave and the lead dioxide formation wave can correspond to intermediate lead oxides, like Pb_3O_4, and/or are due to the buffer, which is known to form a very stable lead compound - lead carbonate hydroxide (LCH).

In the lead - water system, experiments were performed in the neutral and basic regions of the pH scale. One experiment though, number 1 in table II, was performed in the acidic region and should have given plumbous ions. The current started fairly high, 6.3 ma/cm^2, but did not maintain that level for long, as would be expected in the case of corrosion. It went down to 0.3 ma/cm^2, which is still quite high, thus indicating that whatever formed on the surface was not highly protective. The infrared reflection spectrum of the sample, Figure 17a, was obtained and some interesting features can be noted:

1) The spectrum, Figure 17a, is similar to the

transmission spectrum of the buffer, Figure 17c. From the sixteen bands that appear below 1000 cm^{-1} in the transmission spectrum, fourteen can be matched with bands in the reflection spectrum, these bands match exactly or were shifted 5-10 wavenumbers which is well within the expected magnitude of shifts due to reflection. The two bands that are missing are at 680 cm^{-1} - probably not resolved from the 690 cm^{-1} band - and at 405 cm^{-1}. Two extra bands appeared at 530 and at 365 cm^{-1} and are probably due to orthorhombic (yellow) PbO, these bands are not as sharp as the "organic" bands.

2) The effect of polarizing the light perpendicular to the incident wave gave a spectrum orders of magnitude less sensitive than polarizing the light parallel to the incident wave. (See figures 17b and 17a respectively).

3) The difference in band shape above 1000 cm^{-1} between Figures 17a and 17c - broad vs. sharp - makes it difficult to say if any of the bands in that region are missing in the reflection spectrum obtained from the lead sample or if some of the bands just combined to form broad bands which were not resolved properly. Since we are dealing with polyatomic molecules it is likely that some of the vibrations are parallel to the sample surface and thus cannot be excited by the parallel polarized light, which can excite only those vibrations that have some component normal to the metal

surface.

3.1.1. Immunity Region

Experiments perfcrmed in the immunity region of the Pourbaix diagram, in phosphate buffer, pH=7, confirmed that lead does not go through an oxidation reaction under these conditions. Under all potential conditions below -.42 V NHE, there was a reduction current, reducing whatever species there were cn the surface when the reaction began. The lead samples stayed metallic shiny in the solution throughout all the exposures. Figure 18a shows an infrared reflection spectrum of a lead sample exposed at -.76 V NHE. This sample was not washed with distilled water after being removed from soluticn but was left to dry in air. Upon drying its color changed to light brown with some streaks of interference colors - mostly blue. All the bands that appear in the spectrum can be attributed to lead phosphate (66). Another sample that was exposed for the same length of time under almost the same potential conditions, -.64 V NHE, was washed with distilled water upon removal from solution. Its reflection spectrum, Figure 18b, has some LCH at 1440, 1400 and 840 cm^{-1} in addition to all the lead phosphate bands. There is a possible indication of tetragonal PbO band at 500 cm^{-1}. It can be concluded that the LCH and the tetragonal PbO formed as a result of washing the sample with distilled water. Since lead phosphate is slightly soluble in water it was expected that a strong

rinse of the sample, for a few minutes, would take care of whatever lead phosphate was on the surface, especially if it did not form during the electrochemical exposure but rather from the buffer solution that stayed on the sample surface when it was taken out of the cell. In both cases, rinse and no rinse, the lead phosphate bands appeared in the spectrum thus suggesting some adsorption process in which phosphate molecules adsorbed to the surface of the sample, and changed its potential slightly. The process was not carried far enough to be seen in the sign of the current, which stayed as a reducing current throughout the exposure. Figure 18c shows the spectrum recorded, with the same sample that gave the spectrum in Figure 18a, with the polarizer aligned to transmit the perpendicular, to the incident wave, component of the light.

Exposures in the immunity region of the Pourbaix diagram that were carried out in a bicarbonate buffer, pH=10, gave different results. The current was reducing only during the exposure at -.56 V NHE in which the sample also stayed metallic shiny. The spectrum obtained upon removal from solution indicated the formation of orthorhombic PbO and LCH, Figure 19a. The spectrum was confirmed by Raman spectroscopy (67). This seems to contradict the results of J. Burbank (45), who stated that orthorhombic PbO cannot form above a pH value of 9.4, but due to the reducing current observed throughout the whole exposure it is unlikely that the oxidation was part of the electrochemical

exposure. Therefore it is probably due to air oxidation of the sample after its removal from the reaction cell. Figure 19b shows a transmission spectrum, in KBr, of orthorhombic PbO.

Exposures from -.42 V NHE and above, up to the Pb/PbO line, gave rise to oxidizing currents. During a 20 hour exposure the current density went down to the very low value of .003 ma/cm², thus indicating the formation of a very protective film. The color of these samples was white-gray. Infrared spectra of samples exposed in this region showed the protective film to be LCH, one of the most stable and insoluble compounds of lead. The identification can be seen clearly in Figure 20 where a transmission spectrum of LCH powder is matched against a spectrum obtained from a surface of the sample using the reflection mode. The four strongest bands are matched, and even though there are shifts in the positions of the 1400 and the 400 cm^{-1} bands, up to 60 cm^{-1} in the former case, the identification is positive. The phenomenon of band shifting has been observed before (19) during reflection work; it can be explained by the additional dependence of a reflection spectrum on the refractive index and angle of incidence. More precisely, these shifts result from the inverse dependence of the reflectance on the refractive index, which reaches a minimum on the higher frequency side of the absorption band, thus making it clear why the bands are shifted toward higher wavenumbers. Further confirmation in identification can be

achieved by examining a sample that was exposed for a shorter length of time than the sample that gave the spectrum in Figure 20a. Figures 21a and 21c show the spectra recorded from a sample covered with a thinner LCH film; the two spectra are of the same sample at two extremes of light polarization. Compared to Figure 21b, which is of a thicker film, we see that the 845 cm^{-1} band, which appears in the transmission spectrum but is absent in the thicker film, appears in the thinner film spectrum, Figure 21a. In the same line the 680 and the 690 cm^{-1} bands, which are resolved in the transmission spectrum, Figure 20b, and in the spectrum obtained from the thicker film, Figure 21b, appear as one band at 685 cm^{-1} in the thinner film spectrum, Figure 21a. In Figure 21a there is a shoulder at 510 cm^{-1}, a band at 465 cm^{-1} and another shoulder at 405 cm^{-1}. In the comparable region of the thicker film, Figure 21b, there is only slight hint of a shoulder at 500-510 cm^{-1}, a strong band at 420 cm^{-1} and a weak band at 365 cm^{-1}. The conclusion from comparison in this region is that the thinner film displays a tetragonal PbO band, 465 cm^{-1}, while it does not show in the thicker film which shows only LCH bands. The band at 365 cm^{-1} is probably due to a transition between a lattice vibration mode and a normal mode of vibration of the system, which in this case appears at 420 cm^{-1} and can be assigned to the metal-oxygen stretching (68). This transition, when present, appears always as a weak band attached, within 100 cm^{-1}, on the longer

wavelength side, to one of the fundamental frequencies. The comparison between the samples indicates that upon thickening the film undergoes changes in its crystal structure, thus causing minor changes in its infrared reflection spectrum. Figures 22a and 22b show spectra of LCH recorded, from the same sample, at different angles of incidence. Theory (32) shows:

$$\Delta R = \frac{16\pi d \cos\theta}{\lambda}\left(\frac{n_1 k_1 \sin^2\theta}{n_1^4 \cos\theta} - \frac{n_4 f(n_1\theta)}{k_4^3 \cos^4\theta}\right)$$

that the reflectance, R, is dependent on film thickness, d, and the angle of incidence, θ. Any increase in the film thickness will result in a decrease in the angle of incidence required to obtain the maximum reflectivity from a given sample. The second term in the equation for the reflectance is usually small, since it has in the denominator the extinction coefficient of the metal (k_4) to the third power and the refractive index in the numerator but only to the first power - the two indices are of the same order of magnitude in the wavelength region used in this research (69). Even when the second term becomes of some importance its effect on the change of the angle of incidence as a result of film thickening is the same as that of the first term since it has a cosine of θ in the denominator.

When all the theory is considered it is clear why the sensitivity of recording spectra of a thick film, 24 hours exposure, will be higher at 60-65 degrees, Figure 22b, than

at 75-80 degrees, Figure 22a. The phenomena of band shifting due to changes in angle of incidence can best be seen in Figure 23. Concentrating on the 1400 cm^{-1} band it is seen that in recording the spectrum at 60-65 degrees, Figure 23b, the band was centered at 1440 cm^{-1}, while in recording at 45-50 degrees, Figure 23a, the band was centered at 1400 cm^{-1} - a 40 wavenumber shift on an average change in the angle of incidence of 15 degrees. Most changes are not expected to be so sharp since most spectra are recorded at 60 degrees and above. By moving towards the normal, smaller and smaller angles of incidence, it is seen that the positions of the bands approach those of transmission spectra.

An exposure in a KOH solution, pH=9.7 and potential of -.42 V NHE, was carried out to check if the carbonate buffer was responsible for the oxidizing currents observed in the immunity region. The current in this exposure was reducing thus indicating that the immunity region extended above the -.56 V NHE value that was achieved in the pH=10 carbonate buffer. A poor quality reflection spectrum of that sample was obtained, Figure 24, probably due to the film being very thin. It is probably not an oxidation product film but more likely due to adsorption or from washing the sample, but it shows clearly the presence of LCH, 1400 and 680 cm^{-1} bands, with some other bands of that compound appearing too but they are very weak. The asymmetric band at 500 cm^{-1} is probably due to the presence of tetragonal PbO.

From the exposures in what should have been the immunity region of the lead-water system it is clear that using a carbonate buffer alters the system thus making at least part of this "immunity" region into a passivity region, where LCH forms on the surface and protects it from further corrosion.

3.1.2. PbO Region

The next region of higher potential in the Pourbaix diagram is the PbO region. PbO can exist in at least two distinct polymorphs: red PbO, which is also called litharge or tetragonal PbO, and yellow PbO, which is also referred to as massicot or orthorhombic PbO. The red PbO is the stable form at room temperature, and it exists in equilibrium with the yellow form at 491°c. The yellow PbO can also be stabilized at room temperature, and it probably does so by incorporation of impurities into its crystal lattice (70). Synthesizing the two forms must be carried out carefully, especially for the red PbO (71), since any impurity present will either prevent the formation of or the transformation to red PbO. Red PbO is photoconductive and acts as an n - type semiconductor at low oxygen pressures and as a p - type at high oxygen pressures.

Exposures in the PbO region in pH=7 solutions gave oxidizing currents throughout the region. The final current densities ranged from .025 ma/cm² in a 4 hour exposure to .003 ma/cm² in a 16 hour exposure. In the lower potential exposures, close to the Pb/PbO transition line, samples

stayed shiny during the whole exposure in spite of the oxidizing current. The result was that the film formed on the surface was thought to be thin and obtaining the reflection spectrum was difficult. The spectra obtained from these exposures is seen in Figures 25a, 25b and 25d. All the bands above 500 cm^{-1} can be attributed to lead phosphate, and the band at 480-485 cm^{-1} to red PbO. These exposures fall between the two lower waves in the polarization curve, Figure 15, thus making it possible that the lower wave corresponds to the phosphate and the PbO formation, since that wave is resolved into two waves indicating that two processes occur. The light colored particles seen in the electron micrograph, Figure 26, taken from a sample exposed in that region, were identified with an X-ray energy dispersive analyzer to be lead phosphate particles. This seems to rule out any idea of a thin, protective lead phosphate layer on the surface, which could have been the logical explanation to the low current densities and the almost shiny samples observed in these exposures. It is possible that the phosphate forms in two separate processes, one of them providing the thin protective coating. Indirect evidence for this is the fact that neither form of PbO can form protective films and their region is regarded as corrosion of the metal (7). This is due to their high solubility, which reaches a minimum at pH=9.4, and the photoconductivity of red PbO. When considering the shiny color of the samples and the very low

current achieved - 0.003 ma/cm² - it is likely that the phosphate is the passivating agent in these exposures. The film itself seems to be quite thick as seen from the cracks around the dark particle in the center. That particle was analyzed to be a SiC particle embedded in the soft lead from the grinding process which was part of the surface preparation routine. The SiC particles that were stuck in the lead did not oxidize and grow. This introduced stresses into the film, and as it thickened these stresses resulted in cracks. The grinding step was abandoned after this phenomenon was noticed, and the surface preparation consisted only of chemical cleaning with hot ammonium acetate solution.

Exposure in the upper part of the PbO region, at a potential of .48 V NHE, in phosphate buffered solution, pH=7, resulted in a sample that was very dark. The spectrum obtained, Figure 25c, was identified as due to lead phosphate and red PbO.

Due to the difficulty of synthesizing red PbO a compound for recording a reference spectrum was not prepared. Infrared transmission and reflection spectra of red PbO were reported in the literature, mainly with connection to single crystal and minerology research (42,72-76). Most of the papers (72,74-76) reported only one absorption band, anywhere from 455 to 477 cm^{-1}. The only paper that did spectroscopic analysis and band assignment (42) of red PbO indicated that above 250 cm^{-1}, which is the lower limit of

the spectrometer used in the present research, there are two bands, at 470 and at 278 cm^{-1}. During the present research many PbO spectra were recorded and will be shown later in the text; not all of these spectra showed both bands but some did. Figure 27 is a red PbO spectrum, confirmed by Raman spectroscopy, that clearly shows the two bands, now at 505 and 315 cm^{-1}. The asymmetry and the shifting of the bands are very characteristic of reflection spectra. This figure clearly indicates that a good spectrum, as good as that from a single crystal - sometimes even better, can be obtained using the reflection technique, not to mention the trouble saved in "using" an electrochemical exposure to prepare the compound.

Like the exposures done in the pH=10 buffer solution at the upper part of the immunity region, those that were done in the lower part of the PbO region gave, mainly, the spectrum of LCH, Figure 28. The main difference from previous spectra of this compound are the two distinct shoulders at 510 and 465 cm^{-1}. The possibility of the 510 cm^{-1} band belonging to yellow PbO was ruled out with the help of Raman spectroscopy (67). The band at 465 cm^{-1} would, naturally, be assigned to red PbO, but in this way the 510 cm^{-1} will be left unidentified, unless we assign the 465 cm^{-1} band to the ICH - it has a distinct shoulder at 460 cm^{-1} in its transmission spectrum - and the 510 cm^{-1} band to red PbO. We already observed a red PbO band at 505 cm^{-1}, Figure 27, thus making it reasonable to assign the 510 cm^{-1}

band to red PbO. An electron micrograph, Figure 29, of this sample was taken, and it reveals a rough but ordered surface which definetly has a film on it. There is a possibility of lead compound particles, but they were not resolved.

Moving up in the PbO region, pH=10, major changes in the samples exposed were observed. Their color was not light-gray any more but rather black. The most impressive aspect of these exposures was the high current density obtained, even after 18.5 hours exposure. The current densities ranged from 6.3 ma/cm² for a 1.5 hour exposure to 2.5 ma/cm² for an 18.5 hour exposure. These were three orders of magnitude higher than currents observed where LCH formed, indicating that the red PbO films that formed were not protective. Figure 30 shows spectra recorded in the PbO region between .02 V NHE and .24 V NHE. Figures 30a and 30b show spectra of one of the longest exposed samples - 18.5 hours - which probably had the thickest film of all samples exposed in that region. Figure 30a was taken at one extreme of light polarization which is thought to produce parallel polarized light; the two red PbO bands are observed at 480 and 310 cm^{-1}. The other extreme of light polarization gave the spectrum seen in Figure 30b. It was expected that this polarization would not be sensitive enough to observe any absorption, but it is clearly seen that the two bands are there, even though the 480 cm^{-1} band was shifted to 505 cm^{-1} and the overall appearance is less symetric than the spectrum obtained with the light polarized parallel to the

incident plane. Intuitivly this makes sense, since the less sensitive perpendicular polarization, which has a node of the electric field vector in the plane where the reflection occurs, will have a finite magnitude of that vector some distance from the reflection plane. If the film is thick enough and the light penetration is deep enough, on the order of a wavelength, this perpendicular polarized light will assume finite values for its electric field vector while still within the film, thus making it possible for vibrational excitation. A shorter exposure, 1.5 hours, produced the spectrum shown in Figure 30c, in this case only one band of the red PbO was observed, and it appeared at 540 cm^{-1}. The identity of the red PbO compound was confirmed by X-ray and Raman spectroscopy. Samples exposed for an intermediate length of time - 5 hours - showed a weak presence of LCH as can be seen in Figure 30d, but there is no doubt that, even at that stage, red PbO was the main constituent of the surface layer which contributed to the spectrum.

3.1.3. Pb_3O_4 Region

J. Burbank wrote the only paper (45) we found that claims the formation of Pb_3O_4 in aqueous solutions. None of the exposures done during this research, in any of the regions, produced a spectrum that unquestionably could be identified to be that of Pb_3O_4. Pb_3O_4, which is called red lead or minium, can be made by heating up PbO_2 (43). An

interesting point is that there is tetragonal PbO, tetragonal PbO_2 and Pb_3O_4 is also tetragonal, thus making it easier to introduce any of the oxides into the other lattices. From simple stoichiometric addition it is seen that a combination of 2PbO and PbO_2 will produce Pb_3O_4. If during our exposures in the Pb_3O_4 region we actually formed a lattice with PbO and PbO_2 in it, it is clear why the actual Pb_3O_4 spectrum was not observed in any of the exposures. A possible kinetic effect in the formation of Pb_3O_4 can not be ruled out.

Exposure in phosphate buffer, pH=7, in the Pb_3O_4 region, at a potential of .67 V NHE, produced a dark - gray sample. Current densities were not as high as in the exposures in the upper part of the PbO region but were still fairly high, 0.3 ma/cm². Figures 31a and 31c show spectra obtained from the sample at different light polarizations. The problem with the assignment of the bands is that Pb_3O_4 and lead phosphate have bands in very close proximity, and with the possible shift in band position due to reflection, it was not possible to determine if any Pb_3O_4 existed in the sample. Indirect evidence, like color of the sample - dark gray - instead of the bright orange color that was under the surface film reported by Burbank (45), indicated against the formation of Pb_3O_4 in any of those samples. The 455-60 cm^{-1} band, Figure 31a, can be assigned as the strongest Pb_3O_4 band, as seen in the reference transmission spectrum of the compound, Figure 31d. The bands at 540,365 (sh) and 265

cm^{-1} can also be attributed to Pb_3O_4, but at the same time its more likely that the 455-60 and the 265 cm^{-1} bands are red PbO bands and the rest are lead phosphate bands. Figure 31b gives the spectrum of the same sample when no polarizer was used in the light path. There is a marked decrease in the sensitivity and the intensity of this spectrum compared to the spectrum recorded with the polarizer alligned to transmit the parallel component, Figure 31a. Exposing a sample in a bicarbonate buffer at comparable potentials did not seem to form Pb_3O_4 either. The sample was dark-gray and the current was of the same order of magnitude, even after 6 hours exposure. The spectrum, Figure 32, has indications of LCH and red PbO, but there is also a slight possibility that Pb_3O_4 is present, based on the 470 and 375 (sh) cm^{-1} bands. An x-ray diffraction pattern of the sample did not reveal any new data. This was expected, since x-ray diffraction patterns from thin oxide films on a lead substrate produced a strong lead diffraction pattern which probably masked some of the film peaks, thus preventing complete identification. An electron micrograph of the sample, Figure 33, did not help, since it shows only a film-coated surface. All the cracks, shown in Figure 33, are probably due to stresses introduced into the surface during sample preparation.

3.1.4. PbO_2 Region

Like PbO lead dioxide has two polymorphs, the tetragonal and the orthorhombic forms. The formation of the two

polymorphs is pH dependent. The electrical conductivity of PbO_2 is high and it is considered to be an intrinsic semiconductor (47). Lead dioxide is an important compound since it constitutes the positive electrode in lead-acid batteries. Unfortunately neither form of PbO_2 exhibits any absorption bands in the near and middle regions of the infrared spectrum. This lack of spectrum has been reported in the literature (73,76). The only paper that claimed the recording of of the infrared spectrum of PbO_2 (74) admitted that many contaminants were present in many of the samples. An attempt to record the transmission spectrum of PbO_2 powder - confirmed by X-ray to be pure tetragonal PbO_2 - did not produce any measurable absorption bands in the 1500-250 cm^{-1} range. With this in mind it is clear that it is not possible to rule out the formation of PbO_2 in any of the exposures. Indirect evidence like color and current density should help in characterizing the species formed. Due to some of the films being very thin the possibility of X-ray diffraction patterns helping in solving the identification problem was low, but it was tried anyway.

Exposures in the PbO_2 region in a phosphate buffer, pH=7, at .99 V NHE, produced a gray sample. The change in current magnitudes during the exposure indicated the possibility of two processes occuring, the current went steadily down, then after 1 hour climbed up, and then started down again. Current densities were fairly high - 0.6 ma/cm^2. An electron micrograph of the sample did not

reveal any particles on the surface. Figure 34a shows the spectrum obtained from this sample. The important bands are at 470 and 370 cm^{-1}; all the other weak bands are lead phosphate bands. The two bands do not correspond to yellow PbO formation, since the high frequency band should appear above 500 cm^{-1}. The bands correspond well with the possibility of Pb_3O_4 formation even though some of this compound's bands are missing, as seen in comparison with a reference transmission spectrum of Pb_3O_4, Figure 31d. It is possible though that some of the Pb_3O_4 bands are not excitable in the reflection mode. PbO_2 is known to decompose in light and give the lower oxides (54), this was demonstrated with a laser, and the film's Raman spectrum was recorded (67). This can explain, in part, the change in current during the exposure and the spectrum that was recorded.

More spectra were recorded of this sample with different angles of incidence and numbers of reflections. Figure 34b is a single reflection spectrum recorded at an angle of incidence of 65 degrees. Using the same angle of incidence but a higher number of reflections, 2-3, produced a somewhat weaker spectrum, Figure 34c. This spectrum is not as highly asymmetric as the single reflection spectrum; this can only be attributed to the different number of reflections used in recording the spectrum. The change in symmetry is not explained by reflection since more reflections should introduce more information to the light while at the same

time they decrease the overall radiation. It can be caused by a non-specular reflection from the surface, which in other words caused the light to fall in subsequent reflections at a wide range of angles making the spectrum a diffusion - specular combination spectrum. Figure 34d was recorded using even more reflections; the 370 cm^{-1} band is almost undetectable and is seen only as a weak shoulder. The interesting thing is the 470 cm^{-1} band which looks now as if it is composed of two bands at 485 and at 470 cm^{-1}. Repeated spectra under the same conditions proved that this was not instrument noise. The 470 cm^{-1} band, along with the possible band at 270 cm^{-1}, more than hints for the presence of PbO. The presence of PbO does not contradict what was said before, since the decomposition products of PbO_2 can be any intermediate oxides between PbO_2 and PbO inclusively. To close this line a spectrum was recorded at 70 degrees incident radiation with 1-2 reflections, Figure 34e. The spectrum is almost non-informative and contains only the 300 cm^{-1} band of red PbO.

The conclusions from all these recordings is that the film is quite thick, the recording at 65 degrees incident angle was better than recording at 70 degrees, and that the optimum number of reflections for this film is not as low as was expected, indicating that the surface is quite a good reflector in this infrared region. PbO has been stated to be a good mirror in a large interval of the infrared radiation (42), and this is in agreement with the results

presented.

Moving up in the PbO_2 region to 1.08 V NHE, pH=7, and exposing a sample for 3.5 hours produced a surface black in color which seemed thick but was difficult to obtain a spectrum from, since no distinct bands could be located.

Exposures in pH=10 in the PbO_2 region were done in potentials ranging from .75 V NHE to 1.08 V NHE. In the .75 V NHE exposures, with exposures times ranging from 2.5 to 5.5 hours, there is a difference in the spectra obtained. Figure 35a shows the spectrum obtained from the sample exposed for 2.5 hours; there is only one band at 470 cm^{-1}. The sample color was black, but the spectrum can be attributed to red PbO. In the 5.5 hour exposure the current went down to value of 3.8 ma/cm^2, but then started up again and stopped around 6.3 ma/cm^2. The sample looked dark-gray and when checking for a photoelectric effect by illuminating the entire electrochemical cell with 150 watt lamp, there was an increase in the overall current by about 3 ma. The change was not larger since the experiment was conducted in a lighted room and with the extra light we probably caused saturation of the current. The spectrum obtained from that sample, Figure 35b, is highly asymmetric, but the existance of red PbO is confirmed. The bands due to PbO in this spectrum are the 540 and the 290 cm^{-1} bands. The direction of band shift is in agreement with the film wavelength relations. The 500 cm^{-1} band is thought to be of some intermediate lead oxide that formed during the exposure, and

its presence was hinted in the change of the magnitude of the current. Exposures done at a higher potential, .83 V NHE, gave samples with colors ranging from blue-gold to gray, depending on length of time exposed. The current exhibited the same behavior of down, up and down again as was observed at the lower potential, but, inspite of all this, the spectrum was not much different from that recorded before. It displays an extra band at 365 cm^{-1}, Figure 35c, which can be due to Pb O or any of the intermediate oxides. Figure 36 shows one band of red PbO from a sample exposed in that region, that was recorded at 3 different angles of incidence - 60,65 and 70 degrees. It is clearly seen that the optimum angle is around 65 degrees, probably between 60 and 65 degrees.

An electron micrograph of sample exposed at .83 V NHE, Figure 37, shows only film and no particles.

During the analysis of all the exposures in the PbO_2 region it must be taken into consideration that most of this region lies above the oxygen evolution line, shown as line b in Figure 14. This means that another process - water decomposition - takes place and probably influences the surface reactions. The effect of this process on the exposures was not studied in this research.

3.2. Lead-Water-Chloride

The lead electrochemical exposures in solutions

containing chloride ions were conducted in an identical manner to the exposures in nil chloride solutions.

The Pourbaix diagram of the system, Figure 38, was calculated, Appendix II. In the lower potential region, below 0.2 V NHE, the reactions and the species present were after the work done by Appellet (64). The diagram was calculated while taking into account the concentration of chloride ions used in this research, 0.1M. This in turn affected the concentration of lead ions in solution independent of pH and potential as seen in reaction 3 Appendix II.

3.2.1. $PbCl_2$ Region

Most of the experiments, as before, were conducted in pH=7 and pH=10 solutions. One experiment and a matching electrochemical polarization curve, Figure 39, were performed in 0.1M HCl. During this electrochemical exposure the current was very high, and there was a possibility of overloading the potentiostat and having insufficient current to keep the potential steady. The sample looked gray while in solution but became yellowish upon drying. The auxilliary electrode was also covered with some dark material. Figure 40 shows the spectrum recorded from that sample. The two spectra were recorded at identical light polarization settings but different angles of incidence. The spectrum was identified to be that of yellow PbO, and a transmission spectrum of yellow PbO appears in Figure 19b.

The material on the auxilliary electrode was scraped off, and its Raman spectrum was obtained and identified to be that of yellow PbO (67). As mentioned before, yellow PbO is the high temperature polymorph of the lead monoxides, but is known to be stable in the presence of minute amounts of some materials (70), even at room temperature. The infrared spectrum - transmission and reflection - of yellow PbO appears in the literature (42,72,77), but the only reliable source seems to be the one paper that is devoted to the infrared spectra measurements of the lead monoxides (42). This paper lists 3 bands for yellow PbO above 250 cm^{-1}: at 500,356 and at 290 cm^{-1}. This corresponds well to the spectra in Figure 40 which show bands at 500,385 and 305 cm^{-1}. The presence of yellow PbO on the auxilliary electrode hints towards the conclusion that yellow PbO does not form via a direct electrochemical process but rather is a byproduct of such a process. This observation is in agreement with a paper (45) that suggested the possible mechanism for the formation of yellow PbO to be through the plumbous ion, Pb^{++}:

$$Pb^{++} + H_2O = PbO\ (Y) + 2H^+$$

This explains why yellow PbO is seen in acidic solutions. Since the $Pb^{++}/HPbO_2^-$ transition line in the Pourbaix diagram (7) is at pH=9.4, it is understood that the lack of Pb^{++} ions in highly basic solutions will also prevent the formation of yellow PbO.

This experiment was performed in a region of the

pourbaix diagram, Figure 38, in which there should be an equlibrium between the solid phase of $PbCl_2$ and the two dissolved substances of Pb^{++} and Cl^-. Lead chloride does not exhibit absorption bands in the infrared region investigated in this research. It is considered to be quite a good material for infrared windows (40), due to its good transparency and a relatively low solubility in water. In view of all this the lead-water-chloride system should have been investigated with a complimentry technique to infrared spectroscopy, which should be sensitive to the lead chloride compounds. This was done in a separate study using Raman spectroscopy (67).

3.2.2. Exposures in pH=7 (0.1M Cl^-) Phosphate Solutions

The electrochemical polarization curve in phosphate buffer containing 0.1M chloride ions, Figure 41, shows only one small wave which is at too low a potential to correspond to the $Pb/3PbO \cdot PbCl_2$ transition line in the Pourbaix diagram.

Samples that were exposed in the immunity region of the Pourbaix diagram, Figure 38, all the way up to the $Pb/3PbO \cdot PbCl_2$ transition line gave reducing currents through all the exposures. When the samples were taken out of solution they looked the same as when put in. The infrared reflection spectrum was obtained easily but was of fairly low intensity, as is showen in Figure 42. The bands correspond to those of lead phosphate. Three different lead

phosphates are known: meta, ortho and pyro phosphate. All of these compounds have their absorption bands in a very close region which complicates their exact identirication. The only compound that has a band in the 670 cm^{-1} region is the meta phosphate but it is unlikely that this is the compound that formed, and the 670 cm^{-1} band is probably due to LCH.

In the experimerts performed in the lower part of the $3PbO \cdot PbCl_2$ region, Figure 38, at -.11 V NHE the current went down fast indicating a quick formation of a protective layer. At the end of a 17 hour exposure the current was 0.02 ma/cm^2, and the samples had some interference colors on them, mostly blue. Figure 43a shows the spectrum obtained before washing the sample with distilled water. By comparison to Figure 43b, which was obtained after washing the sample, it is seen that the appearance of the spectrum is the same except that the low frequency bands are better resolved after washing the sample. No improvement of the baseline below 500 cm^{-1} was possible with this sample. Another sample, expcsed under identical conditions, Figure 43c, gave a spectrum that could be interpreted as either a mixture of red and yellow PbO or as just yellow PbO. Electron micrographs of these samples at 500X, Figure 44, and at 5000X, Figure 45, magnifications were obtained. The light colored particles were identified, as in the nil chloride solutions, to be lead phosphate particles. The surface film was characterized, with an X-ray energy

dispersive analyzer, to have lead, but nothing else was detected. This is in agreement with the infrared results indicating PbO formation, since the X-ray energy dispersive analyzer can not detect oxygen. No chlorides were detected in the surface film thus indicating that the monoxides were the only species present in the film.

Several experiments were conducted in solutions having 0.01M and 0.5M concentrations of chloride ions. These experiments were done in the $3PbO \cdot PbCl_2$ region of the Pourbaix diagram, Figure 38. In the 0.01M chloride ion solution the current was an order of magnitude higher than in those exposures carried out in 0.5M chloride ion solutions. Figure 46a shows the spectrum obtained from the exposure in the low concentration chloride solution. Besides the lead phosphate bands one can see a distinctive shoulder at 520 cm^{-1}, a band at 470 cm^{-1} and another shoulder at 375 cm^{-1}. This spectrum can be identified as a red and yellow PbO mixture and it was confirmed by X-ray diffraction and Raman spectroscopy (67). The high concentration chloride solutions gave the spectrum seen in Figure 46b. The bands below 600 cm^{-1} are not resolved and the overall spectrum is weaker. Electron micrographs of these samples were obtained, and there is a marked difference between the low concentration chloride exposure, Figure 47, and those performed in the high concentration chloride solutions, Figures 48 and 49. The crystals in Figures 48 and 49 were identified to be pottasium chloride

(KCl) which precipitated out of solution due to its high concentration there, but there was, probably, some impurity or surface effect on this precipitation since KCl did not exceed its solubility product in solution.

Electrochemical exposures in the upper part of the $3PbO \cdot PbCl_2$ region, Figure 38, gave a spectrum of red PbO only.

Exposures in the PbO_2 region, Figure 38, gave a very dark sample. The infrared reflection spectrum was obtained, Figure 50, and it has again an indication of red and yellow PbO, Figure 50a. Scale expansion of 5X was tried in the vicinity of the important bands, and the spectrum obtained is seen in Figure 50b. The bands are clear and strong, but it was impossible to adjust the baseline, mainly due to the reflection attachments, which are trial and error instruments and do not provide any accurate way to measure and reproduce the exact angles of incidence, and to the angles of the directing mirrors with respect to the infrared spectrometer. Figure 50c is a spectrum obtained from the same sample with the polarizer aligned to transmit the perpendicular component of the light.

The only big difference, so far, in comparison with the nil chloride exposures is the formation of the yellow form of PbO in solutions containing chloride ions. Since trace amounts of the chloride ions were expected to prevent the yellow to red PbO transformation, no chloride concentration effect was observed, even when there was a change in the

concentration of chloride ions by an order of magnitude from the usual working conditions.

3.2.3. Exposures in pH=10 (0.1M Cl^-) bicarbonate solutions

The electrochemical polarization curve in a bicarbonate buffer solution containing 0.1M chloride ions, pH=10, Figure 51, looks very much the same as the polarization curve of the comparable nil chloride solution, Figure 16. Comparing the Pourbaix diagrams of the systems, Figures 14 and 38, it is clear that the polarization curve in the chloride containing solution should have at least one transition wave less than the polarization curve that was run in the nil chloride solution at pH=10.

No yellow PbO was expected to form in pH=10 solutions, even in those containing chloride ions. In the exposures performed in a bicarbonate buffer at low potentials - immunity and the lower part of the $3PbO \cdot PbCl_2$ regions, Figure 38 - LCH formed, which is comparible tc the processes in nil chloride solutions. Sample colors were from light gray to some that had interference colors on them. Throughout this region current densities were approximately the same indicating that identical processes might be taking place. Spectra obtained, not shown, were identical to those obtained in the comparible exposures in nil chloride solutions, Figure 21a, and were identified, as before, to be of LCH.

Moving up in the $3PbO \cdot PbCl_2$ region of the Pourbaix diagram, Figure 38, the exposures gave red PbO. Current densities were high compared to the exposures that gave LCH, this is expected in the formation of red PbO which is a nonprotective oxide.

An exposure in the PbO_2 region, Figure 38, gave very high currents, 5.0 ma/cm^2. Its infrared reflection spectrum was obtained, Figure 52, and it shows a medium broad band between 450 and 600 cm^{-1}. This band is clearly resolved into two weak bands. The spectrum looks like it could match the infrared spectrum of lead dioxide given in the literature (74) but that spectrum does not seem to be too reliable. This paper states that the lead dioxide spectrum consists of one weak and broad band between 585 and 465 cm^{-1}. The high current densities observed are in agreement with the good conductivity of PbO_2, but at the same time could be in part from the oxygen evolution process.

Not much information was expected to be gained from the infrared reflection spectra of lead samples exposed in solutions containing chloride ions. This was mainly due to the lack of absorption bands of the lead halides in the infrared region of the spectrometer used during this research. The results, in pH=10 solutions were almost identical to those obtained in nil chloride solutions, and no significant difference can be pointed out.

3.3. Lead-Water-Sulfate

The electrochemical behavior of lead in sulfuric acid is by far the single most widely investigated system of lead electrochemistry. The importance of the lead-sulfuric acid system is based on the extensive use of lead-acid batteries in many modern applications, from cars to submarines.

The Pourbaix diagrams of the system, Figures 53 and 54, were calculated, Appendix III. Two diagrams are presented for two different concentrations of sulfate ions - 1N and 0.1M. The diagram was calculated before (48), but the use of newer data (65) shows that some changes do occur. These changes are mainly in the $PbO \cdot PbSO_4$ region which is seen, Figure 53, to expand towards higher and lower pH values, relative to the diagram that was published (48).

3.3.1. Exposures in 0.1M Sulfuric Acid

The electrochemical polarization curve of lead in sulfuric acid, Figure 55, shows one strong and sharp wave at -.26 V NHE which can clearly match the $Pb/PbSO_4$ transition line in the Pourbaix diagram, Figure 54.

The infrared transmission spectrum of lead sulfate powder was recorded and is compared, Figure 56, to the infrared reflection spectrum obtained from a lead sample exposed in 0.1M sulfuric acid, pH=0.9, at -.02 V NHE. The lead sample surface was confirmed by Raman spectroscopy (67) to be covered with $PbSO_4$. The two spectra in Figure 56 do not look the same at first sight but at least three of the

bands can be matched easily: the 960, 628 and the 595 cm^{-1} bands. The other bands, all of them above 1000 cm^{-1}, can also be matched if some literature data is used, but before that it is clear that the resolved bands in the reflection spectrum could be hidden under the poorly resolved, strong and broad band in the transmission spectrum which covers over 250 wavenumbers, from 950 to 1200 cm^{-1}. The 1220 cm^{-1} band which is the strongest in the reflection spectrum can be either from the shifting of the 1160 cm^{-1} band in the transmission spectrum, or a combination band of two fundamentals as is seen in the case of gypsum (78), or even a combination of these two possibilities.

Figure 57a shows the spectrum obtained from a lead sample exposed in the immunity region of the Pourbaix diagram, Figure 54, in 0.1M H_2SO_4, at -.40 V NHE. The current was reducing during the whole exposure. The spectrum obtained upon removal from solution was identified as $PbSO_4$ and red PbO. This spectrum, Figure 57a, has the same band appearance as the reflection spectrum presented in Figure 56b, but it is seen now that the 1220 cm^{-1} band is at 1160 cm^{-1}, which is more like the transmission spectrum of $PbSO_4$, thus hinting that the origin of the 1220 cm^{-1} band is from the 1160 cm^{-1} band in the transmission spectrum, and the shift is due to reflection phenomenon and thickening of the film. The formation of red PbO can be explained to be from the "wet" oxidation of the sample after removal from the cell and not as part of the electrochemical process. An

x-ray diffraction pattern of this sample was completely uninformative and showed only the lines of lead metal (cubic), thus supporting the idea of a very thin film (<1000 angstroms). Figure 57b shows a spectrum recorded from the same sample but with the polarizer aligned to transmit the perpendicular component of the light.

An electron micrograph of the sample, Figure 58, shows a surface with scattered lumps of particles on it. These are probably lead sulfate which did not have the time to crystalize properly upon drying of the sample. Unfortunately it was not possible to identify the particles using an x-ray energy dispersive analyzer since the lead and the sulfur lines are very close and could not be resolved.

Pavlov (50,53) and Ruetschi (55) investigated the anodic layer, formation and composition, on lead electrodes in sulfuric acid solutions. Their results were that between -.34 V NHE and .32 V NHE the anodic layer consists only of $PbSO_4$, from .32 V NHE to 1.52 V NHE the layer composition is more complicated having $PbSO_4$ in the solution-electrode interface. Under the $PbSO_4$ layer they reported the formation of compounds like, red PbO and $PbO \cdot PbSO_4$ which are usually observed only in basic solutions. During that research, which was based on x-ray diffraction analysis of the lead electrodes, it was suggested (50) that a non x-ray technique should also be used, mainly due to the problems encountered with identification of some of the compounds x-ray diffraction patterns.

Electrochemical exposures within the potential boundaries set by Pavlov (50) in which only the formation of $PbSO_4$ was observed gave infrared reflection spectra that confirmed these results. An example of such a spectrum is seen in Figure 56b.

A good example of the dependence of the reflection spectrum on the angle of incidence is given in Figure 59. Figure 59a was recorded at 60-65 degrees incident angle and the spectrum obtained is clear and sharp. Recording at lower angles of incidence, 45 and 30 degrees, Figures 59b and 59c respectively, showed spectra that, while they still are resolved, are of much worse quality than that recorded at 60-65 degrees. The spectra recorded at low angles of incidence, Figures 59b and 59c, look more like the transmission spectrum of the $PbSO_4$ powder, Figure 56a. This is reasonable when considering that these spectra were recorded at angles of incidence closer to the normal to the surface. Another feature that can be pointed out from these spectra is the change in the relative intensity of some of the bands with a change in the angle of incidence. Going from 60 to 45 to 30 degrees the bands at 1200 and 1030 cm^{-1} change their relative intensity, so do the two sharp bands at 630 and 585 cm^{-1}. This can not be explained throughly without knowing the optical constants of the film at the wavelength of the abscrption bands.

Electrochemical exposures done at .48 V NHE and .80 V NHE gave results that at least on the shorter

exposures, up to 7 hours, confirmed the results reported by Pavlov (50). Figure 60a shows a spectrum obtained from an exposure done in the region where only $PbSO_4$ form on the surface, at -.02 V NHE, while Figure 60b, at .80 V NHE, shows a spectrum that is identified to be a mixture of $PbSO_4$ and red PbO. These identifications were confirmed by Raman spectroscopy (67). The explanation given by Pavlov for the formation of red PbO, which usually forms only under basic conditions, was that as a result of the $PbSO_4$ crystals growth on the electrode surface, the diffusion of sulfate ions towards the lead electrode was hindered thus causing the pH value under the surface film to rise and become more basic. Electron micrographs of such surfaces were taken, Figures 61 and 62, at magnifications of 500X and 2000X respectively.

A series of seven exposures was done at .80 V NHE. The only difference between the exposures was the exposure time, ranging from 20 minutes to 20.5 hours. In the first three exposures - 20 minutes, 1.5 and 2.5 hours - the current densities observed kept on going down steadily as the exposure time grew. It started with .94 ma/cm² at the end of a 20 minutes exposures and went down to 0.25 ma/cm² for a 2.5 hour exposure. During these exposures sample colors changed from yellow-pink to blue to gray green. Spectra obtained were stronger for the 1.5 and the 2.5 hour exposure than that obtained from the sample exposed for 20 minutes. There is no difference though in the spectra of the 1,5 and

the 2.5 hour exposures. There is an indication of red PbO in the 20 minutes exposure, Figure 63a, and the 1.5 hour exposure, Figure 63b, it is not seen in the spectrum obtained from the sample exposed for 2.5 hours, Figure 63c, but it should have been there and probably was not resolved.

Things changed somewhat in the 3.5 hour exposure. Trials to record the spectrum upon removal from solution did not produce a good spectrum, Figure 64a, which still can be identified as $PbSO_4$, but it has anabnormaly weak bands above 1000 cm^{-1}. This spectrum was recorded at 60 degrees. After letting the sample dry in air for 24 hours its spectrum was recorded again, Figure 64b, this time giving a much better spectrum but still not as good as those obtained from the short time exposures. Figure 64b was recorded using 65 degrees incident angle. Using even higher angle, 65-68 degrees, gave a better spectrum which is identical in appearance to those recorded in the shorter exposures, and it has a clear indication of red PbO, Figure 64c.

The next exposure was 7 hours long. No meaningful spectrum was obtained in the first four hours after removal of the sample from the solution, and it had a very weak and broad band around 800 cm^{-1}. After letting the sample dry in air for two days an excellent $PbSO_4$ spectrum was recorded, which also had a red PbO band.

The longer exposures, 16 and 20.5 hours, gave samples gray to dark gray in color, but the main difference was that their spectrum was completely different from those obtained

from the shorter exposures. Figure 65 shows the spectra obtained at two different settings of light polarizations.

Two logical explanations exist for the series of reactions observed at .80 V NHE. The first explanation is the possible trapping of water molecules in the film, and, while the film was not too thick, these molecules could still diffuse to the surface and evaporate. While in the film these water molecules could cause masking of the spectrum in the longer wavelength region, thus explaining the difficulty of obtaining a spectrum upon removal from solution. In the longer exposures, 16 and 20.5 hours, the film was probably too thick for the water molecules to diffuse to the surface or they already were bonded as a chemical complex. This explanation can be supported by the fact that these samples, 16 and 20.5 hours exposures, still gave the same spectra even after 20 days drying in air. Water has a medium and broad band centered at 750 cm^{-1}, and this is close enough to the 800 cm^{-1} band seen in Figure 65b, which cause the major difficulty in identifing the surface film. The presence of $PbSO_4$ in the spectra is clear and can also be supported by electron micrographs of those samples that showed the exact same crystals as the shorter exposed samples. Raman spectra of the longer exposed samples did not help to solve the problem since they only showed $PbSO_4$ and red PbO bands (67), but if water were present the Raman spectra could not help much since water is a poor Raman scatterer.

AD-A058 883 RHODE ISLAND UNIV KINGSTON DEPT OF OCEAN ENGINEERING F/G 11/6
CHARACTERIZATION OF CORROSION FILMS ON LEAD BY INFRARED REFLECT--ETC(U)
AUG 78 A GOLDFARB, C BROWN, R HEIDERSBACH N00014-76-C-0889

UNCLASSIFIED TR-5 NL

2 OF 2
ADA
058883

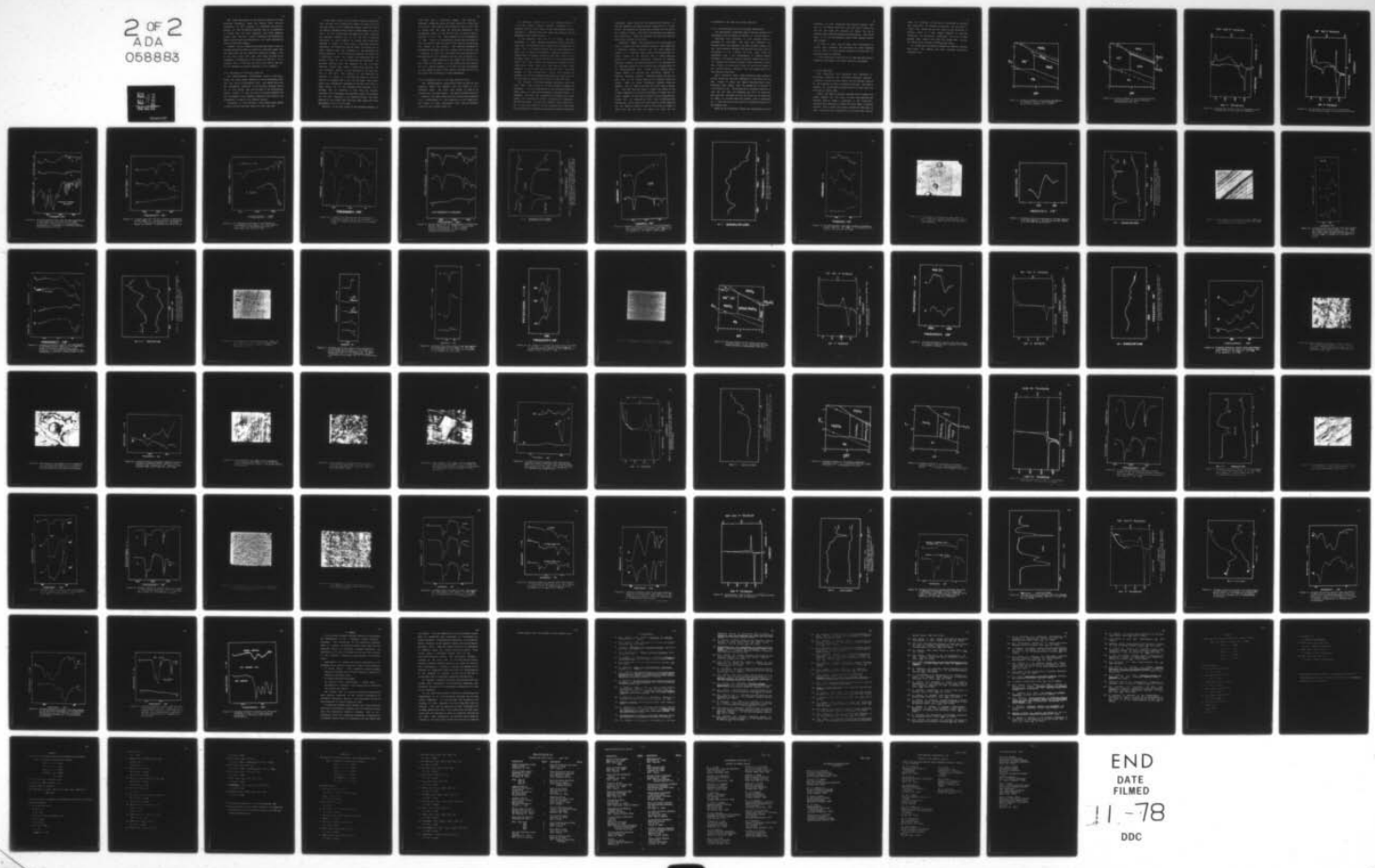

END
DATE
FILMED
11-78
DDC

The other explanation is the possible formation of lead bisulfate ($Pb(HSO_4)_2$) under the surface film. Not much information on this compound is available, but using an analogy to other bisulfate compounds (79) it is reasonable to assume that the lead bisulfate has a band, probably strong, near 800 cm^{-1}. Since no bisulfate was detected by Raman, which should have detected it, this whole explanation does not have much support.

Besides the two possibilities mentioned above, there is another explanation which is based on a published paper (80) that deals with the low temperature spectrum of $PbSO_4$. This is the only paper that says that $PbSO_4$ has one of its fundamental frequencies in the vicinity of 800 cm^{-1}. It is unlikely that if this was true that, this band at 800 cm^{-1} was not observed from other exposures in this research.

3.3.2. Exposures in 0.1M K_2SO_4 (pH=5.75)

The electrochemical polarization curve in 0.1M K_2SO_4, Figure 66, looks almost identical to the polarization curve that was run in 0.1M sulfuric acid. This agrees well with the information presented in the Pourbaix diagram, Figure 54, of the system. The two big waves in the polarization curves, Figures 55 and 66, are at the same potential and they correspond to the $Pb/PbSO_4$ transition line, which is pH independent, as seen in the Pourbaix diagram.

Exposures at -.62 V NHE gave a dark sample which showed a strong red PbO spectrum, Figure 67, with some LCH.

In the $PbSO_4$ region of the Pourbaix diagram, experiments were carried out to compare the effect of using 0.1M K_2SO_4 solution, which is not a buffering system, versus the use of the regular phosphate buffer with an added amount of sulfate ions. In the latter case the sample had a dark color and the spectrum obtained was of red PbO with a possible indication of small amounts of yellow PbO, Figure 68a. Exposing a sample in 0.1M K_2SO_4 at identical potential conditions and almost the same pH value, the current was 20 times smaller than that observed in the phosphate plus sulfate exposure. In the 0.1M K_2SO_4 exposure the sample had a white-gray color. All these are indications that the species formed in the two exposures were different. The spectrum obtained from the exposure in the 0.1M K_2SO_4 solution, Figure 68b, shows a clear $PbSO_4$ spectrum. The only different feature in this spectrum is the very sharp band at 450 cm^{-1}. The position of the band makes it possible to assign it to red PbO, but based on this band shape it is unlikely that it is a red PbO band. The sulfate group has a fundamental frequency at 450 cm^{-1} (79) which is Raman active but is not allowed in the infrared. It is possible that the sulfates in that film are somewhat distorted, thus overcoming the selection rules, and allowing the 450 cm^{-1} frequency to be infrared active. The Raman spectrum of this sample gave the usual $PbSO_4$ bands with some enhanchment of the 450 cm^{-1} band.

Exposure in the PbO_2 region of the Pourbaix diagram, at

1.08 V NHE, gave a gray-brown sample. The spectrum obtained, Figure 69, shows the $PbSO_4$ bands and a sharp band at 445 cm^{-1}. This band is not as sharp as the 450 cm^{-1} band in Figure 68b, but they due have some similarity. The interesting thing in the 445 cm^{-1} band is that it shows a shoulder at 470 cm^{-1}. This shoulder can be attributed to red PbO. There is a possibility though that the shoulder and the 445 cm^{-1} band are part of the spectrum of $PbO \cdot PbSO_4$ that formed on the surface. The infrared transmission spectrum of $PbO \cdot PbSO_4$ (41) has a strong band at 420 cm^{-1} and a shoulder at 454 cm^{-1}, and these can match the 445 cm^{-1} band and the 470 cm^{-1} shoulder that are seen in Figure 69.

Since a Raman spectrum of the sample (67) did not show any trace of lead oxide, it is more likely that the band at 445 cm^{-1} and the shculder at 470 cm^{-1} are due to breakdown in the selection rules in the sulfate spectrum, and it fits well since that vibration is doubly degenerate.

3.3.3. Exposures in KCH + 0.1M K_2SO_4 (pH=10.9-11.2)

The electrochemical polarization curve of lead in this solution, Figure 70, exhibits only two waves in its oxidation cycle. The lower wave though is seen to be resolved into two small waves. The upper potential wave has a somewhat odd shape indicating that either many processes occur simultanously or the transition is not a sharp one. The number of waves corresponds well with the Pourbaix diagram of the system, Figure 54.

An exposure carried out in the immunity region, at -.67 V NHE, showed reducing currents throughout the exposure, and the sample color stayed shiny metallic silver. Obtaining a spectrum from that sample was difficult and no meaningful bands could be seen.

A few exposures were run at .24 V NHE. The main difference in these exposure conditions was the length of time they were exposed, which ranged from 3 minutes to 3.5 hours. In the 3 minute exposure the film was probably too thin, and no bands were observed. Exposing a sample for a longer time, 25 minutes, produced a spectrum, Figure 71 that displays bands at the two extremes of light polarization. Figure 71a shows clearly the presence of sulfates, in the broad band around 1200 cm^{-1}, but there is also a clear presence of LCH as seen from the 1450 cm^{-1} band. The other extreme of light polarization, Figure 71b, supports the presence of the two compounds identified in Figure 71a, but it also adds the presence of red PbO, the 460 cm^{-1} band.

The presence of LCH was somewhat disturbing, and a few steps were taken tc get rid of the carbonates presence in solutions. This was complicated by the potassium hydroxide (KOH), which is a very good adsorbant of carbon dioxide. In preparing solutions for exposure the following steps were taken: the solution was boiled - equivalent to degassing - and KOH was added. At this point granular lead, about 50 gr for 3 liter, was added to the hot sclution so it could form LCH and deplete the sclution even more of carbon dioxide and

carbonates, while still hot the solution was filtered - to keep the granular lead away from the storage bottle. In the bottle the solution was purged with nitrogen and the bottle was tightly closed. Just before the exposure the solution was boiled again. After the exposure the sample was quickly dried with a stream of nitrogen.

Comparison samples were exposed for the same length of time, 2.5 hours, and gave different spectra. One sample had a specially prepared solution and the other sample was exposed in a solution where special precautions were not taken. Figure 72 was obtained from a sample that was exposed in a solution especially prepared to minimize carbonate content, an added precaution in this exposure was an overnight purging of the solution with nitrogen while in the electrochemical cell. Figure 73 was obtained from a sample exposed in solution not especially treated to minimize carbonate content. Comparing Figures 72a and 73a show that in the former case all the carbonate bands are weaker. There are other differences between these two spectra, one of them is the 465 cm^{-1} band, seen in Figure 73a. This band does not appear in Figure 72a, which is the matching spectrum, in polarizer settings, of Figure 73a, but rather appears at the other extreme of light polarization, Figure 72b. No explanation other than a different film orientation can be given for these results, since comparing all the bands of Figure 72 with all the bands in Figure 73 shows that all of them are there, but they are not

distributed in the same way in each spectrum.

3.3.4. Lead Exposures for Film Thickness Measurements

The experimental techniques used to measure passive film thicknesses were discussed in section 2.7. of this report.

Exposures were performed in 0.1M sulfuric acid at a potential of .80 V NHE. The lead film thickness was measured before the exposure, for most accurate results, and the after exposure thickness was figured from that value by multiplying it by a factor of 4.12. This factor was determined from a few measurements of exposed samples. Thickness corrections based on density change from lead to the appropriate oxidation product, using literature values, were found to be inaccurate, since the thin films formed in the electrochemical exposures did not always display the bulk material densities.

Short exposures under these conditions were presented before, Figure 60, and were identified to give $PbSO_4$ and red PbO. Figure 74 shows the spectra obtained from a vapor deposited lead sample that was exposed for 15 minutes in 0.1M sulfuric acid. The maximum film thickness obtained, in case all the lead had oxidized, was 2142 ± 61 angstroms. The spectrum obtained is clear and sharp and is identified as $PbSO_4$; no red PbO bands are present, this is reasonable in a thin film that is not much of a diffusion barrier for the sulfate ions.

Based on the literature (19,28) the reflectance and film

thickness, of that magnitude, are linearly related. From this it is clearly seen that a film ten times thinner than the one that gave the spectrum in Figure 74a, can be detected using infrared reflection spectroscopy. This lower limit is in the 200 angstroms range. These results require some remarks:

1) This is true only for $PbSO_4$ which constitutes the surface film examined. The estimation for other compounds can be made if their optical constants are known for the infrared region of interest.

2) The sensitivity obtained can be improved using better reflection attachments and signal averaging techniques.

3.4. Iron Exposures

High temperature iron exposures were conducted as preliminary efforts, for providing reference infrared reflection spectra of iron oxides, and for further research on the passivity of iron in aqueous solutions. The present research is not entirely original and is in part after the work done by Poling (19).

Figure 75a shows a spectrum obtained from an Armco iron sample exposed for 405 hours in 230°, this spectrum was obtained without using a polarizer in the light path. Comparing this spectrum to Figure 75b which shows a spectrum obtained from an Armco iron sample exposed for 288 hours in 230°, this time with a polarizer in the light path, clearly

shows the advantage of the use of a polarizer to increase the sensitivity of recording a spectrum. All the bands in Figure 75b, except the 655 cm^{-1} band, can be attributed to α-Fe_2O_3, which is a very strong absorber of infrared radiation, its extinction coefficient is 4.5 to 22 times greater than those of the other iron oxides (19). The 655 cm^{-1} band can be assigned to γ-Fe_2O_3 and Fe_3O_4.

No difference was observed between the spectra obtained from Armco iron samples and those obtained from vapor deposited iron.

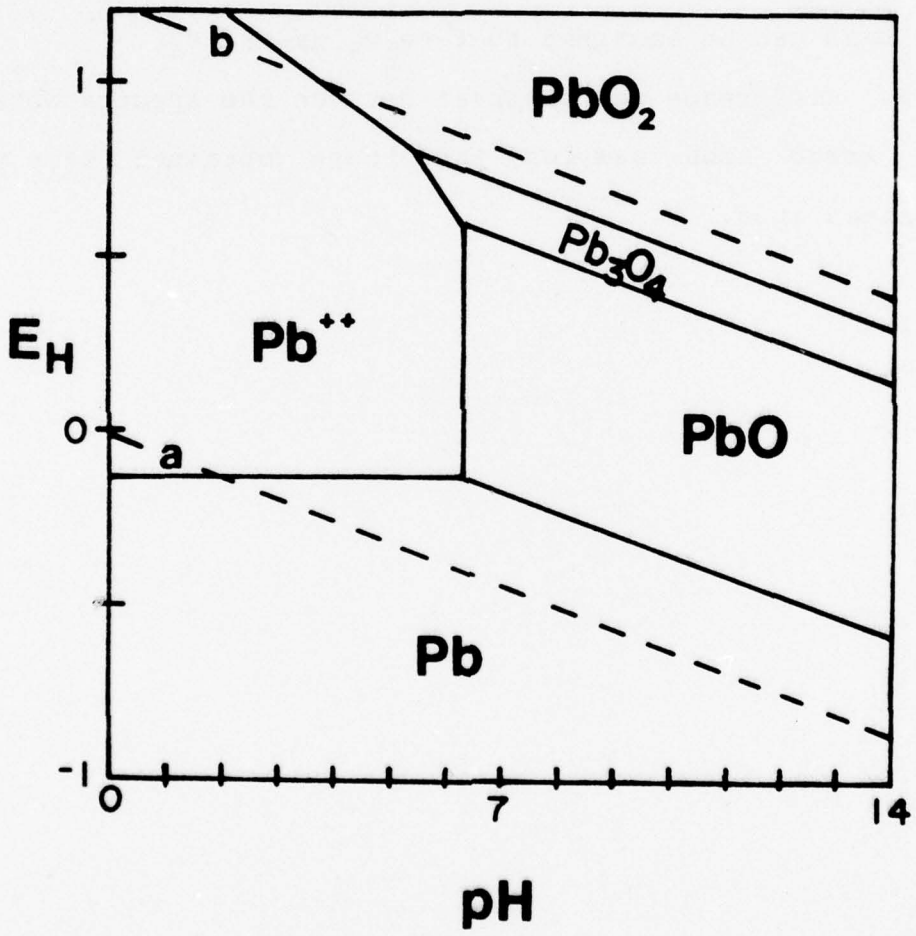

Figure 13. Pourbaix diagram of the system Lead-Water, M. Pourbaix, Atlas of Electrochemical Equilibria, Pergamon, N.Y. (1966).

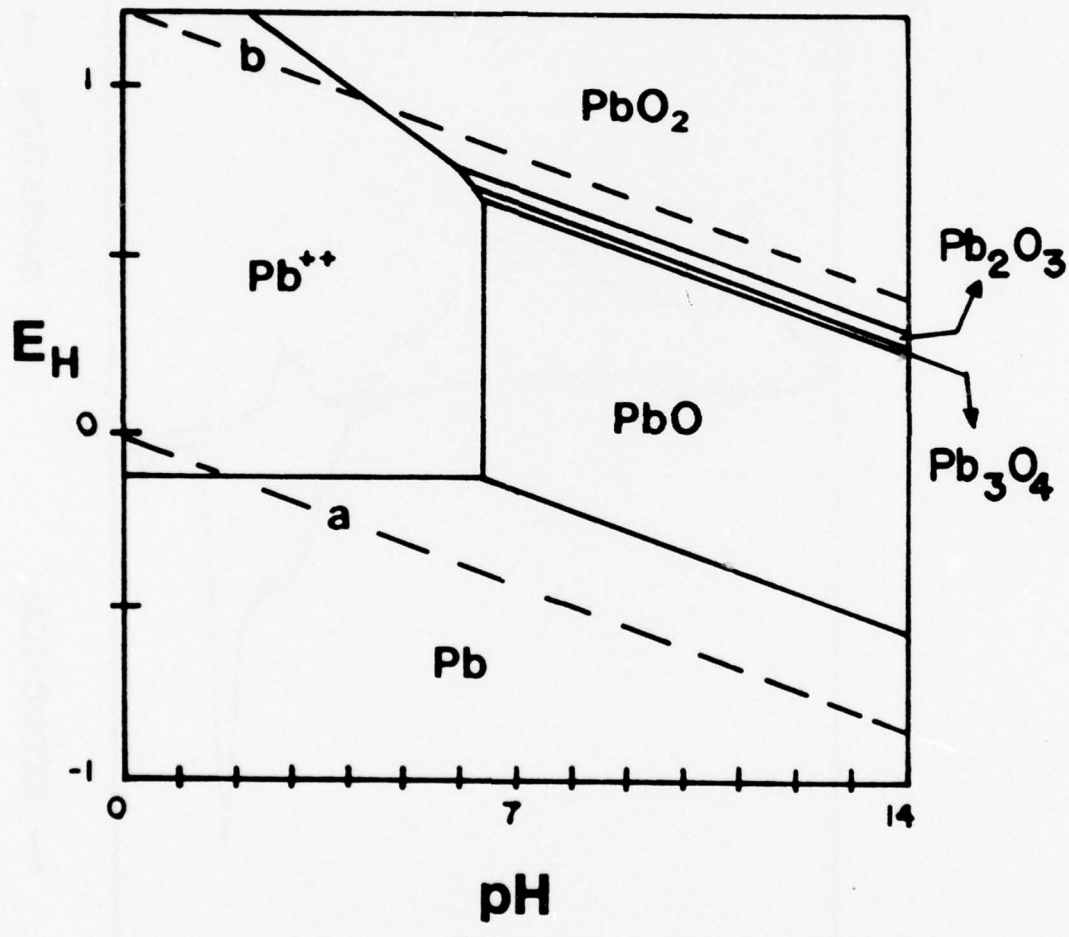

Figure 14. Pourbaix diagram of the system Lead-Water, calculated with the latest available thermodynamic data (65).

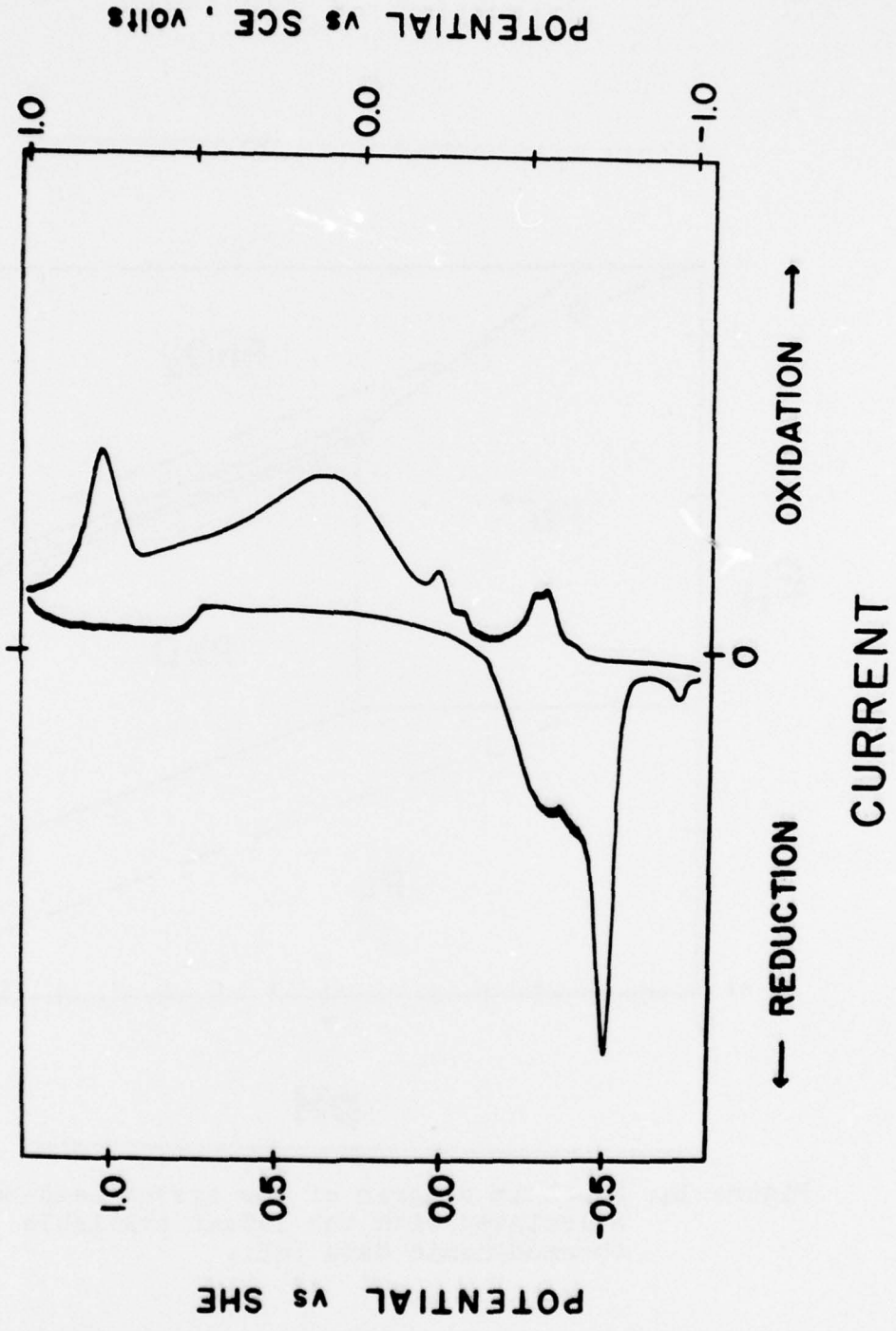

Figure 15. Polarization curve of lead in phosphate buffer solution, pH= 7. Scan rate 40 mv/minute.

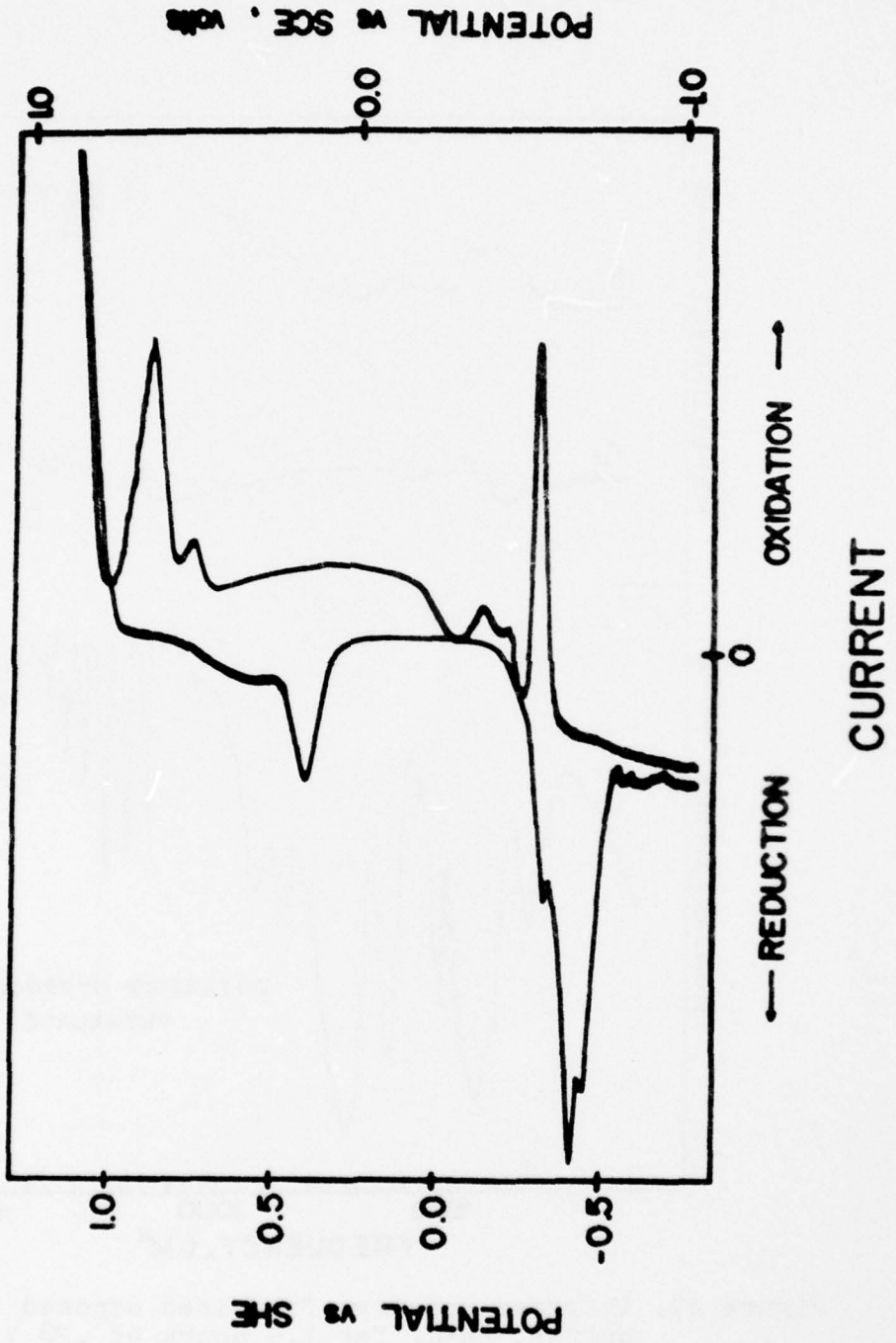

Figure 16. Polarization curve of lead in bicarbonate buffer solution, pH=10. Scan rate 40 mv/minute.

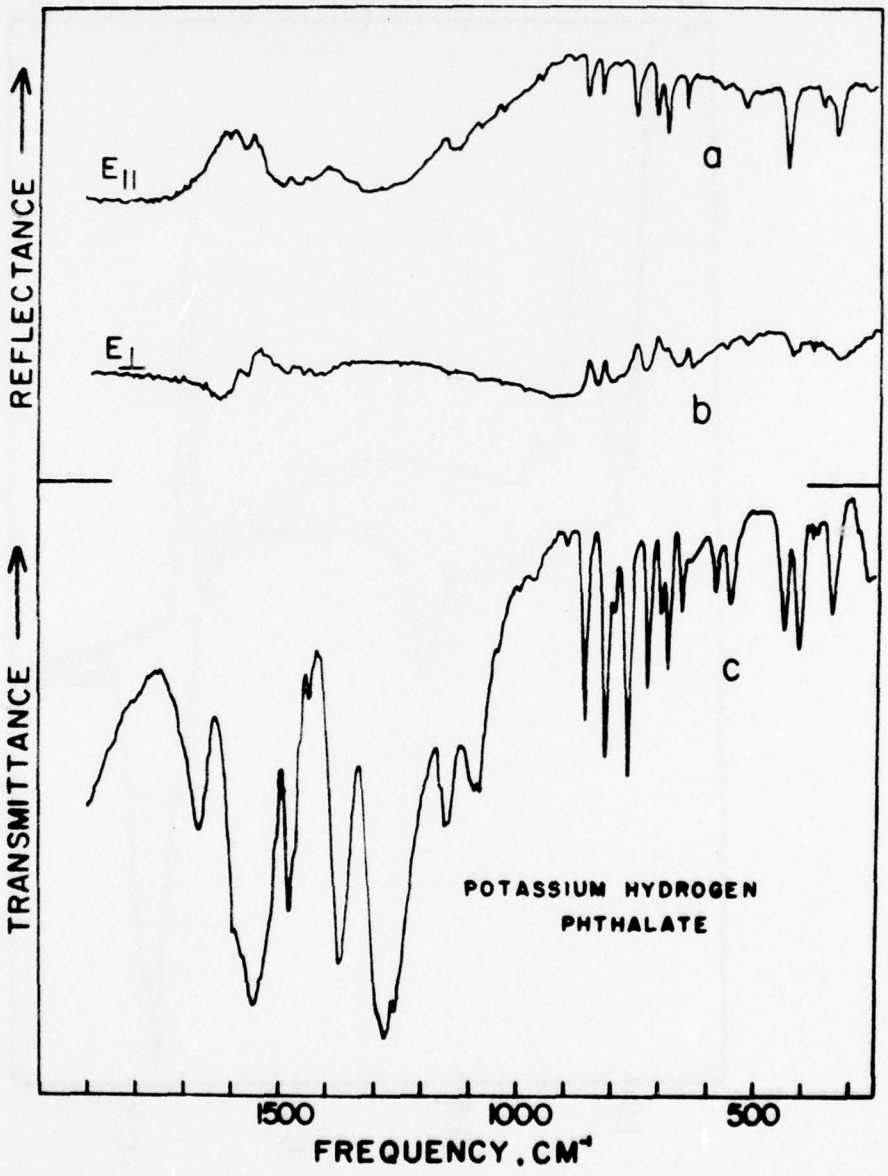

Figure 17. Infrared spectrum from lead exposed in phthalate buffer, pH=4, for 1.5 hours at .28 V NHE. a) Parallel polarization. b) Perpendicular polarization. c) Spectrum of potassium hydrogen phthalate powder, in KBr.

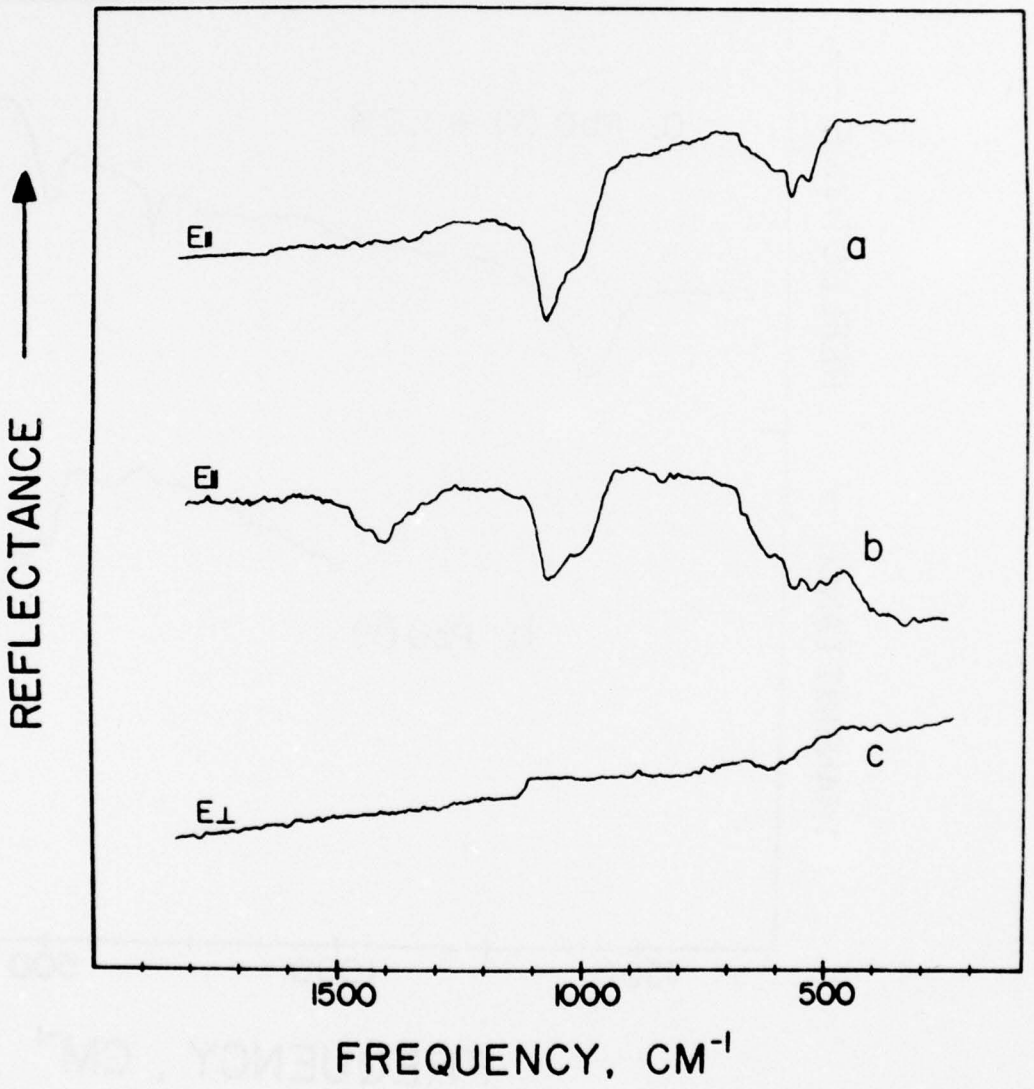

Figure 18. Infrared spectrum from lead exposed in phosphate buffer, pH=7, for 2 hours, parallel polarization a) -.76 V NHE, was not washed. b) -.64 V NHE, sample was washed. c) Perpendicular polarization

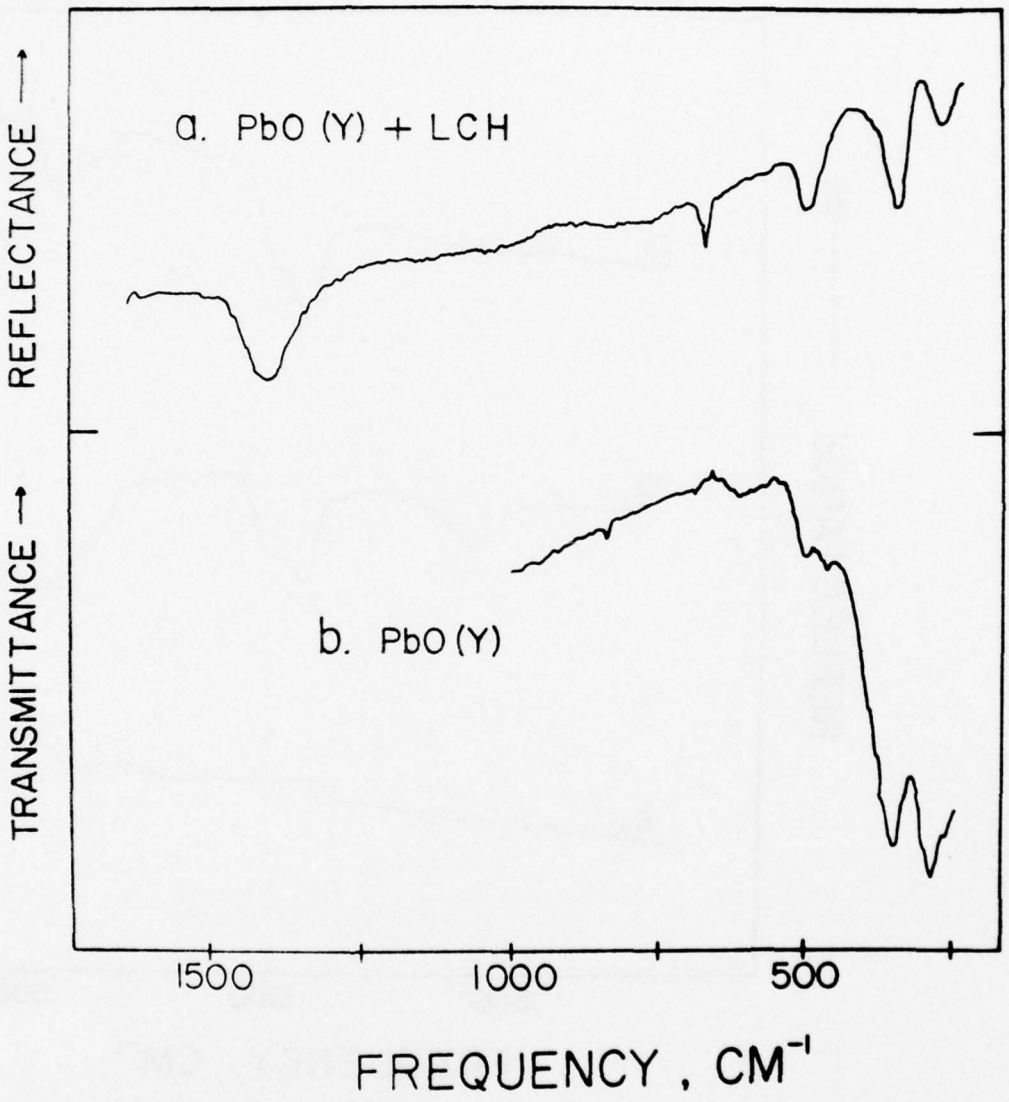

Figure 19. a) Reflection spectrum of lead exposed in bicarbonate buffer, pH=10, for 2.75 hours at -.56 V NHE. b) Transmission spectrum of orthorombic PbO powder, in KBr.

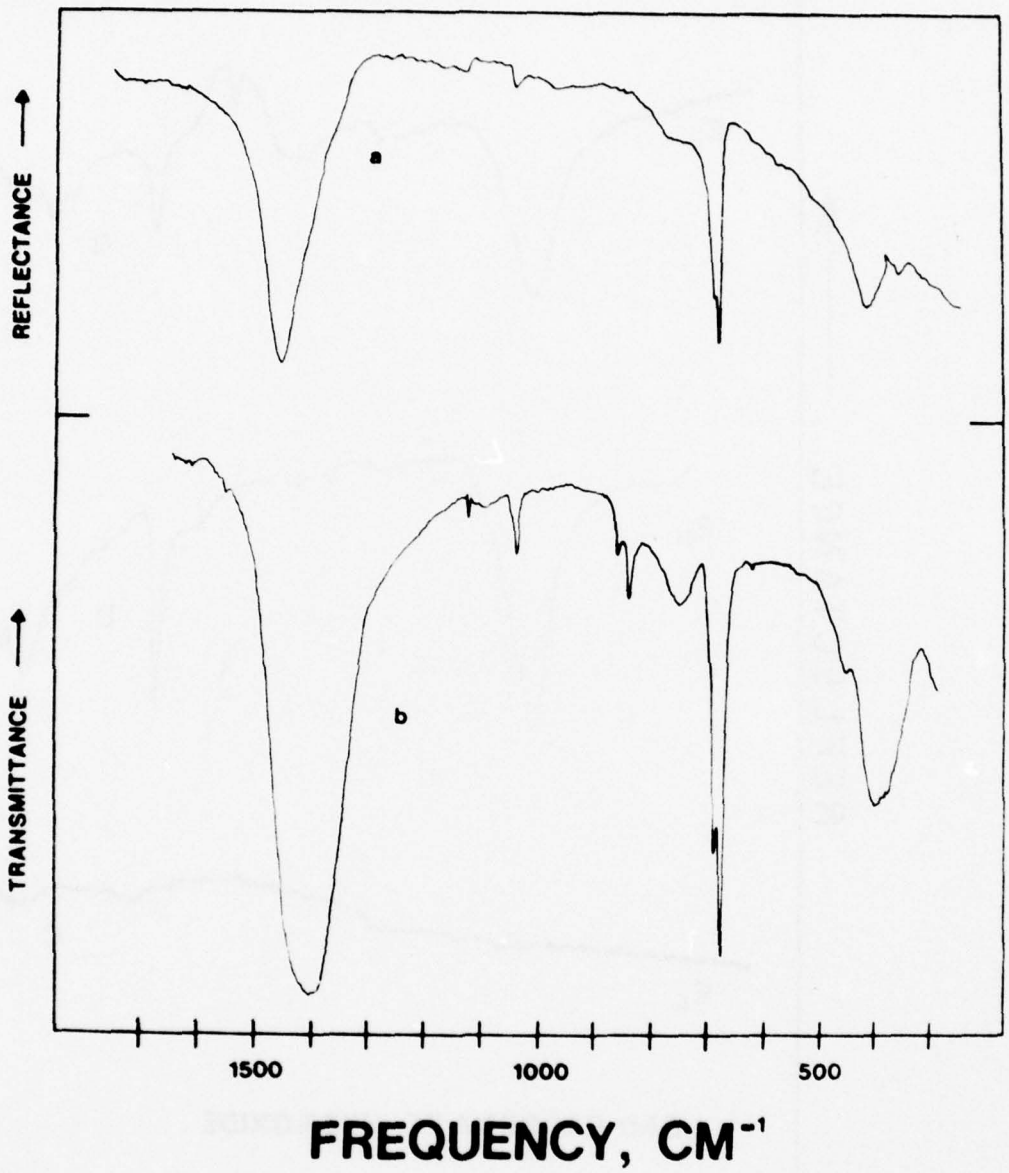

Figure 20. a) Reflection spectrum from lead exposed in bicarbonate buffer, pH=10, for 24 hours at -.42 V NHE. b) Transmission spectrum of LCH powder, in KBr.

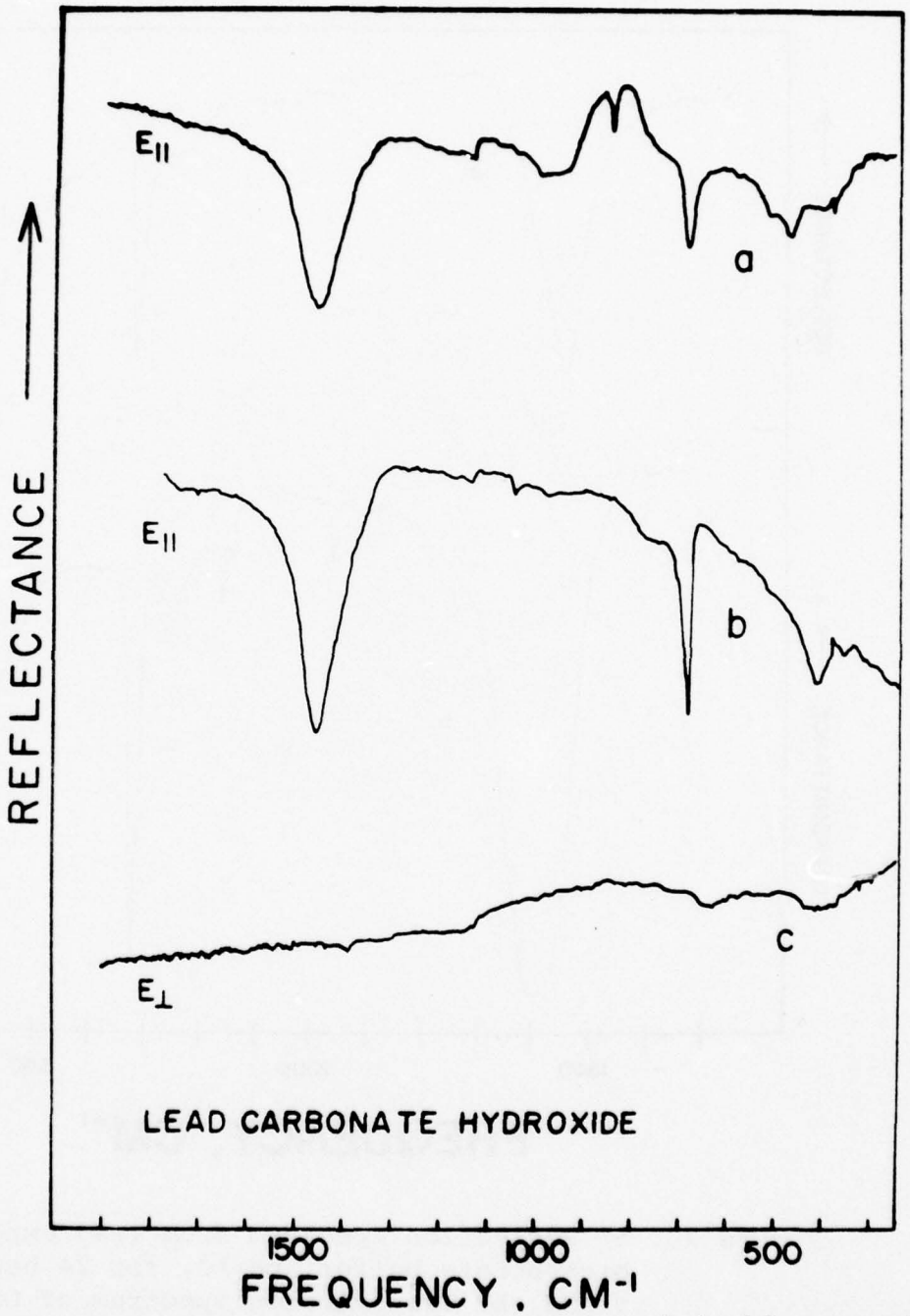

Figure 21. Reflection spectra of lead exposed in bicarbonate buffer, pH=10, at -.42 V NHE. a) For 4 hours, parallel polarization. b) For 24 hours, parallel polarization. c) For 4 hours, perpendicular polarization.

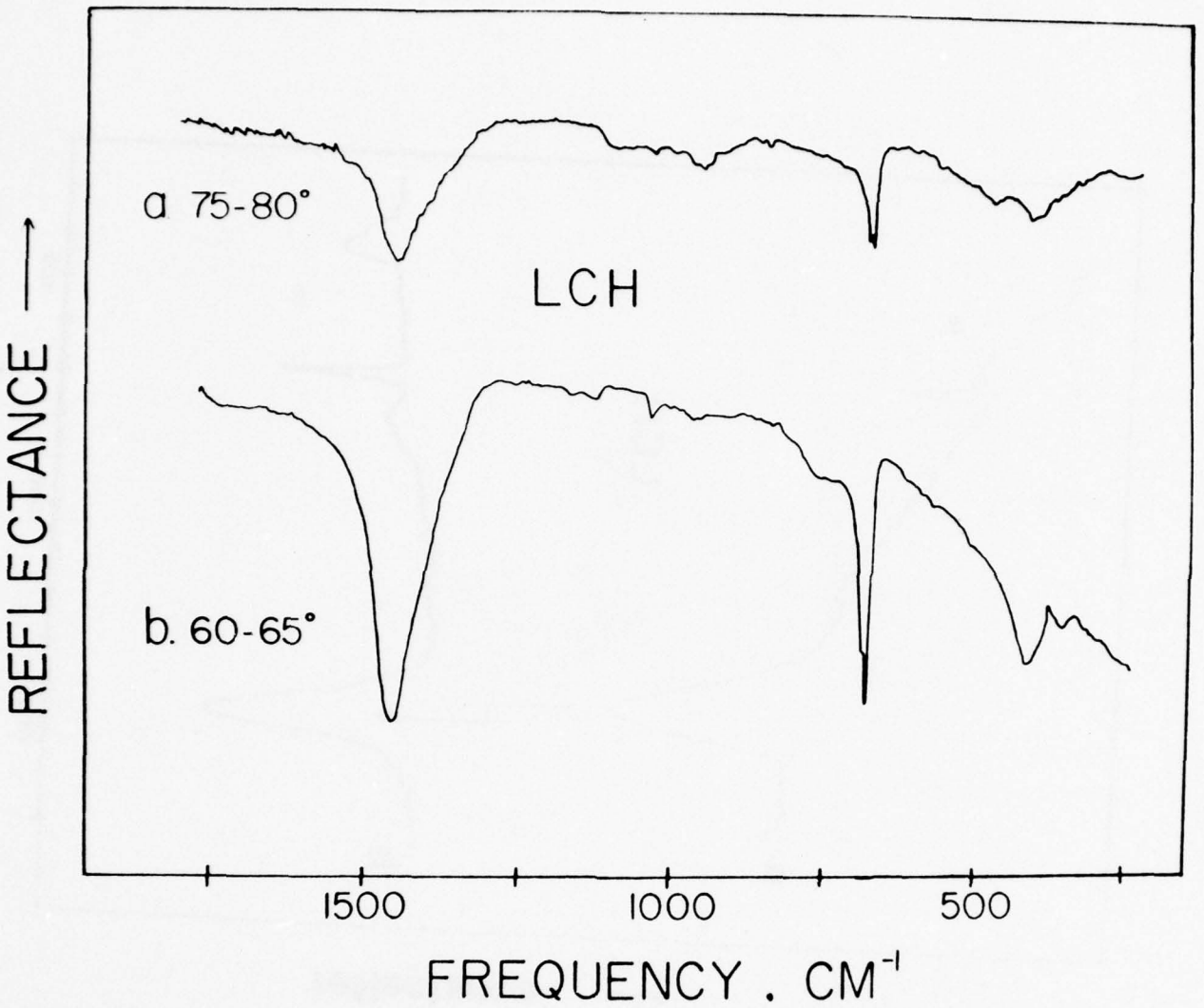

Figure 22. The dependence of the sensitivity of reflection spectra on the angle of incidence, obtained from lead exposed in bicarbonate buffer, pH=10, for 24 hours at -.42 V NHE. a) 75-80° b) 60-65°

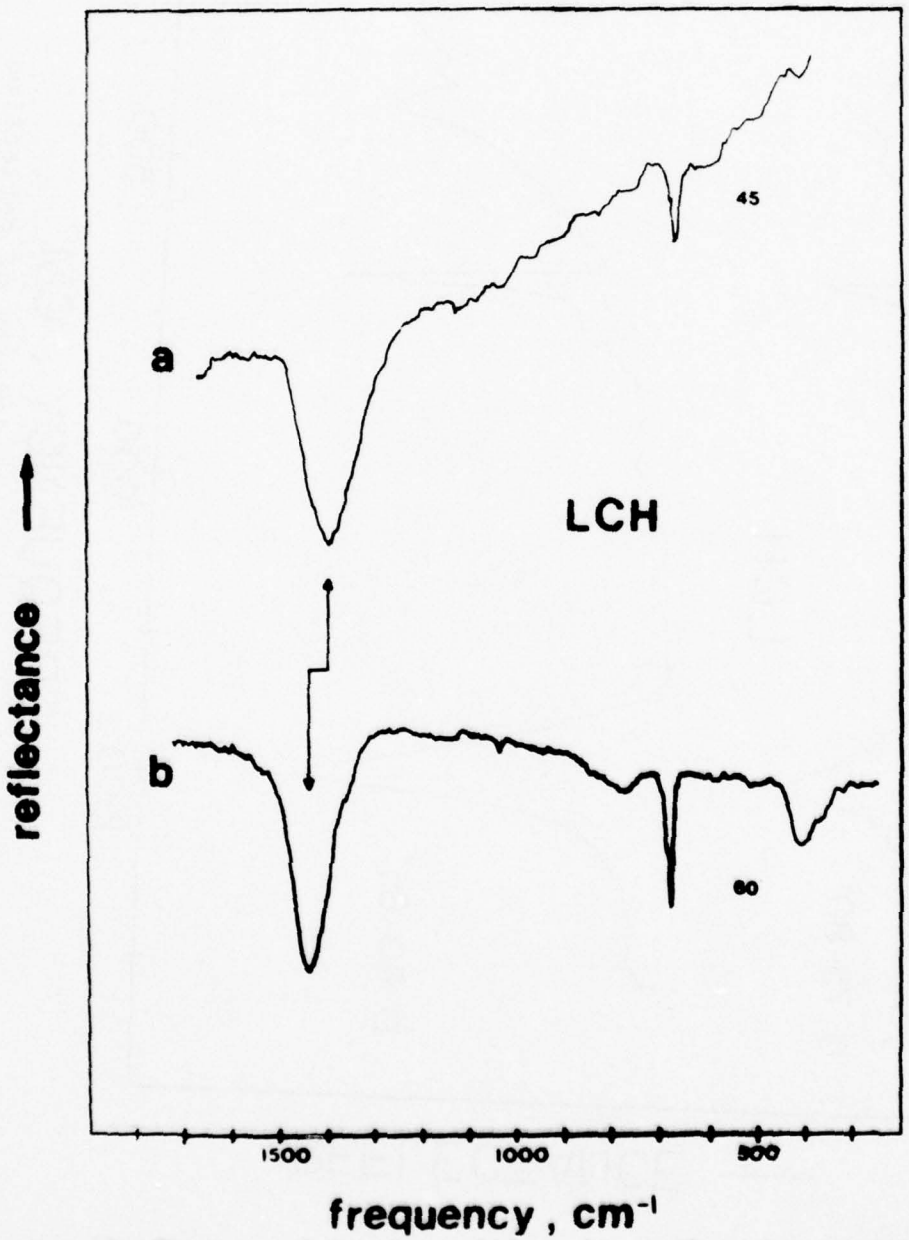

Figure 23. Change of band position in reflection spectra due to the angle of incidence, obtained from lead exposed in bicarbonate buffer, pH=10, for 2.25 hours at -.37 V NHE. a) 45° b) 60°

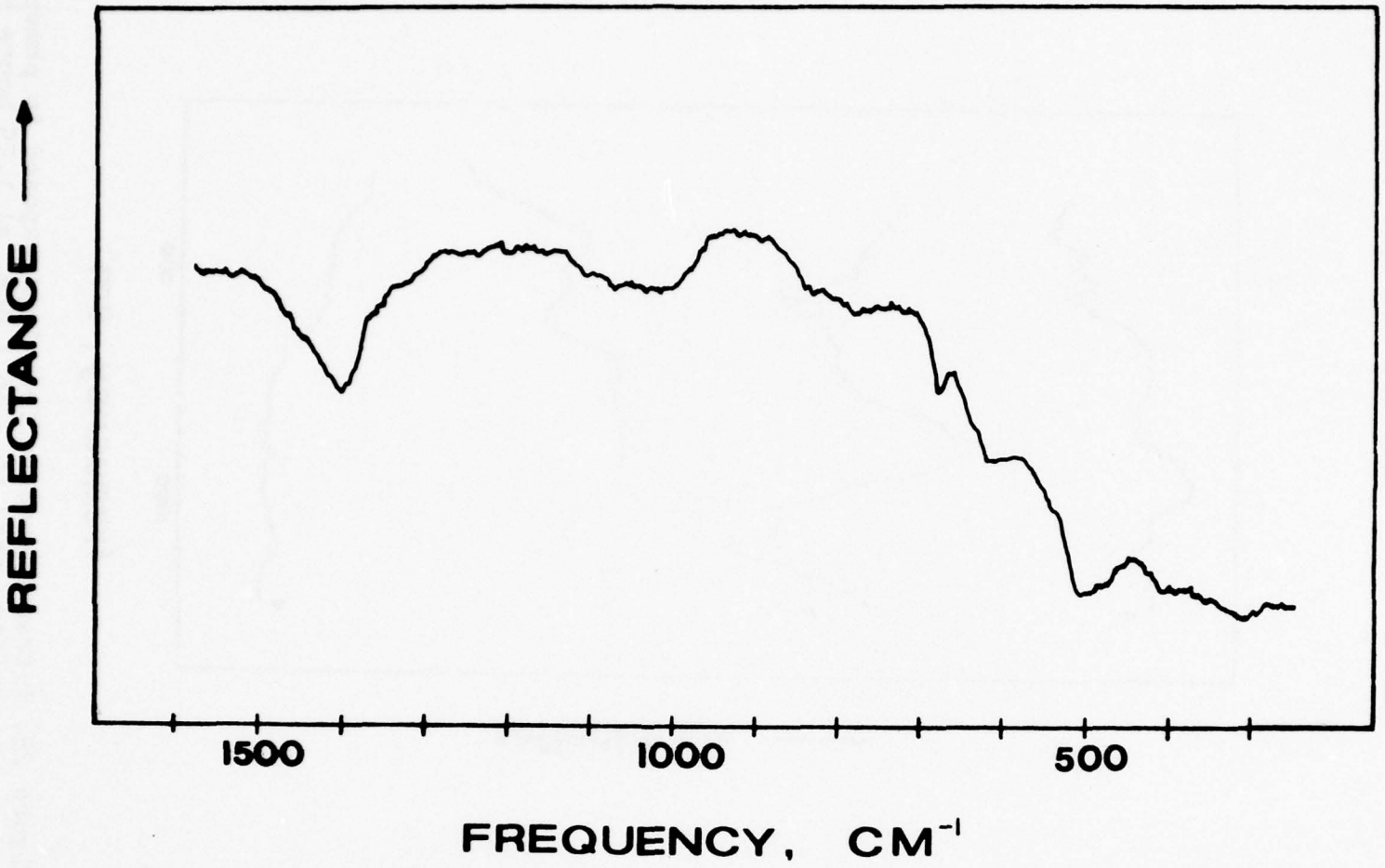

Figure 24. Infrared reflection spectrum obtained from lead exposed in KOH solution, pH=9.7, for 17 hours at -.42 V NHE.

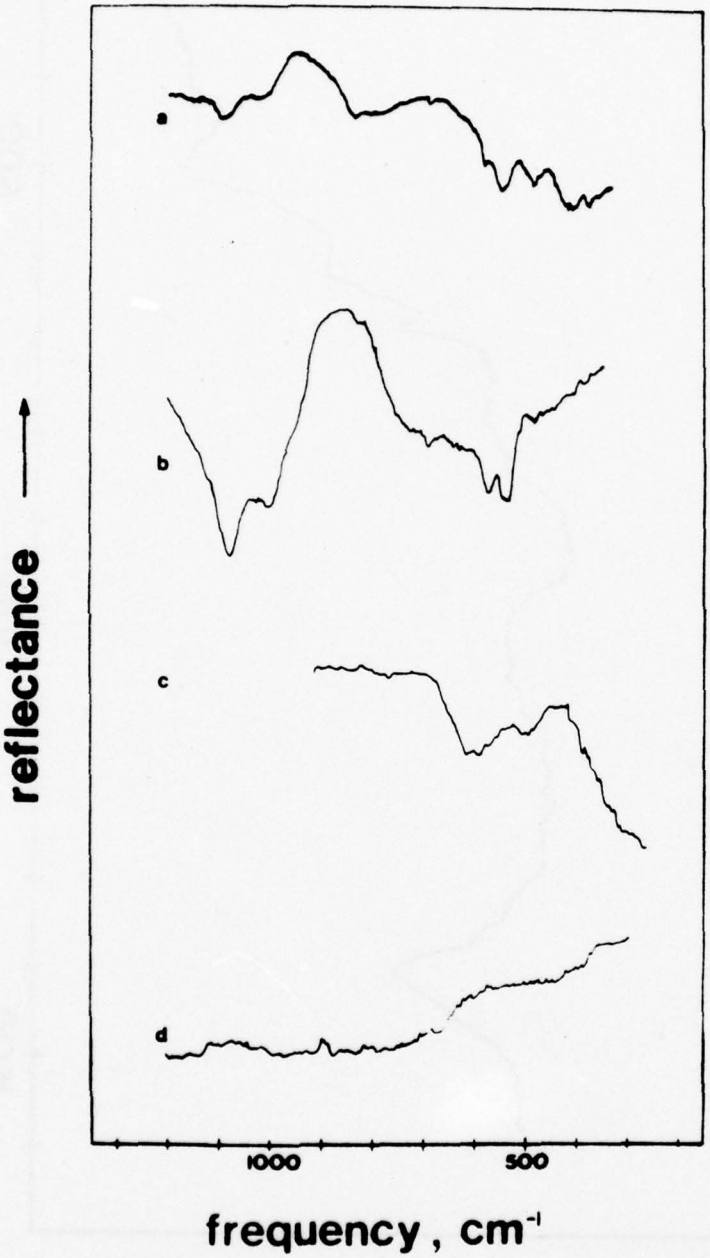

Figure 25. Infrared spectra from lead exposed in phosphate buffer, pH=7 at -.16 V NHE. a) 1.25 hours b) 4.5 hours c) 16 hours d) 16 hours.

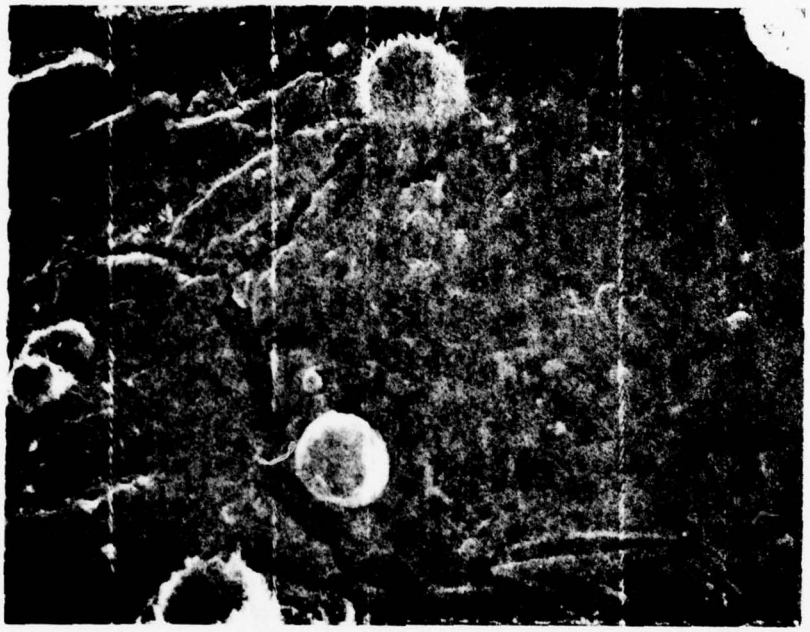

Figure 26. Lead exposed in phosphate buffer, pH=7, at -.11 V NHE for 19 hours. Magnification: 2000X, black particle - SiC, light colored "balls" - lead phosphate.

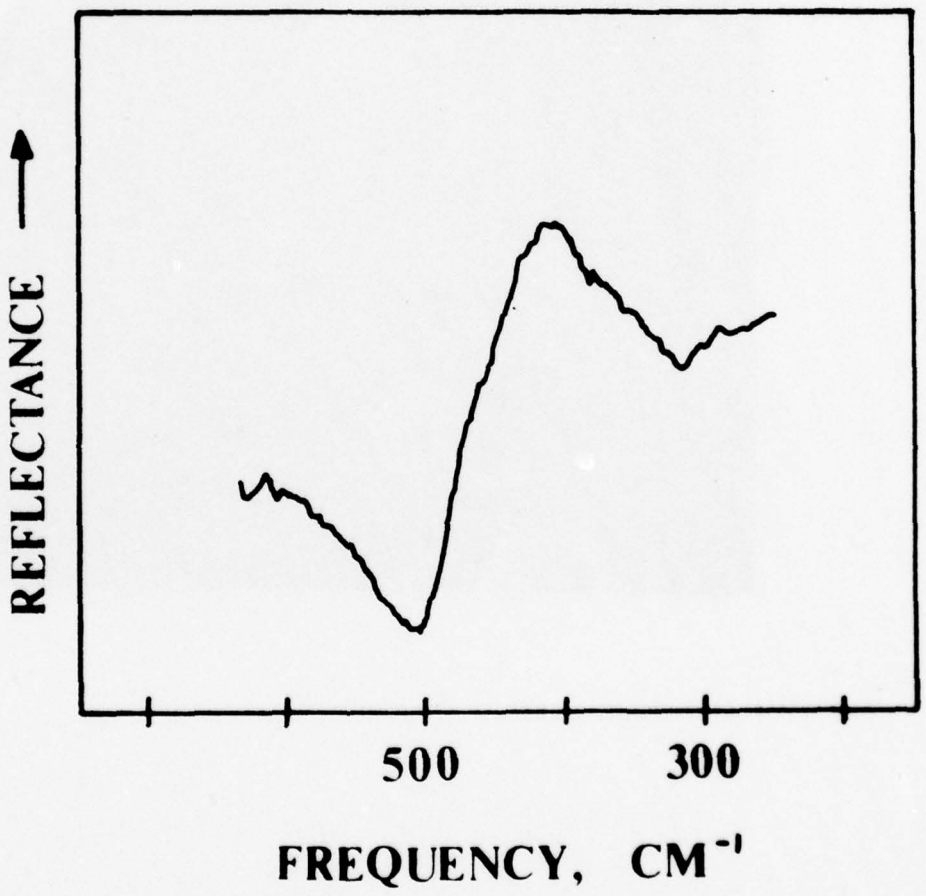

Figure 27. Infrared reflection spectrum of red PbO obtained from lead exposed in bicarbonate buffer, pH=10, at 1.08 V NHE for 14.5 hours.

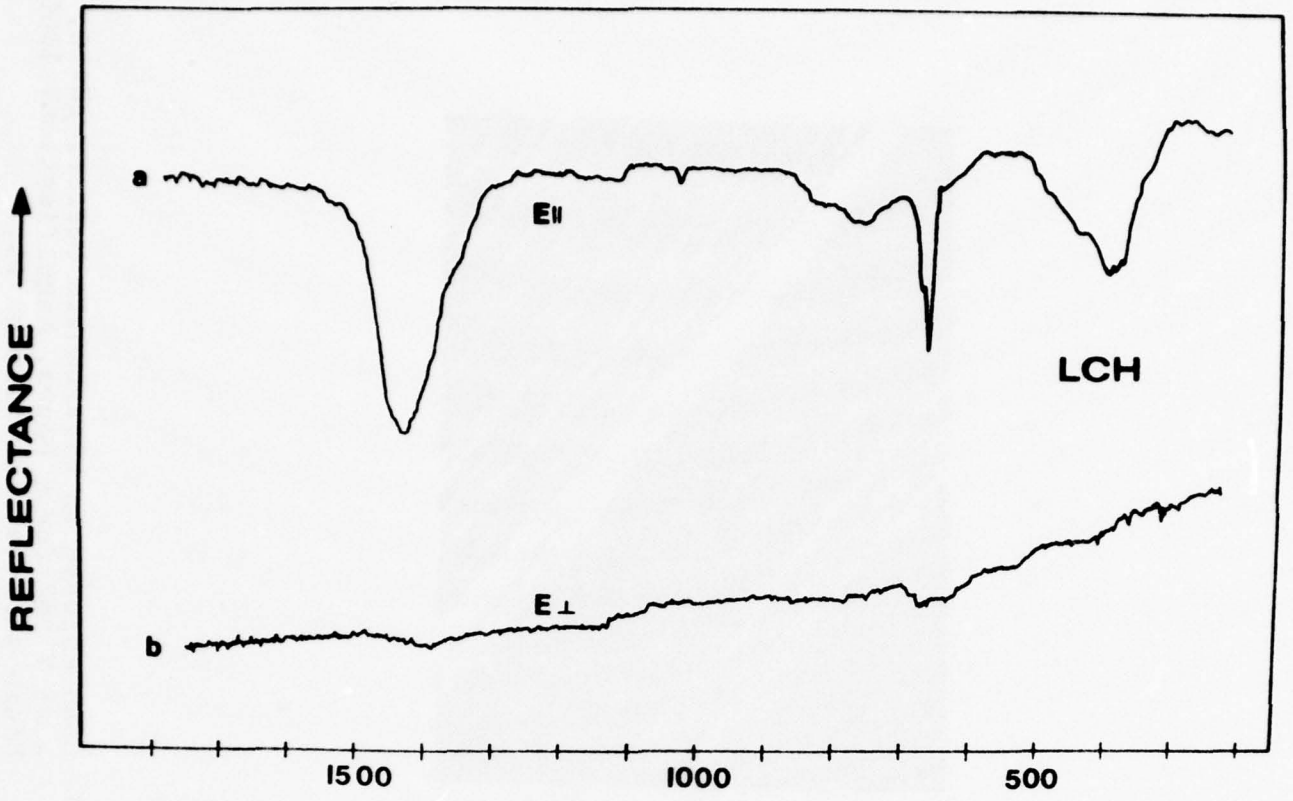

Figure 28. Infrared reflection spectra from lead exposed in bicarbonate buffer, pH=10, at -.28 V NHE, for 4 hours. a) Parallel polarization. b) Perpendicular polarization.

Figure 29. Lead exposed in bicarbonate buffer, pH=10, at -.28 V NHE for 4 hours. Magnification: 1000X. Rough surface with film on it.

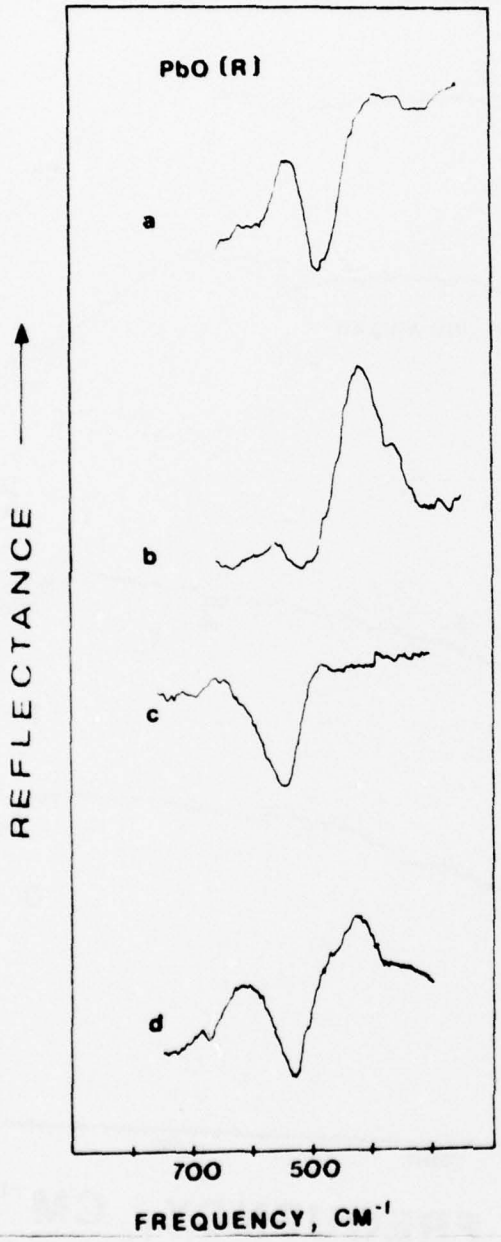

Figure 30. Infrared reflection spectra from lead exposed in bicarbonate buffer, pH=10. a) .24 V NHE, 18.5 hours, parallel polarization. b) .24 V NHE, 18.5 hours, perpendicular polarization. c) .04 V NHE, 1.5 hours. d) .24 V NHE, 5.5 hours.

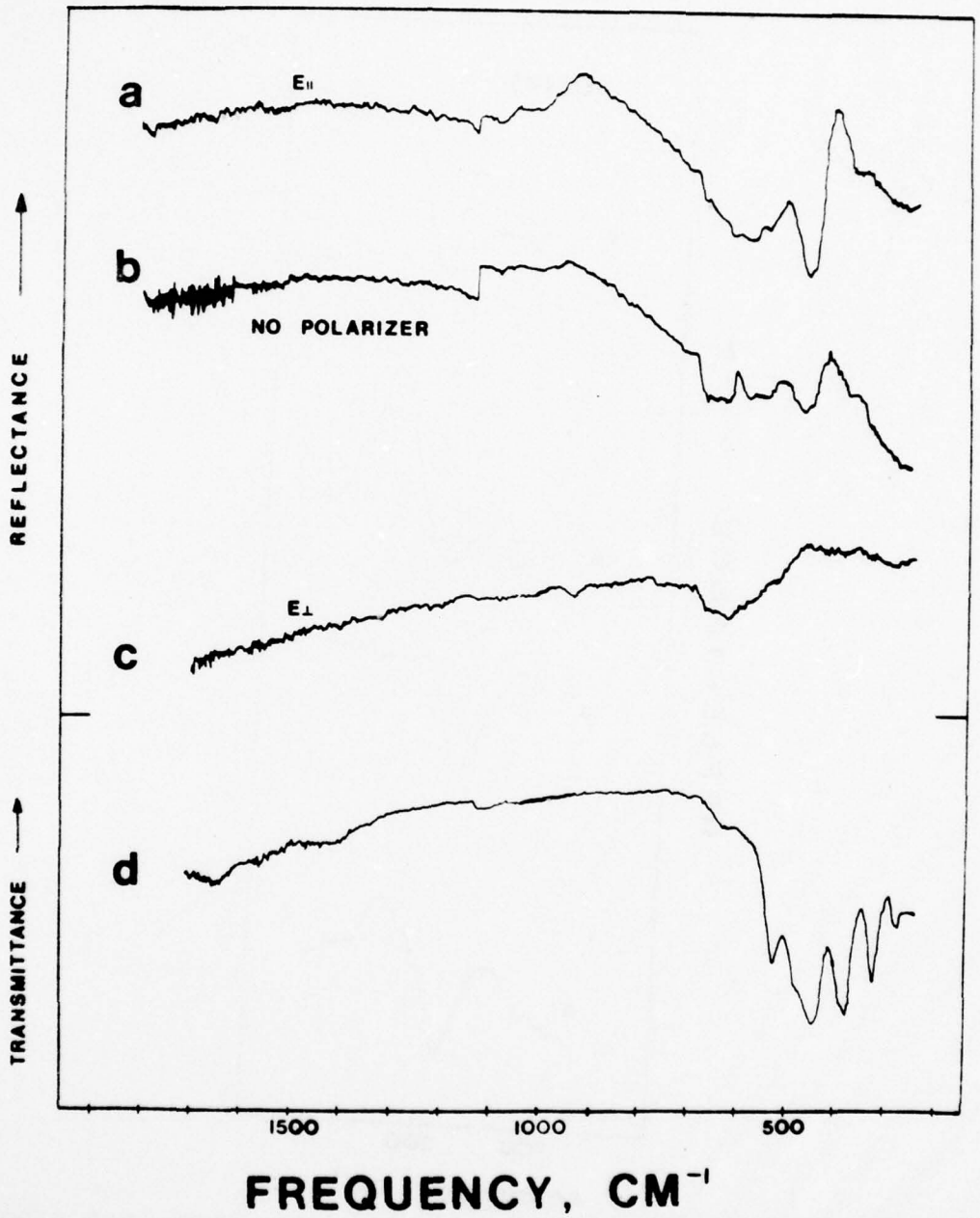

Figure 31. Infrared reflection spectra from lead exposed in phosphate buffer, pH=7, at .67 V NHE for 2 hours. a) Parallel polarization. b) No polarizer. c) Perpendicular polarization. d) Transmission spectrum of Pb_3O_4 powder, in KBr.

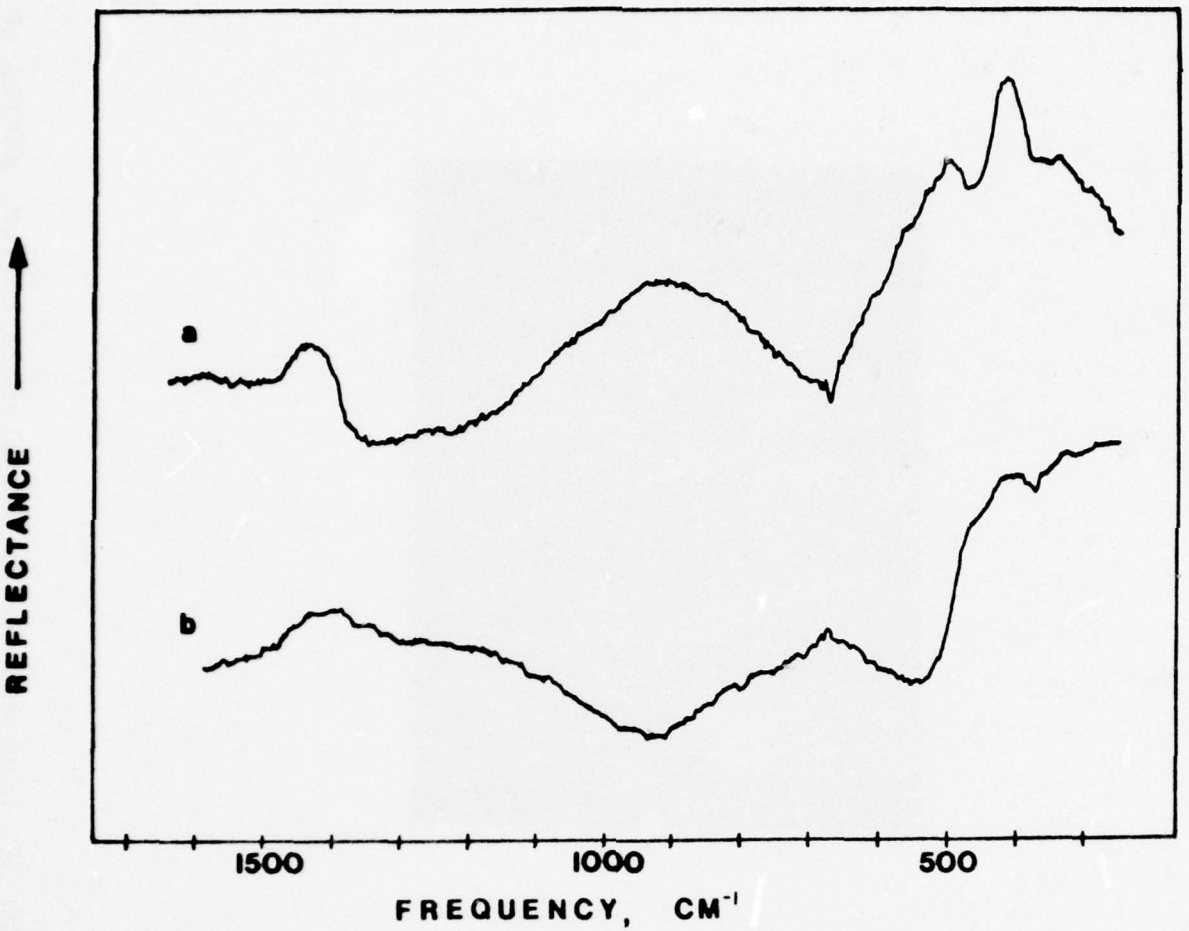

Figure 32. Infrared reflection spectra from lead exposed in bicarbonate buffer, pH=10, at .51 V NHE for 6 hours. a) Parallel polarization. b) Perpendicular polarization.

Figure 33. Lead exposed in bicarbonate buffer, pH=10, at .51 V NHE for 6 hours. Magnification: 1000X. Film coated surface, cracks from sample preparation for SEM.

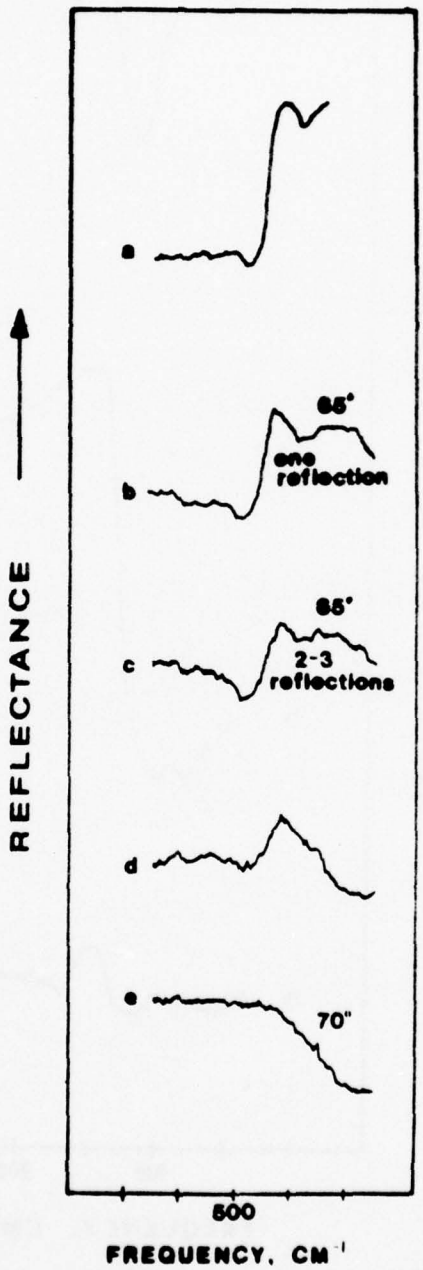

Figure 34. Infrared reflection spectra from lead exposed in phosphate buffer, pH=7, at .99 V NHE for 2 hours. a) Multiple reflections, 60°. b) Single reflection, 65°. c) 2-3 reflections, 60-65°. d) Multiple reflections, 65°. e) 1-2 reflections, 70°.

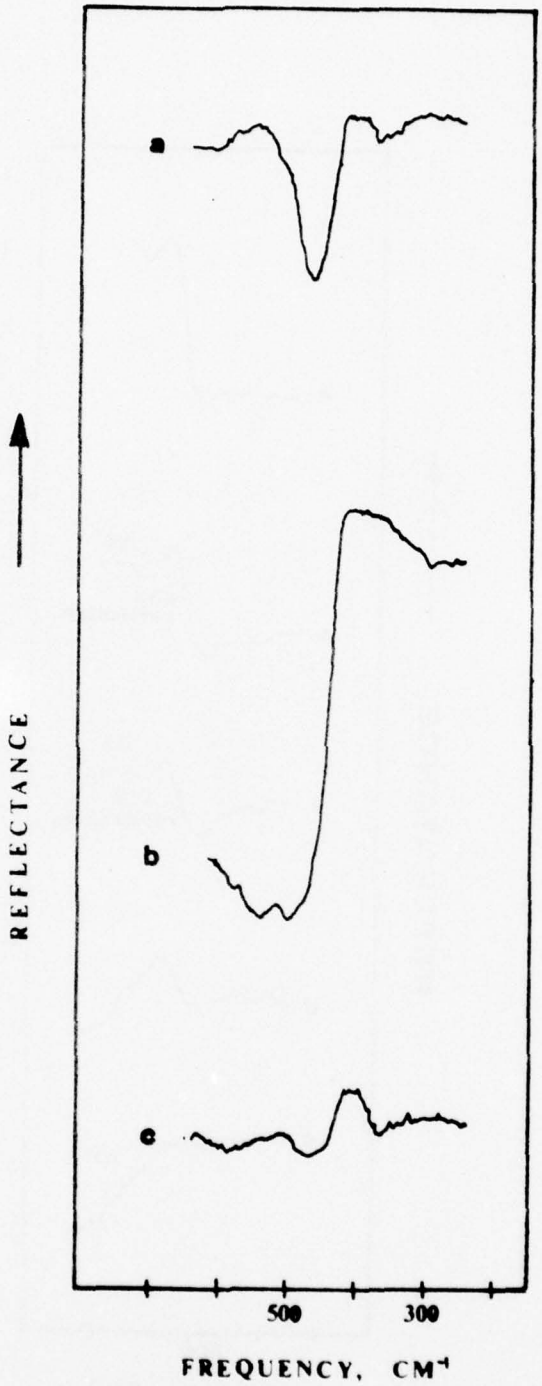

Figure 35. Infrared reflection spectra from lead exposed in bicarbonate buffer, pH=10. a) .75 V NHE, for 2.25 hours. b) .75 V NHE, for 5.5 hours. c) .83 V NHE, for 3.25 hours.

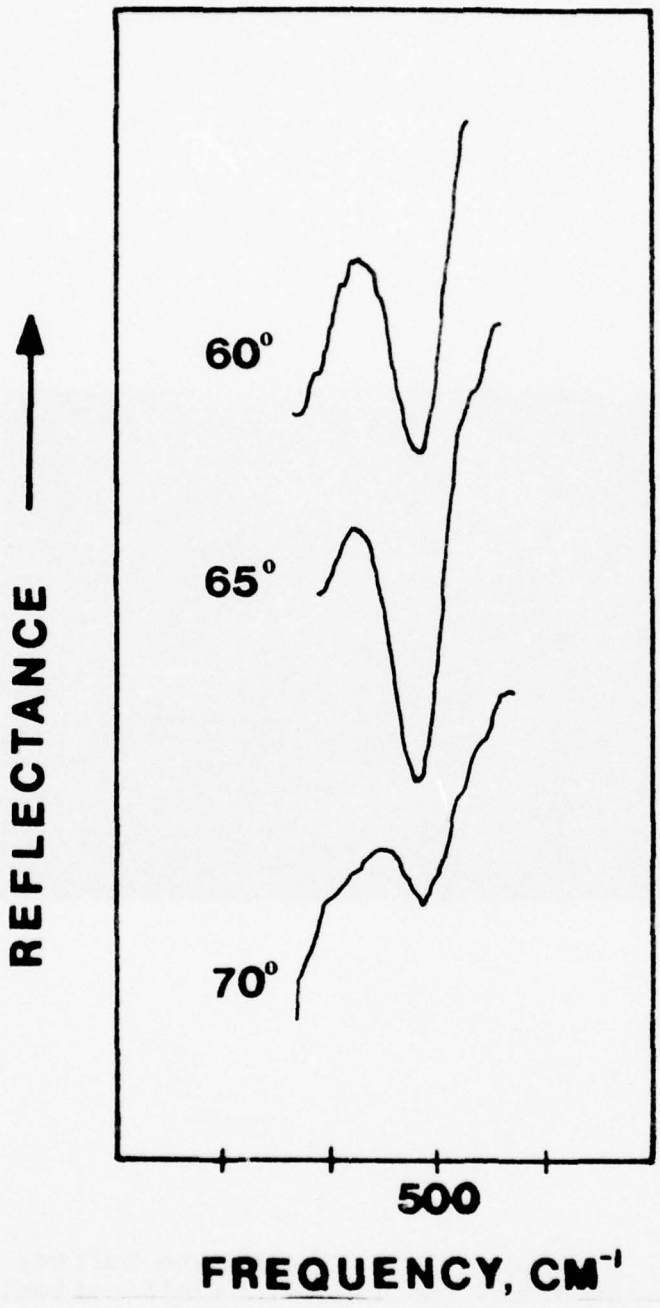

Figure 36. The change of a reflection band due to the angle of incidence, obtained from lead exposed in bicarbonate buffer, pH=10, at .99 V NHE for 17 hours. a) 60° b) 65° c) 70°.

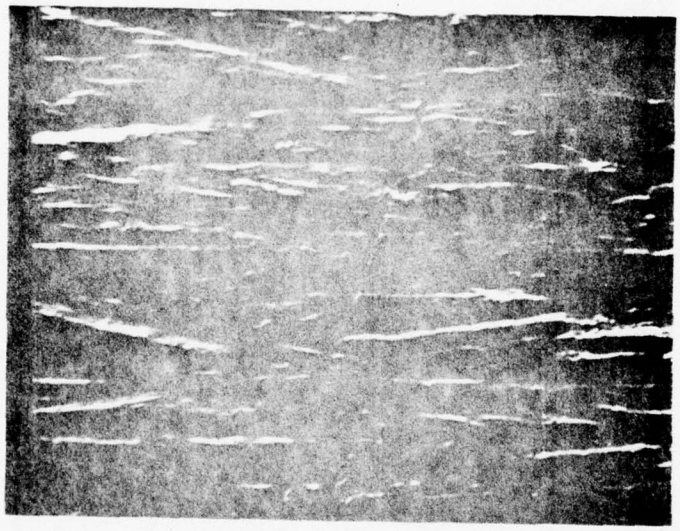

Figure 37. Lead exposed in bicarbonate buffer, pH=10, at .84 V NHE for 1 hour. Magnification: 1000X.

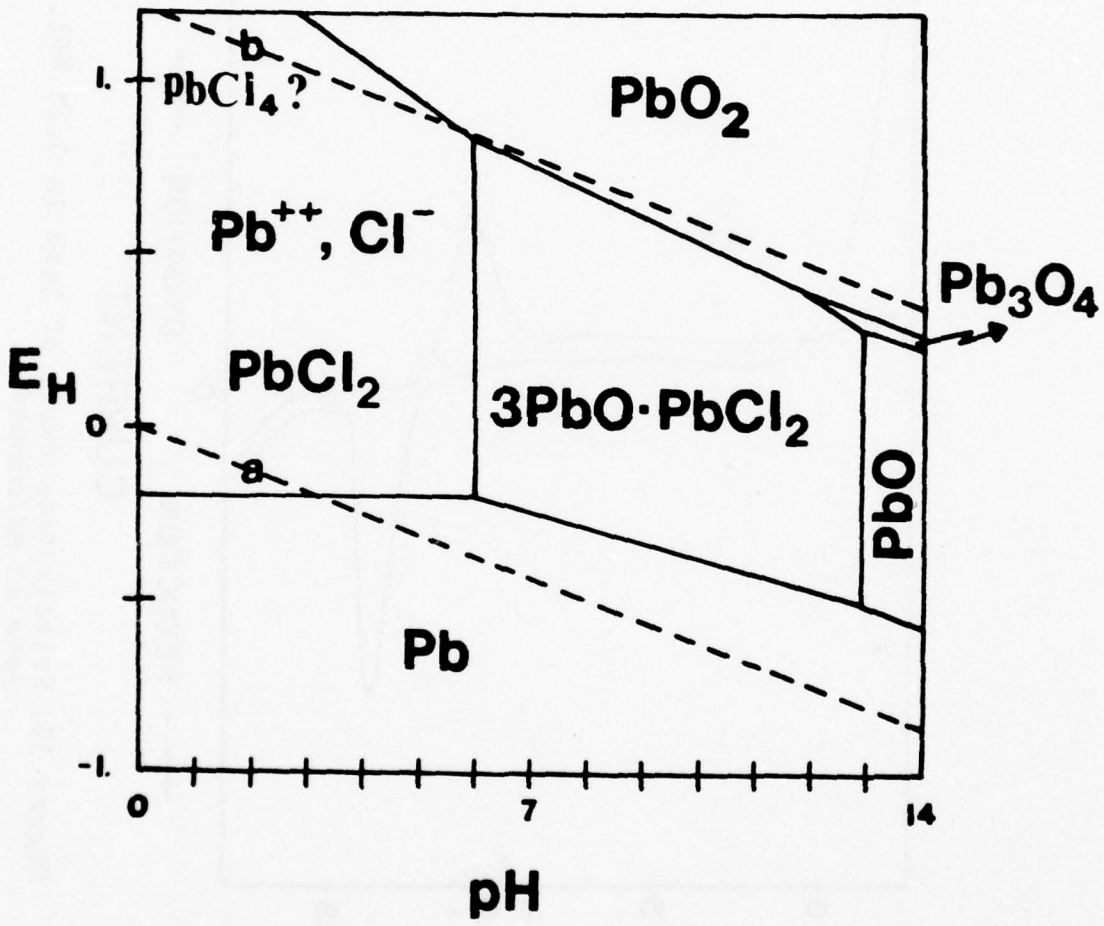

Figure 38. Pourbaix diagram of the system Lead-Water-Chlorides (a_{Cl^-} = 0.1), calculated with the latest available thermodynamic data (65).

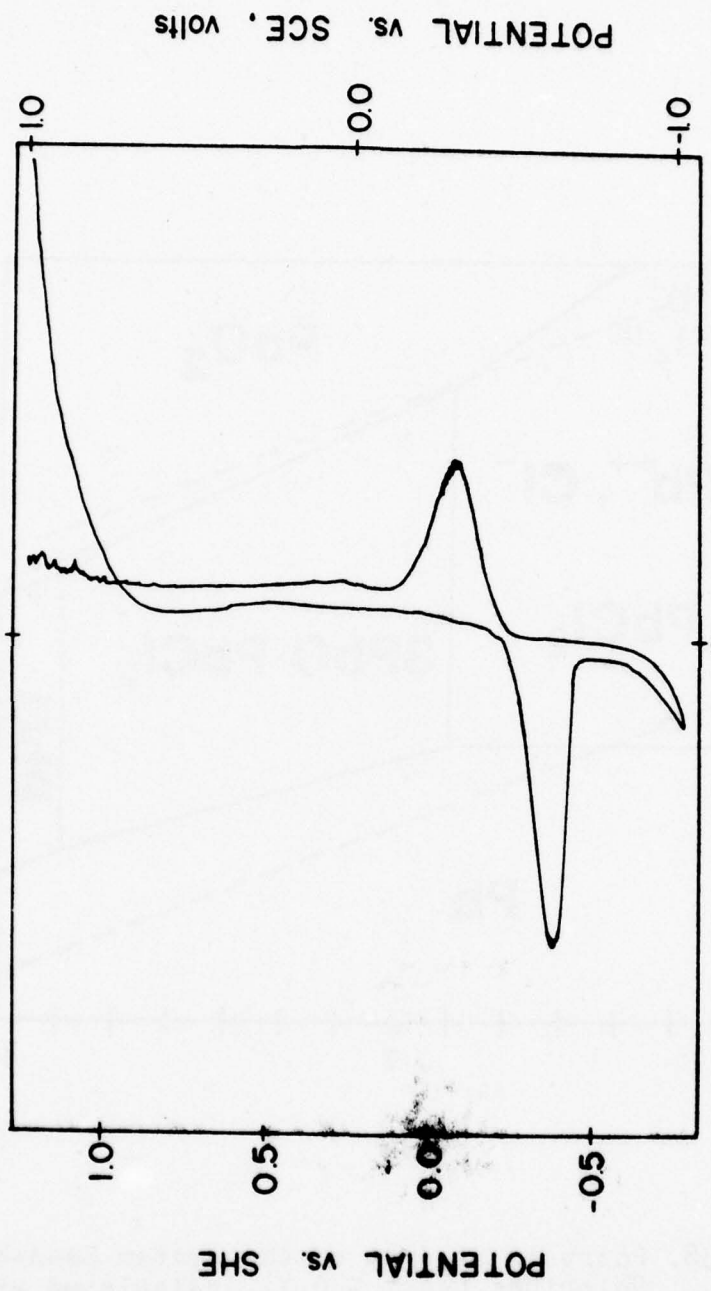

Figure 39. Polarization curve of lead in 0.1M HCl. Scan rate 40 mv/minute.

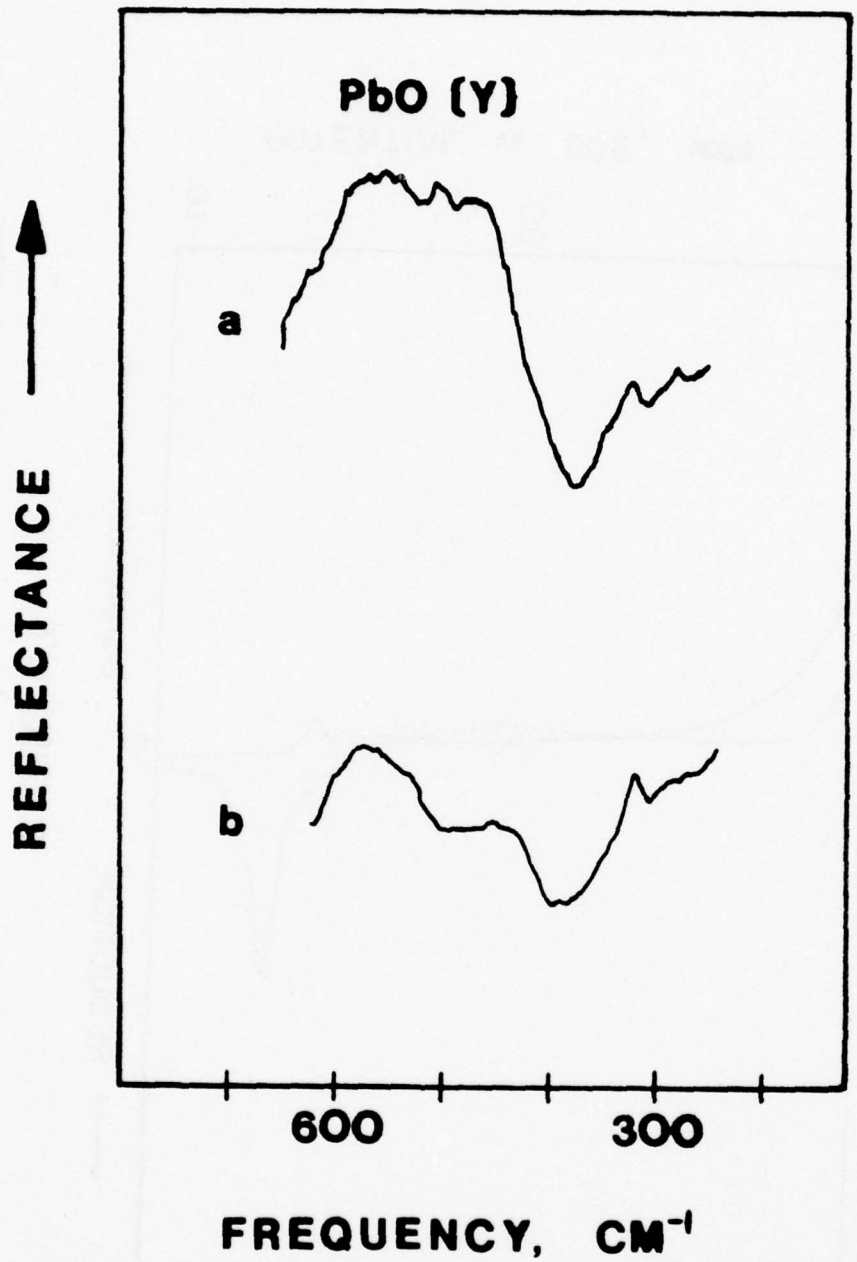

Figure 40. Infrared reflection spectra from lead exposed in 0.1M HCl, pH=1.1, for 1 hour at 1.18 V NHE. a) 65-68° b) 60-65°.

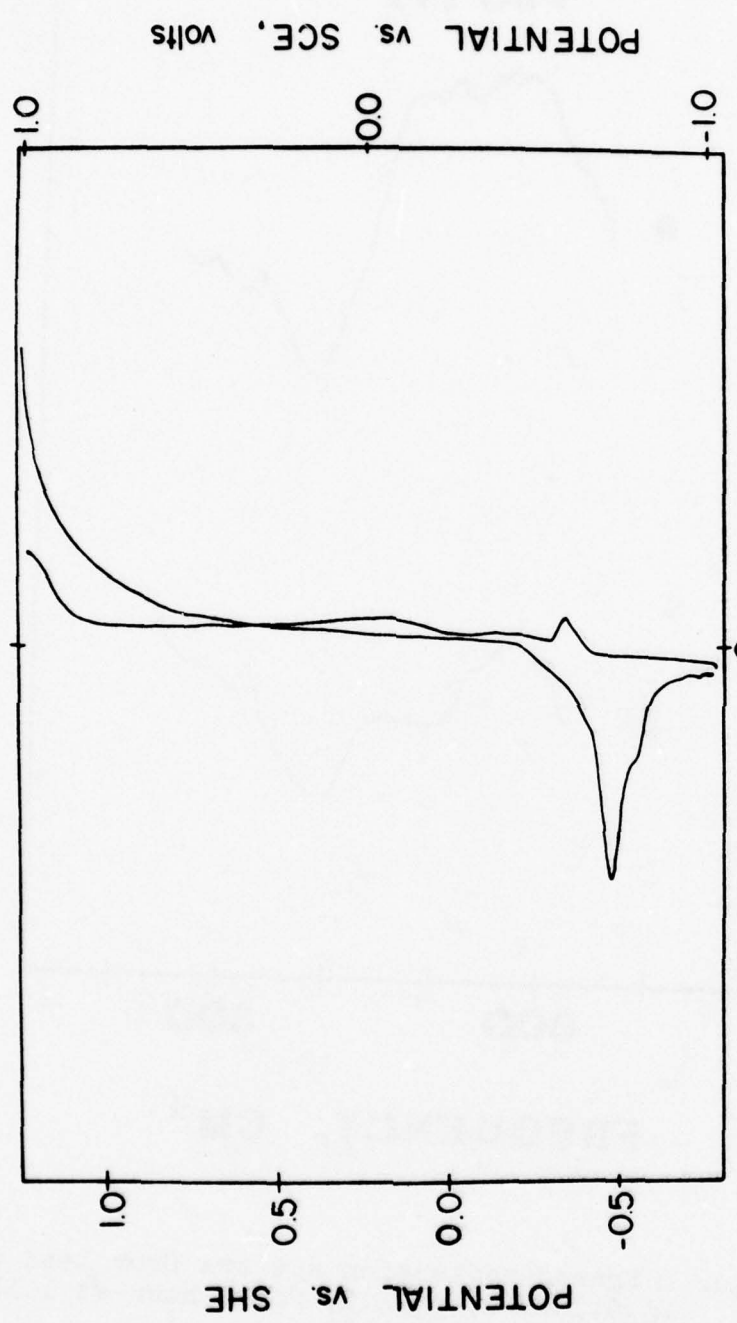

Figure 41. Polarization curve of lead in phosphate buffer with 0.1M chloride ions, pH=7. Scan rate 40 mv/minute.

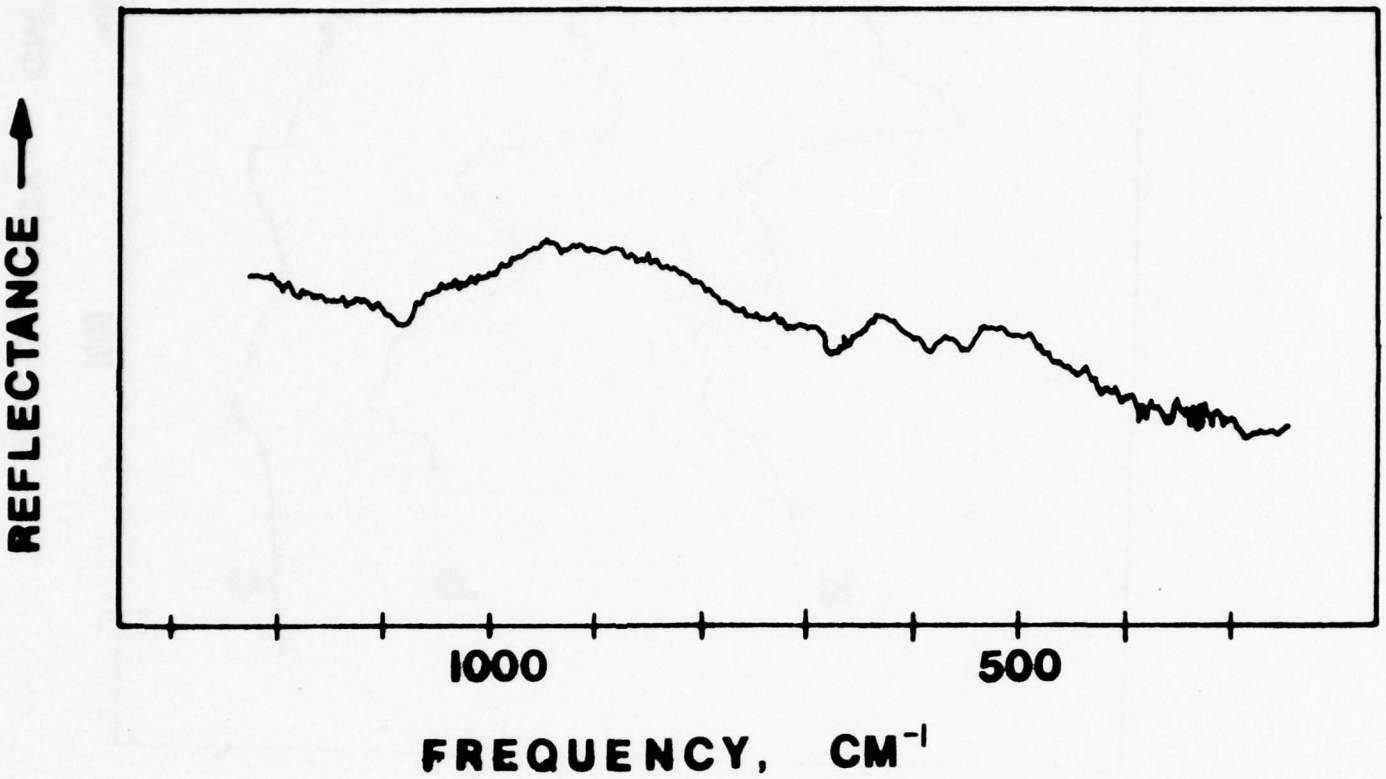

Figure 42. Infrared reflection spectrum from lead exposed in phosphate buffer with 0.1M chloride ions, pH=7, for 25 hours at -.42 V NHE.

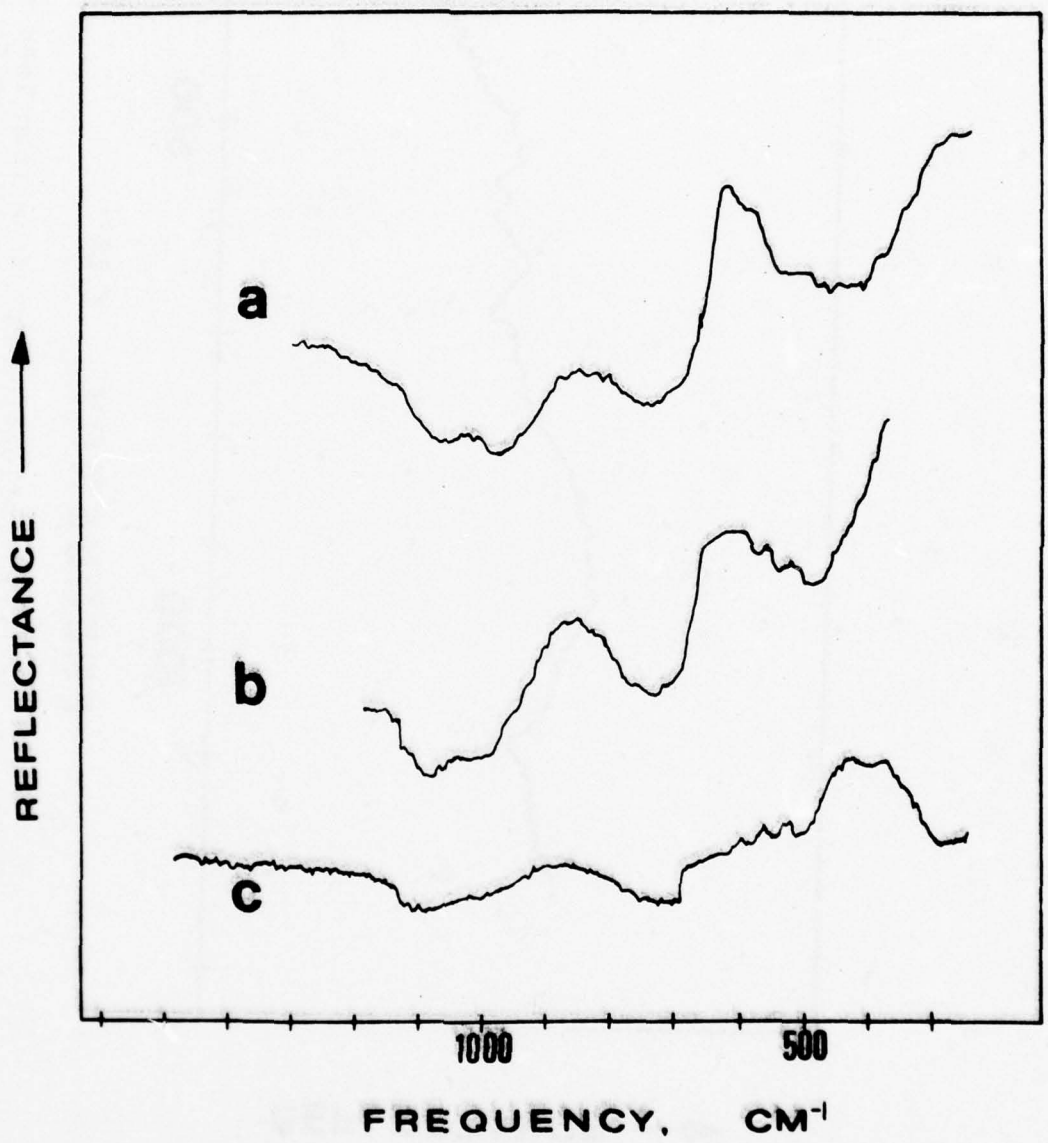

Figure 43. Infrared reflection spectra from lead exposed in phosphate buffer, with 0.1M chloride ions, pH=7. a) and b) 17 hours at -.11 V NHE. c) 16 hours at -.11 V NHE.

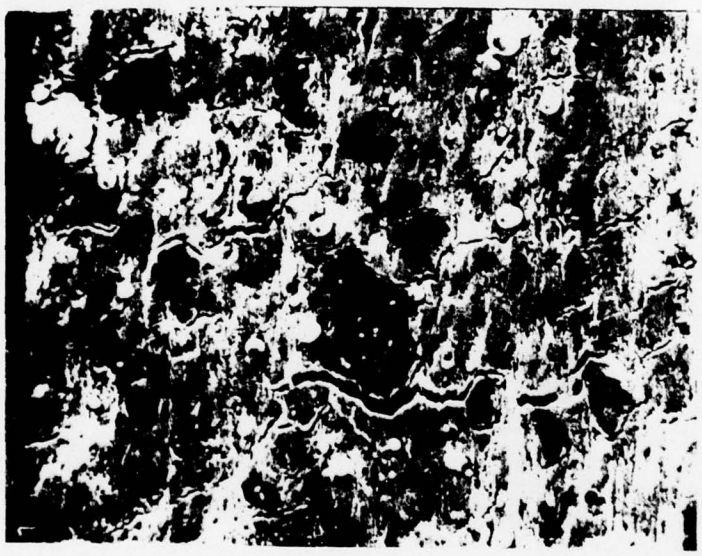

Figure 44. Lead exposed in phosphate buffer, containing 0.1M chloride ions, pH=7, at -.11 V NHE for 16 hours. Magnification: 500X. White colored particles - lead phosphate, no chlorides were detected in the film.

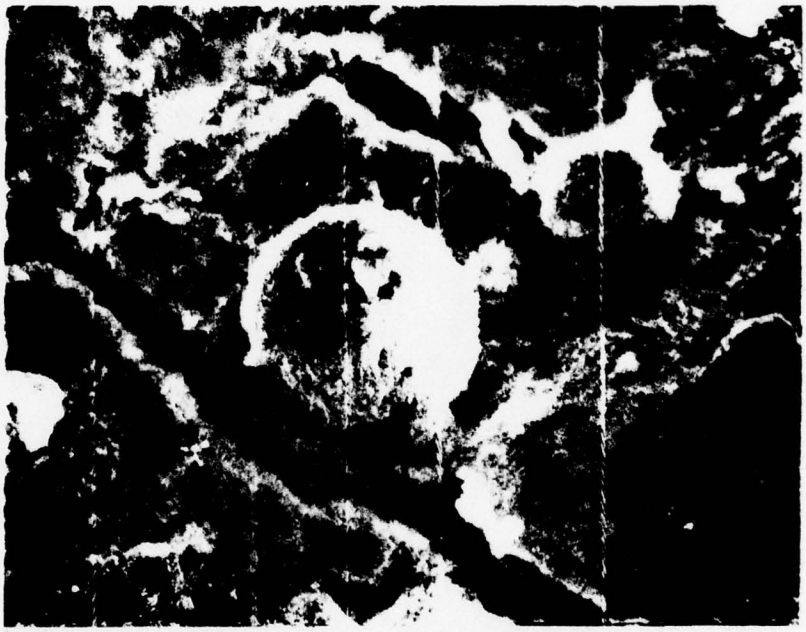

Figure 45. Lead exposed in phosphate buffer, containing 0.1M chloride ions, pH=7, at -.11 V NHE for 16 hours. Magnification: 5000X. Particles - lead phosphate, no chlorides were detected.

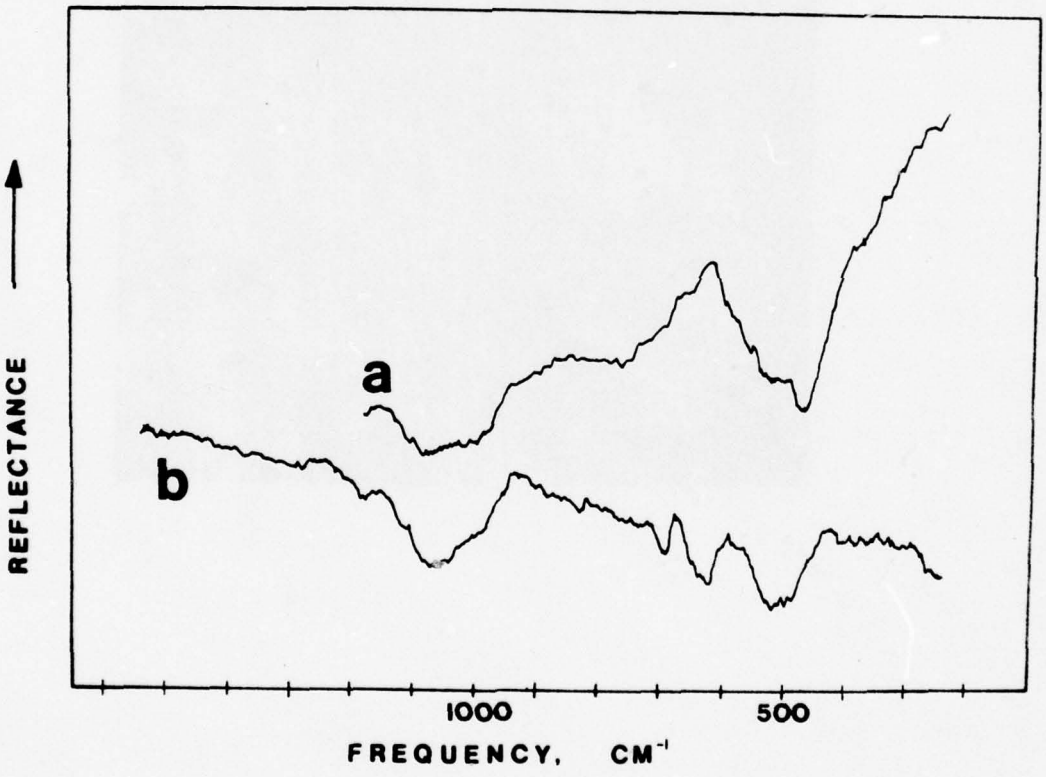

Figure 46. Infrared reflection spectra obtained from lead exposed in phosphate buffer, pH=7. a) 0.01M chloride ions, 3 hours at -.01 V NHE. b) 0.5M chloride ions, 18.75 hours at -.01 V NHE.

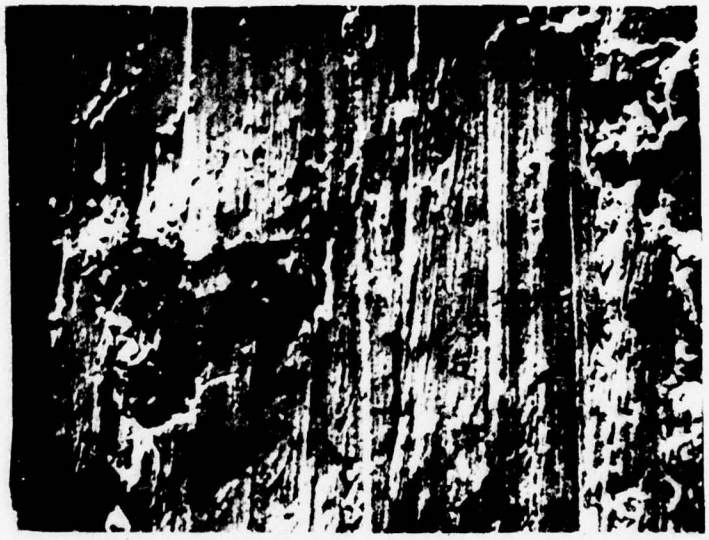

Figure 47. Lead exposed in phosphate buffer containing 0.01M chloride ions, pH=7, at -.01 V NHE for 3 hours. Magnification: 1000X. Film coated surface, no particles.

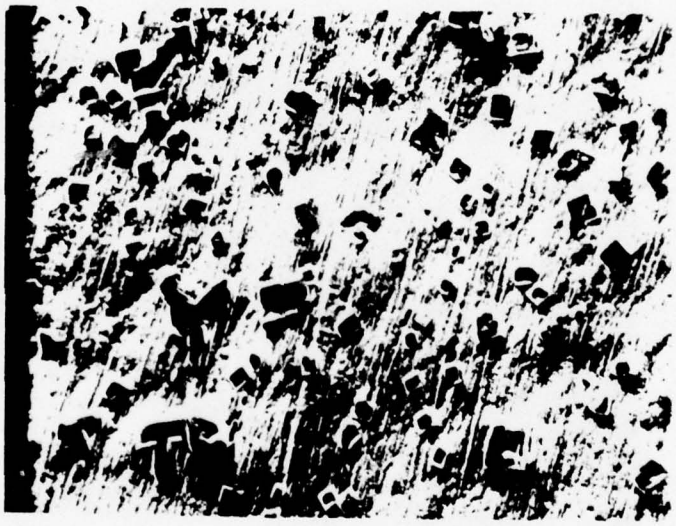

Figure 48. Lead exposed in phosphate buffer containing 0.5M chloride ions, pH=7, at -.01 V NHE, for 18 hours. Magnification: 200X, the crystals were idetified as KCl.

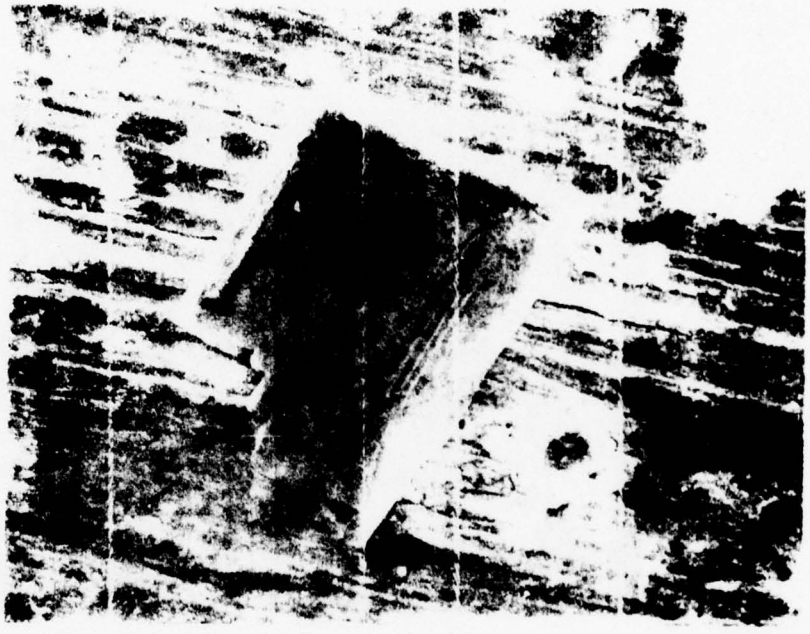

Figure 49. Lead exposed in phosphate buffer containing 0.5M chloride ions, pH=7, at -.01 V NHE, for 18 hours. Magnification: 2000X, the big crystal was identified as KCl, the small as lead phosphate.

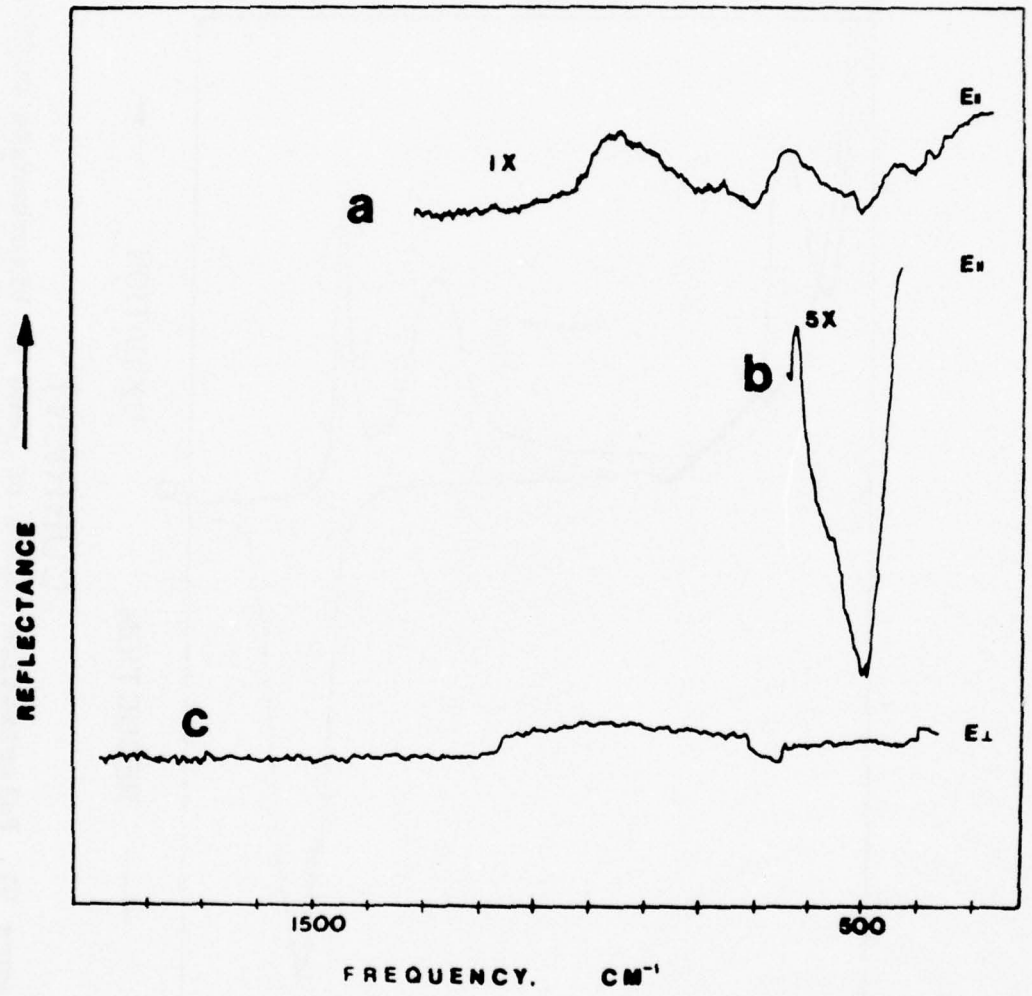

Figure 50. Infrared reflection spectra from lead exposed phosphate buffer containing 0.1M chloride ions, pH=7, for 3 hours at 1.08 V NHE. a) 1X, parallel polarization. b) 5X, parallel polarization. c) 1X, perpendicular polarization.

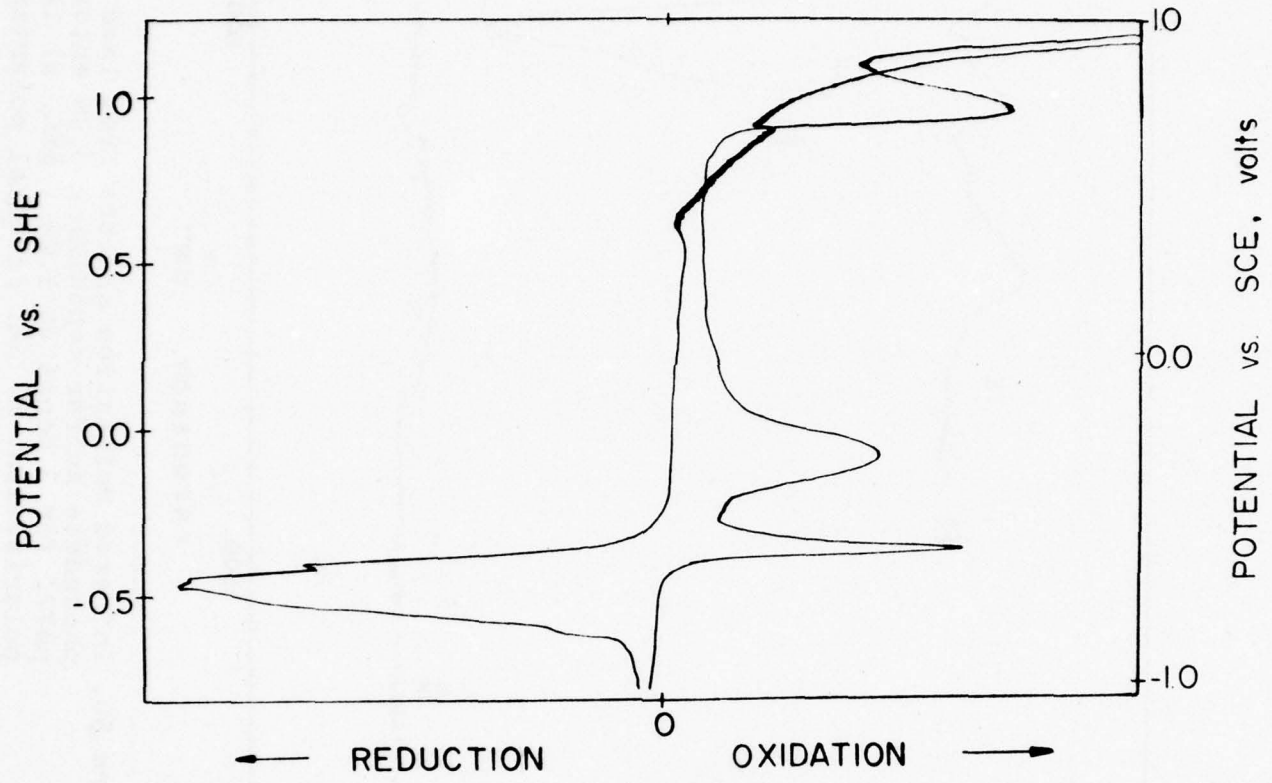

Figure 51. Polarization curve of lead in bicarbonate buffer containing 0.1M chloride ions, pH=10. Scan rate 40 mv/minute.

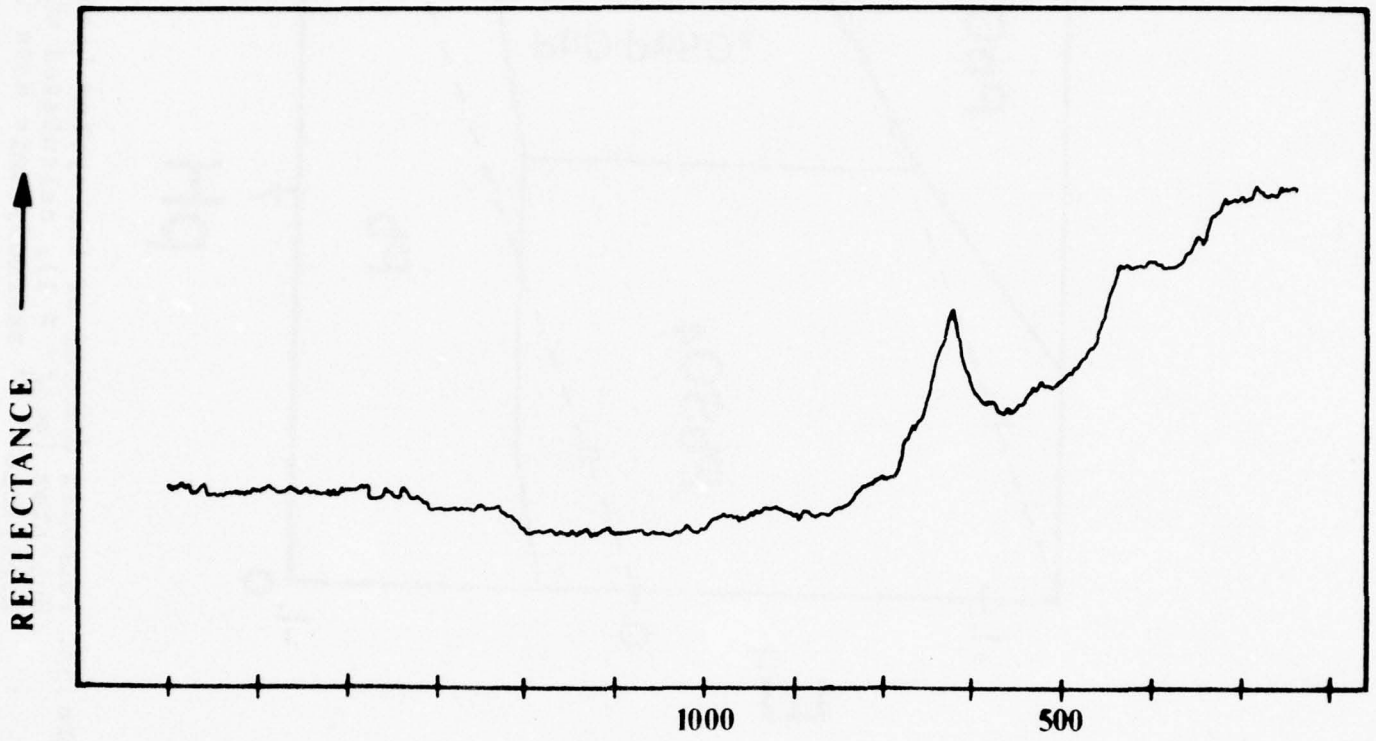

Figure 52. Infrared reflection spectrum from lead exposed in bicarbonate buffer, containing 0.1M chloride ions, pH=10, for 4 hours at 1.08 V NHE.

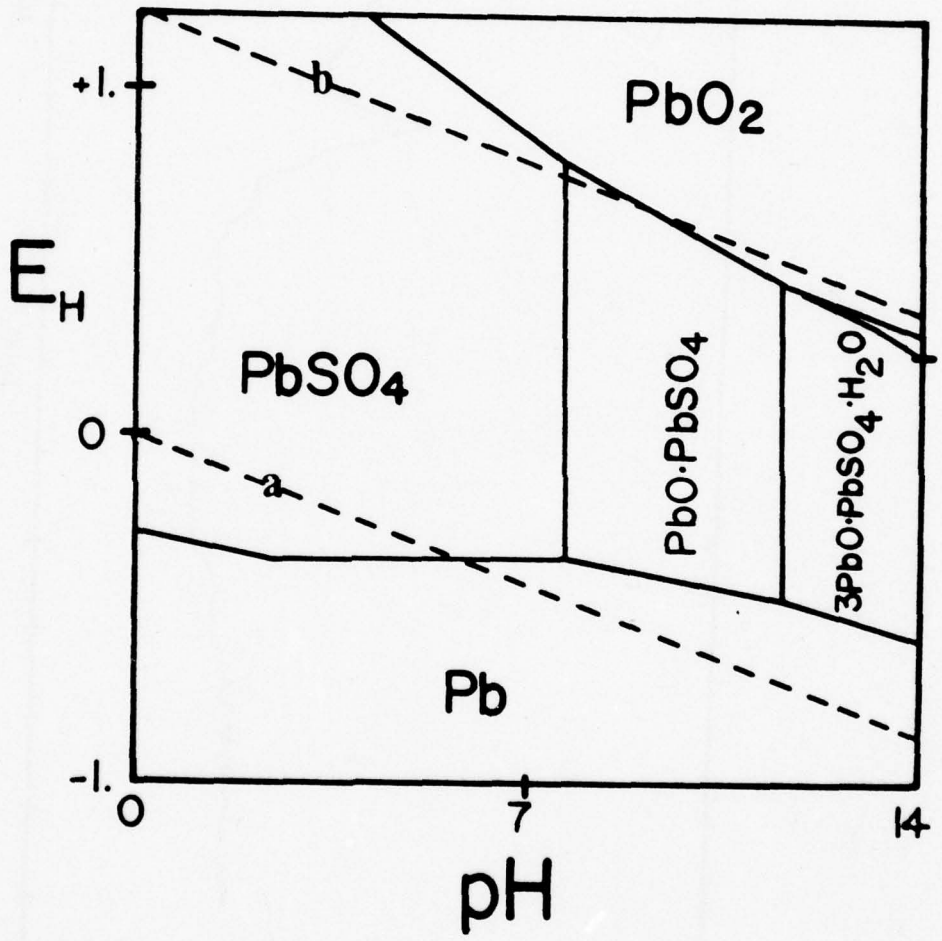

Figure 53. Pourbaix diagram of the system Lead-Water-Sulfates ($a_{SO_4^{--}} = 1$), calculated with the latest available thermodynamic data (65).

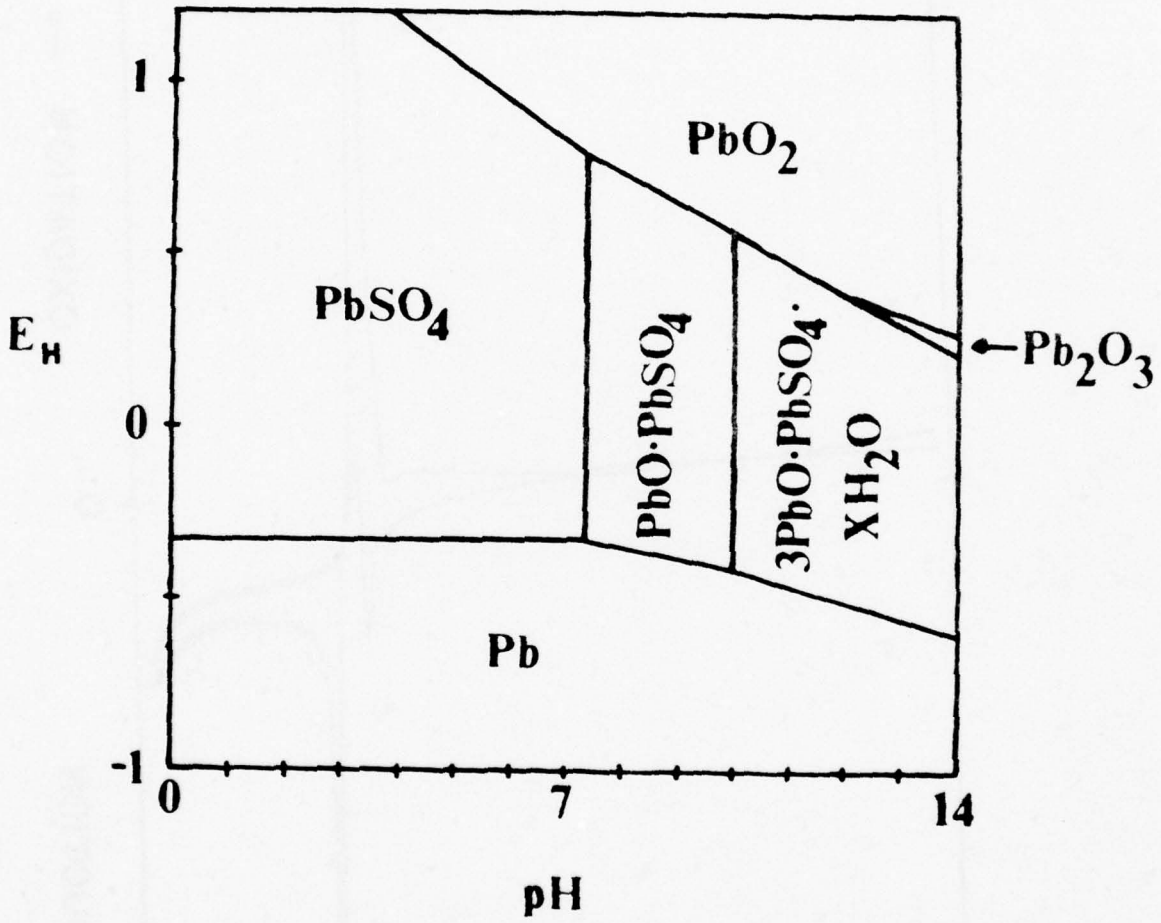

Figure 54. Pourbaix diagram of the system Lead-Water-Sulfates ($a_{SO_4^{--}} = 0.1$), calculated with the latest available thermodynamic data (65).

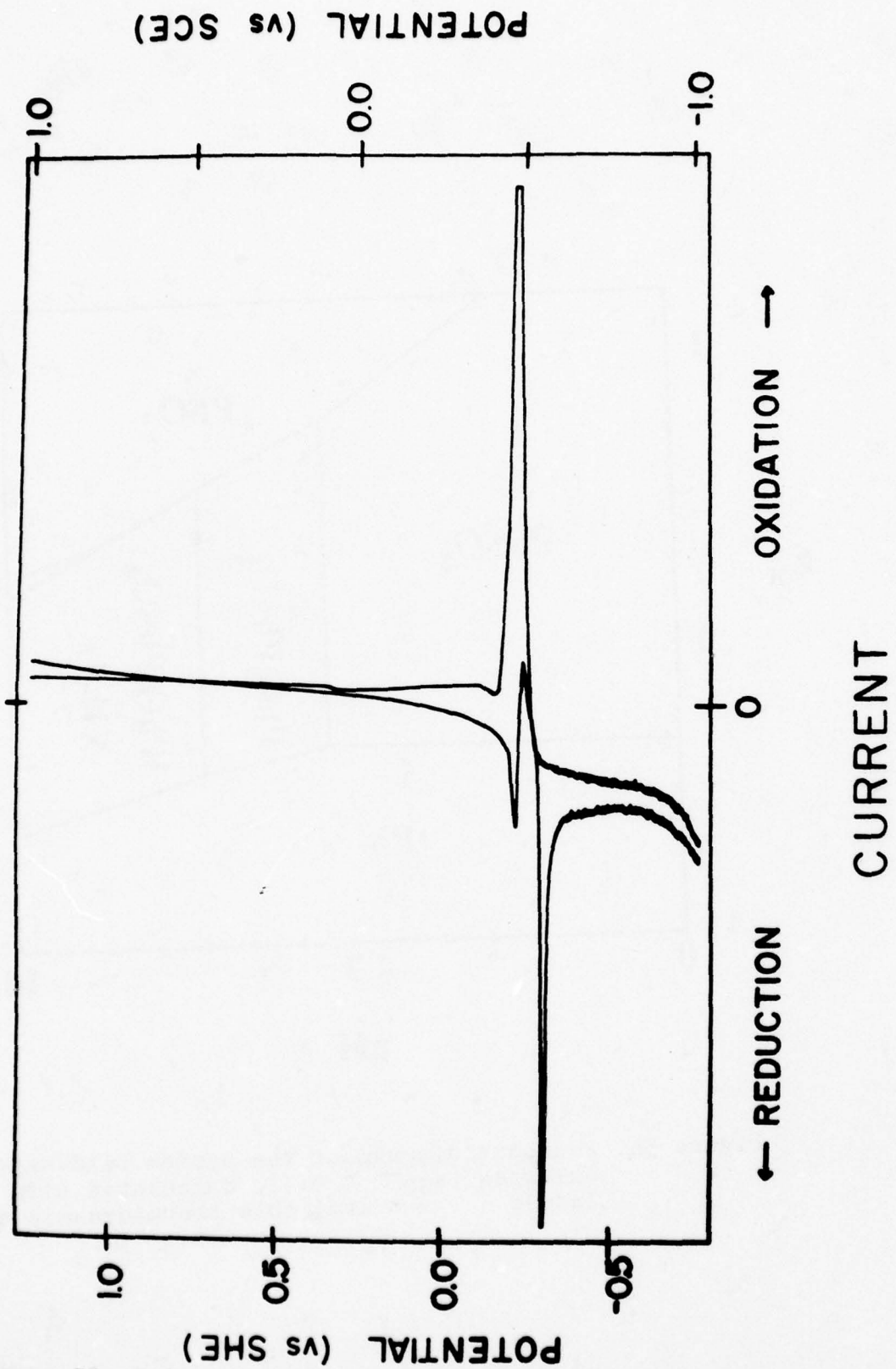

Figure 55. Polarization curve of lead in 0.1M sulfuric acid, pH=0.9. Scan rate 40 mv/minute.

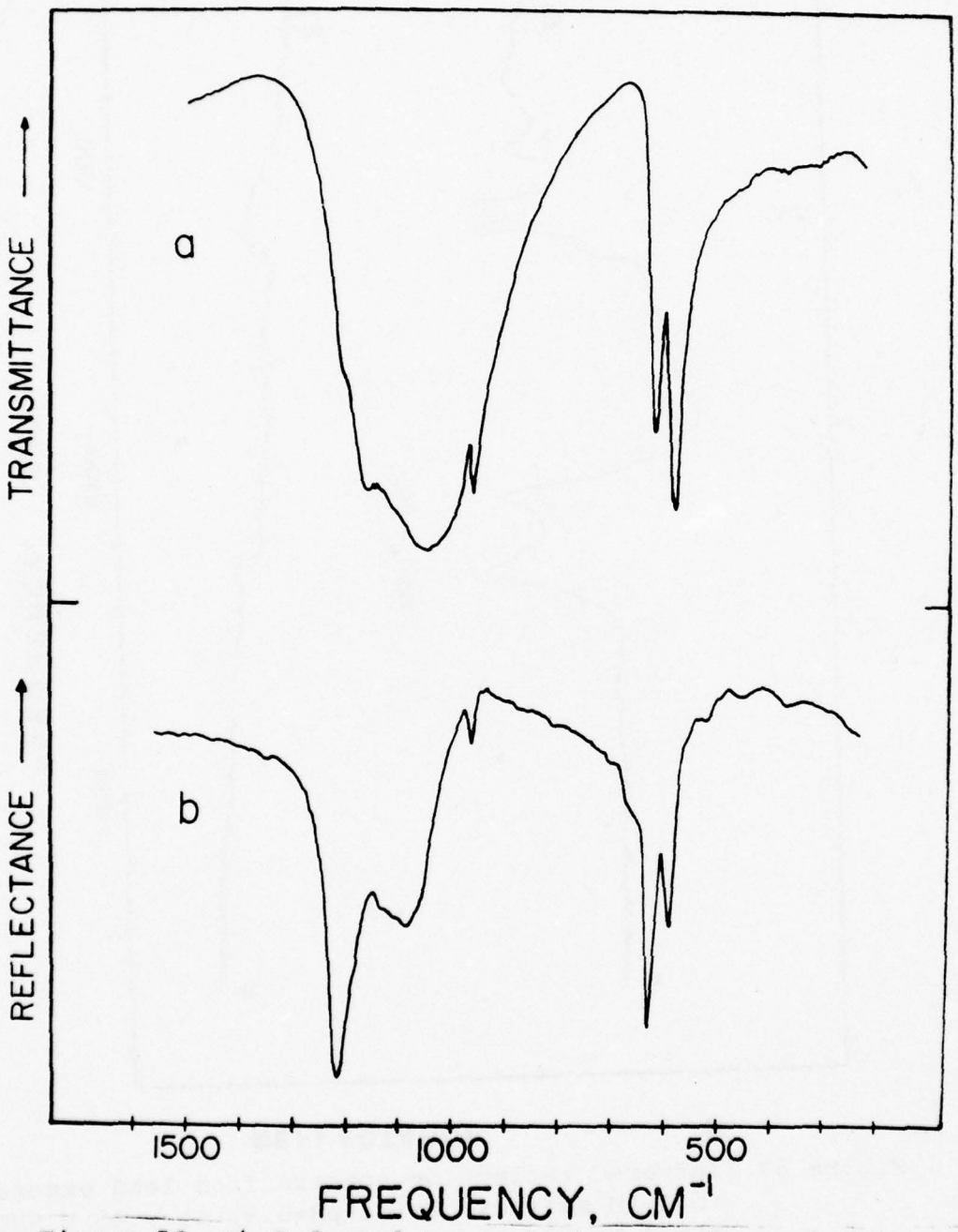

Figure 56. a) Infrared transmission spectrum of $PbSO_4$ powder, in KBr. b) Infrared reflection spectrum from lead exposed in 0.1M sulfuric acid, pH=0.9, for 3 hours at -.02 V NHE.

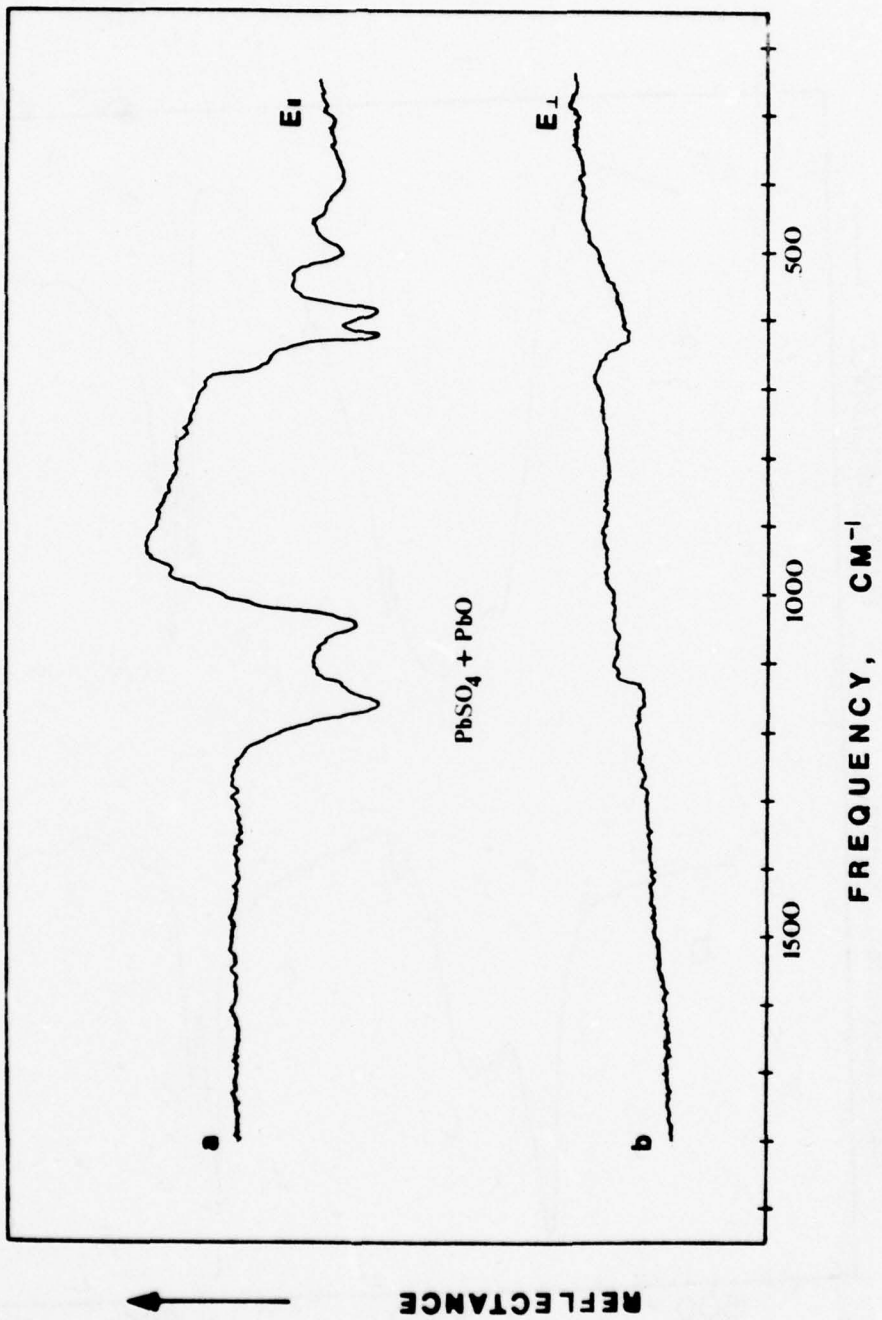

Figure 57. Infrared reflection spectra from lead exposed in 0.1M sulfuric acid, pH=0.9, at -.40 V NHE for 2 hours. a) Parallel polarization. b) Perpendicular polarization.

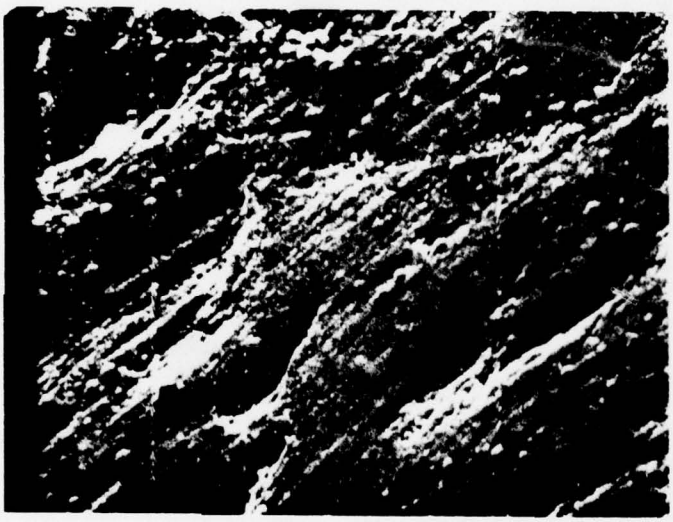

Figure 58. Lead exposed in 0.1M sulfuric acid, pH=0.9, at -.40 V NHE for 2 hours. Magnification: 1000X, particles are probably lead sulfate.

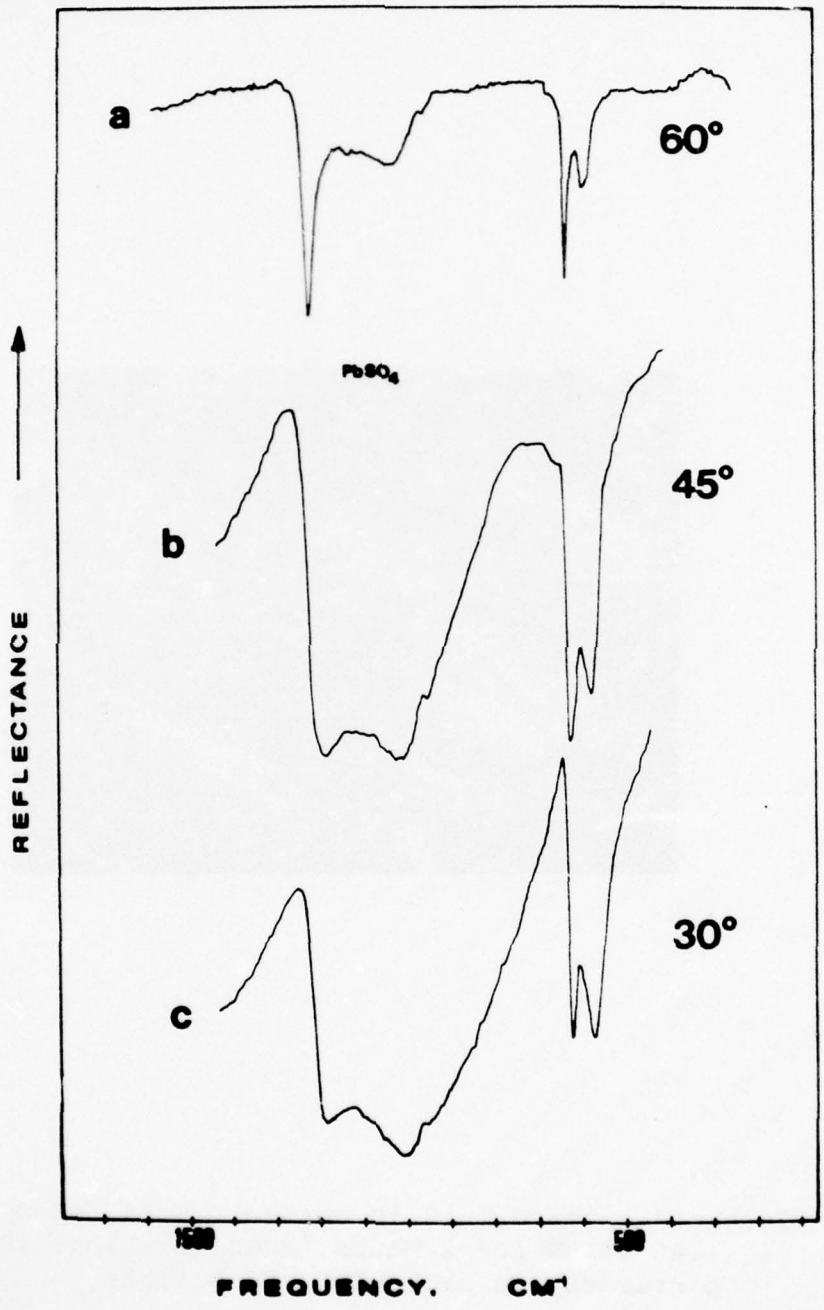

Figure 59. Infrared reflection spectra from lead exposed in 0.1M sulfuric acid, pH=0.9, for 16 hours at -.02 V NHE. a) 60-65° b) 45° c) 30°.

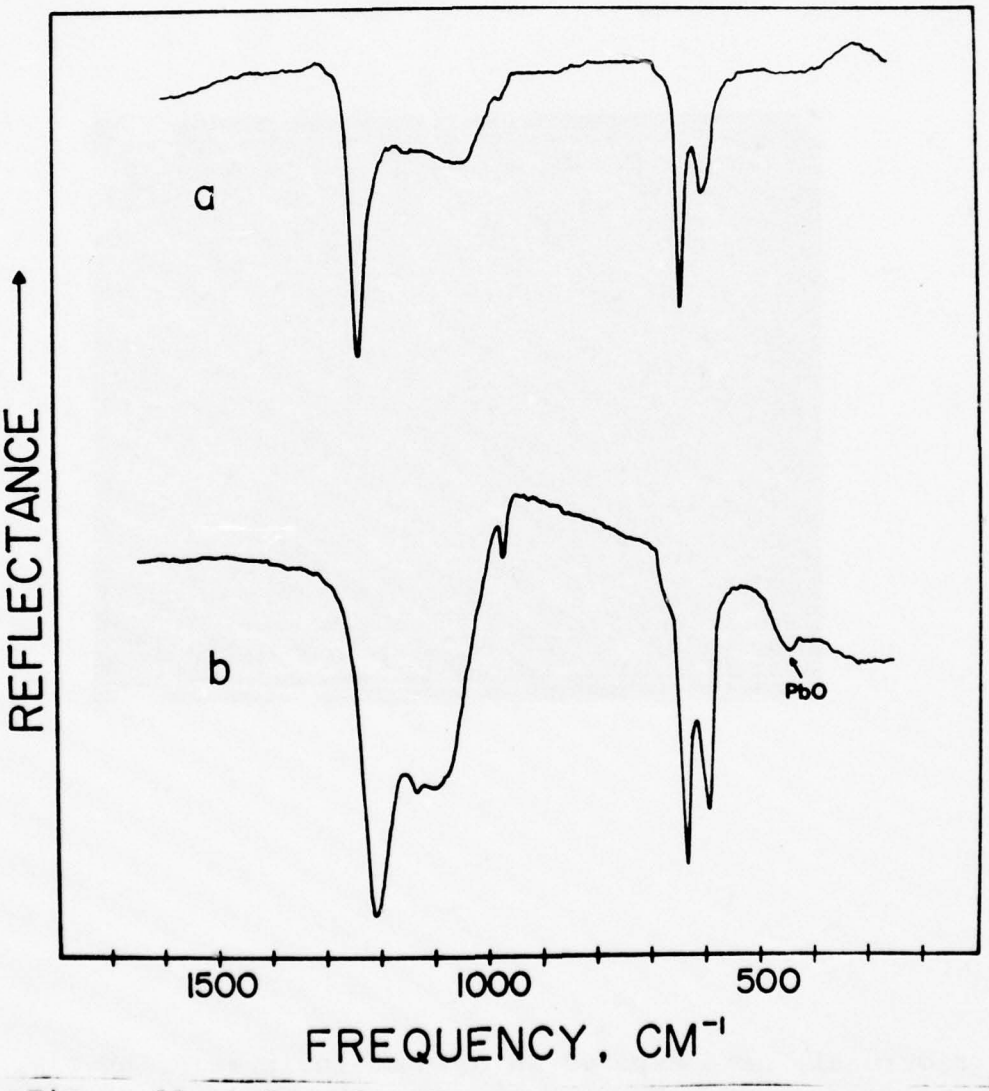

Figure 60. Infrared reflection spectra from lead exposed in 0.1M sulfuric acid, pH=0.9, a) -.02 V NHE for 3 hours. b) .80 V NHE for 1.5 hours.

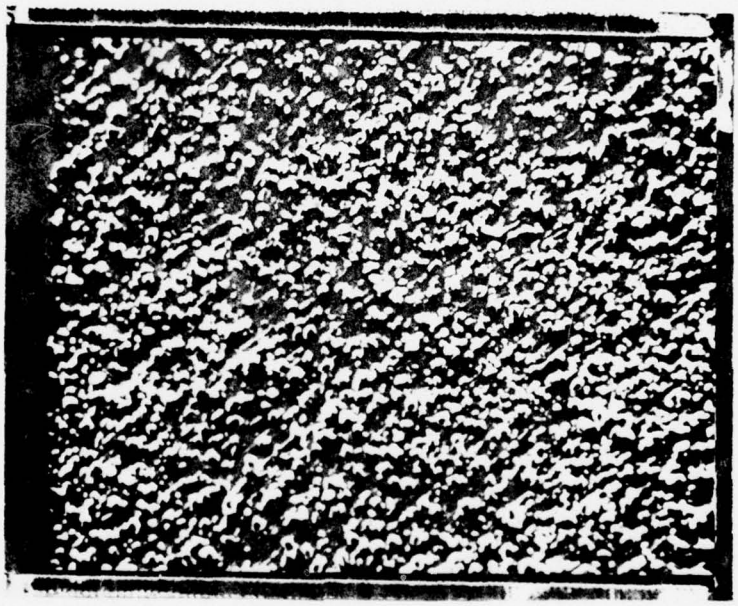

Figure 61. Lead exposed in 0.1M sulfuric acid, pH=0.9, at .80 V NHE for 16 hours. Magnification: 500X, lead sulfate crystals.

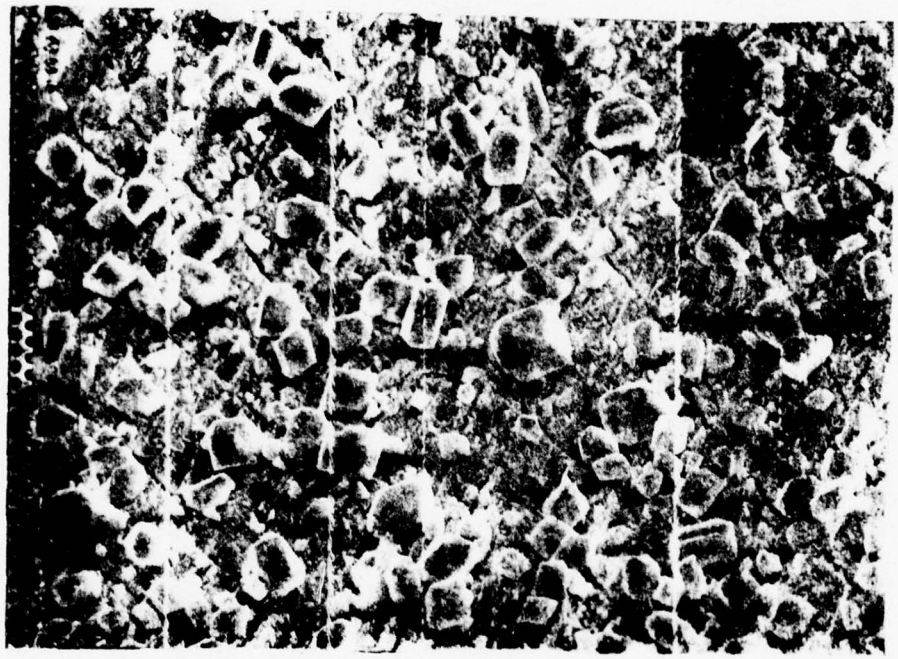

Figure 62. Lead exposed in 0.1M sulfuric acid, pH=0.9, at .80 V NHE for 16 hours. Magnification: 2000X, lead sulfate crystals.

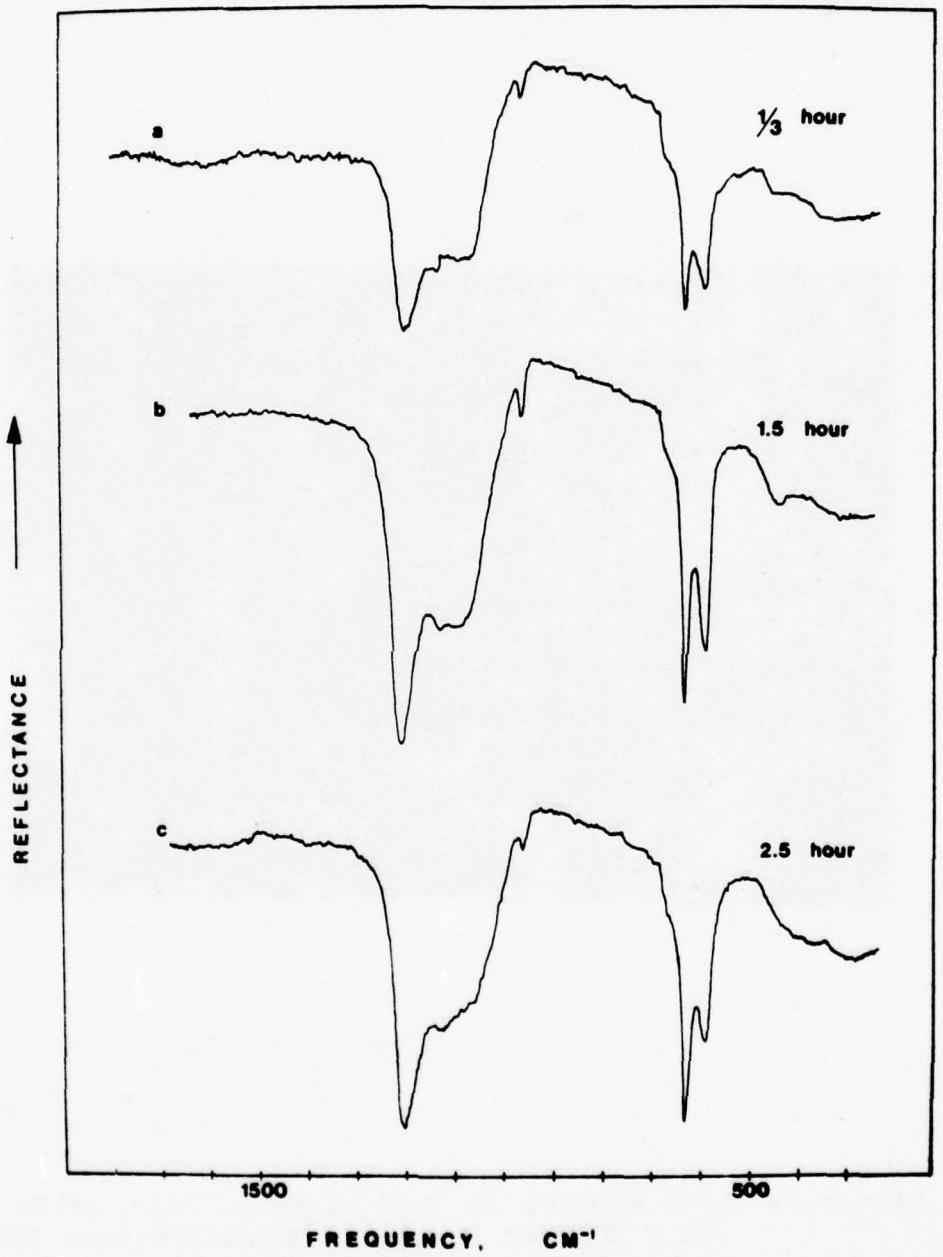

Figure 63. Infrared reflection spectra from lead exposed in 0.1M sulfuric acid, pH=0.9, at .80 V NHE for a) 20 minutes b) 1.5 hours c) 2.5 hours.

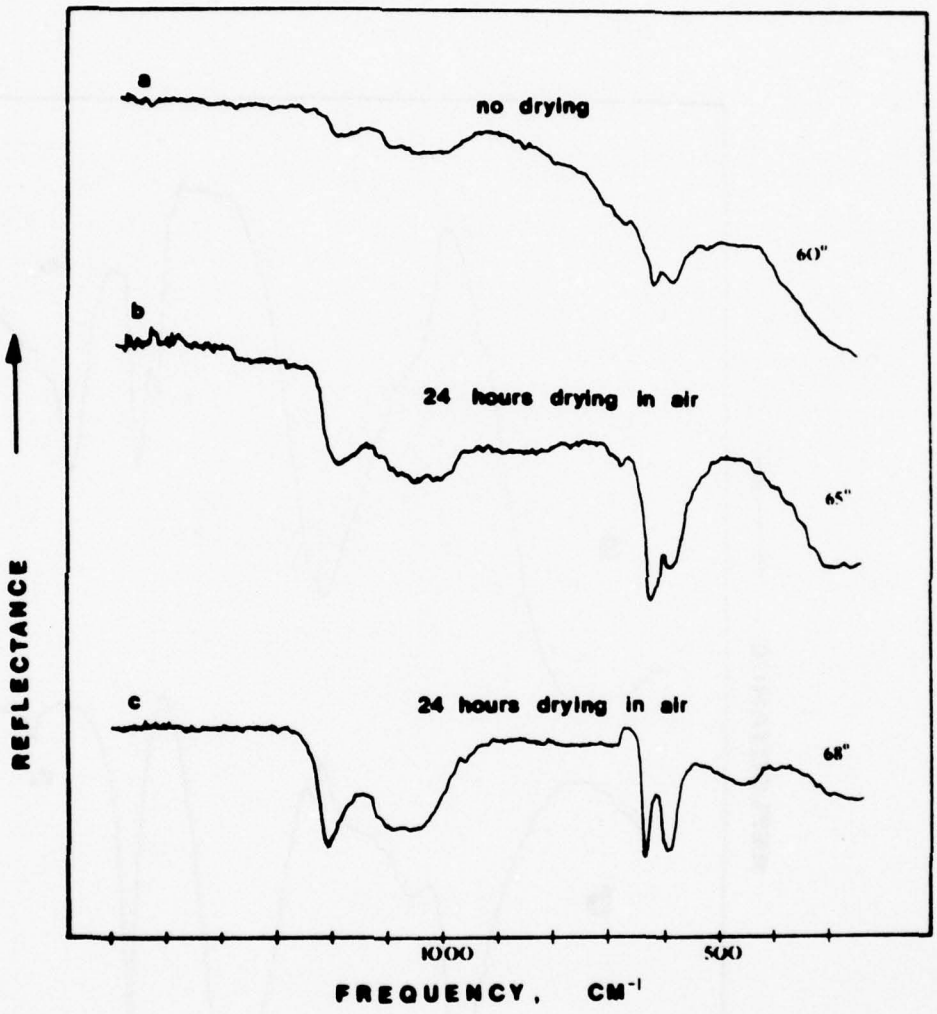

Figure 64. Infrared reflection spectra from lead exposed in 0.1M sulfuric acid, pH=0.9, at .80 V NHE for 3.5 hours. a) 60° b) After drying in air for 24 hours, 65° c) same as (b), 65-68°.

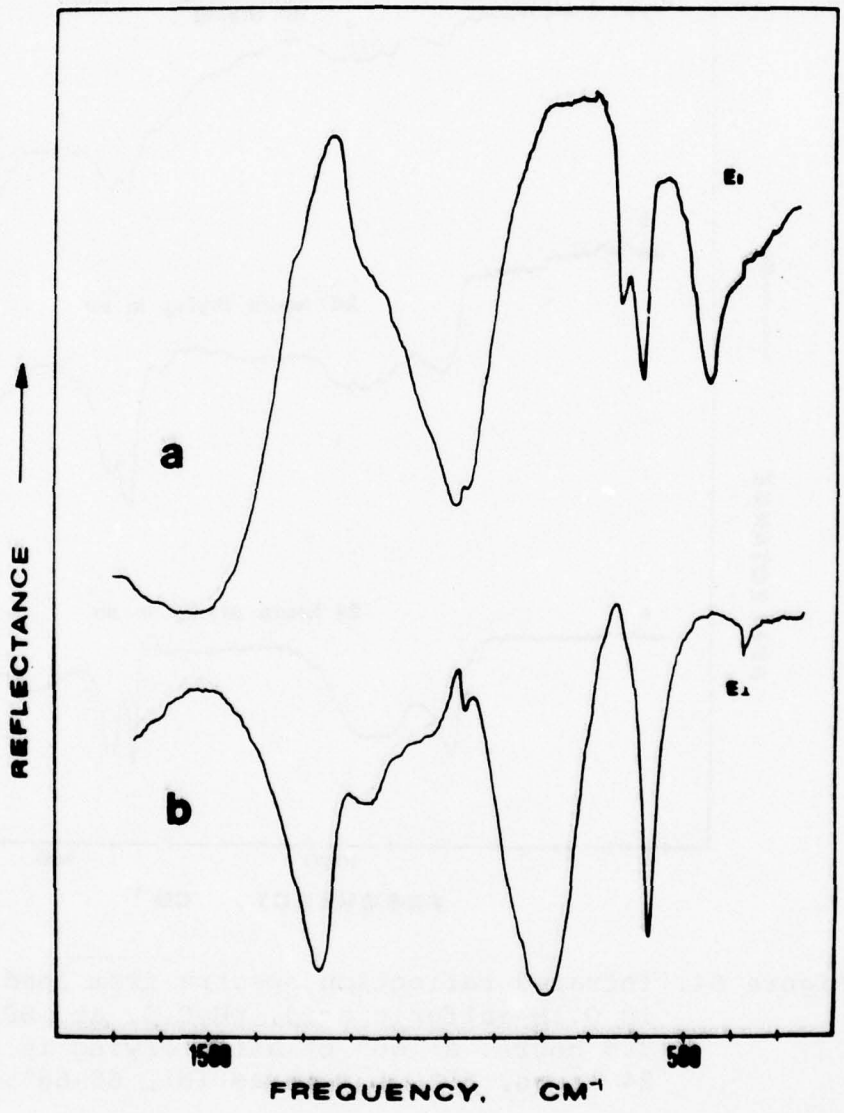

Figure 65. Infrared reflection spectra obtained from lead exposed in 0.1M sulfuric acid, pH=0.9, at .80 V NHE for 20.5 hours. a) Parallel polarization. b) Perpendicular polarization.

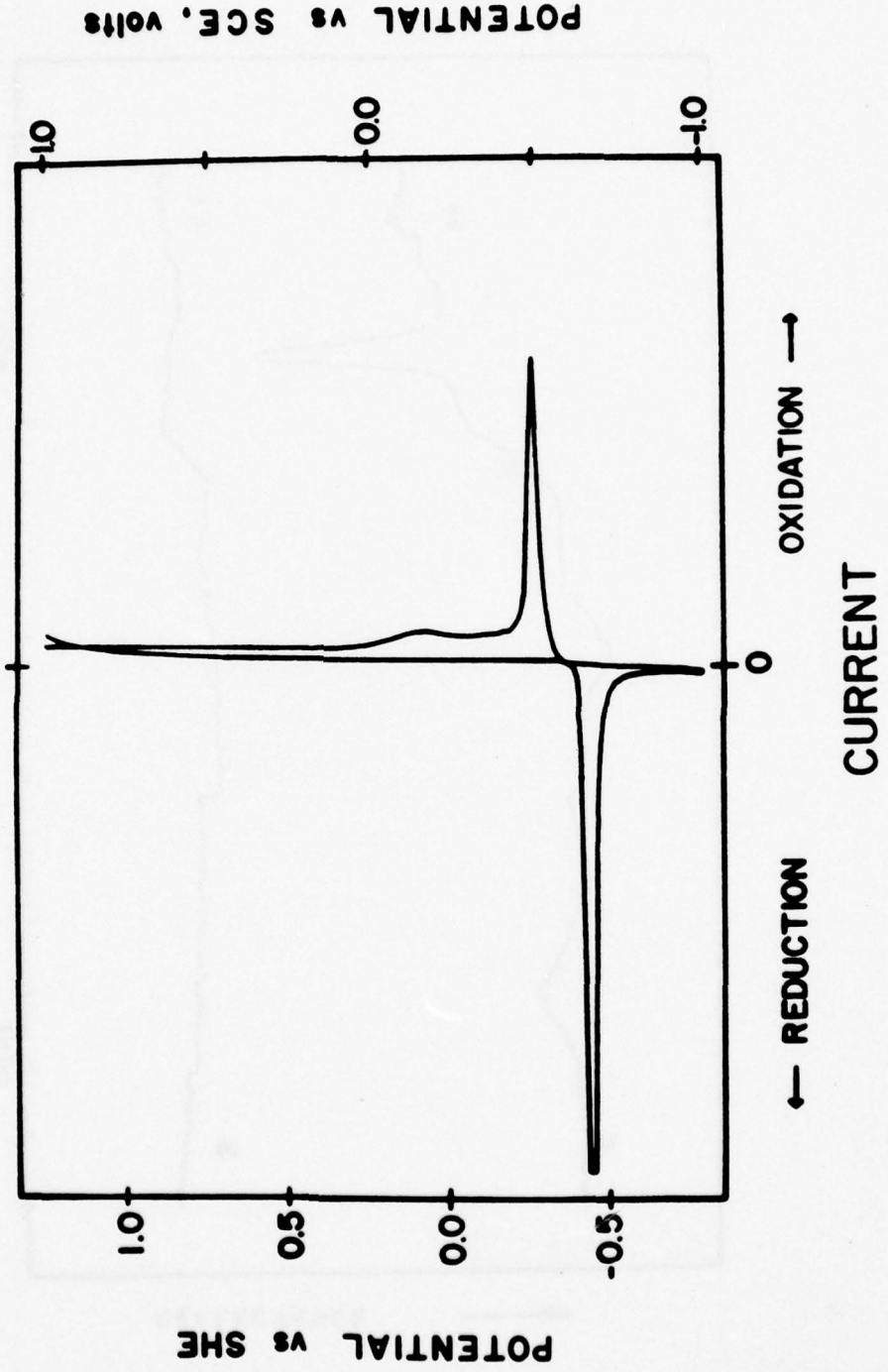

Figure 66. Polarization curve of lead in 0.1M K_2SO_4 solution, pH=5.75. Scan rate 40 mv/minute.

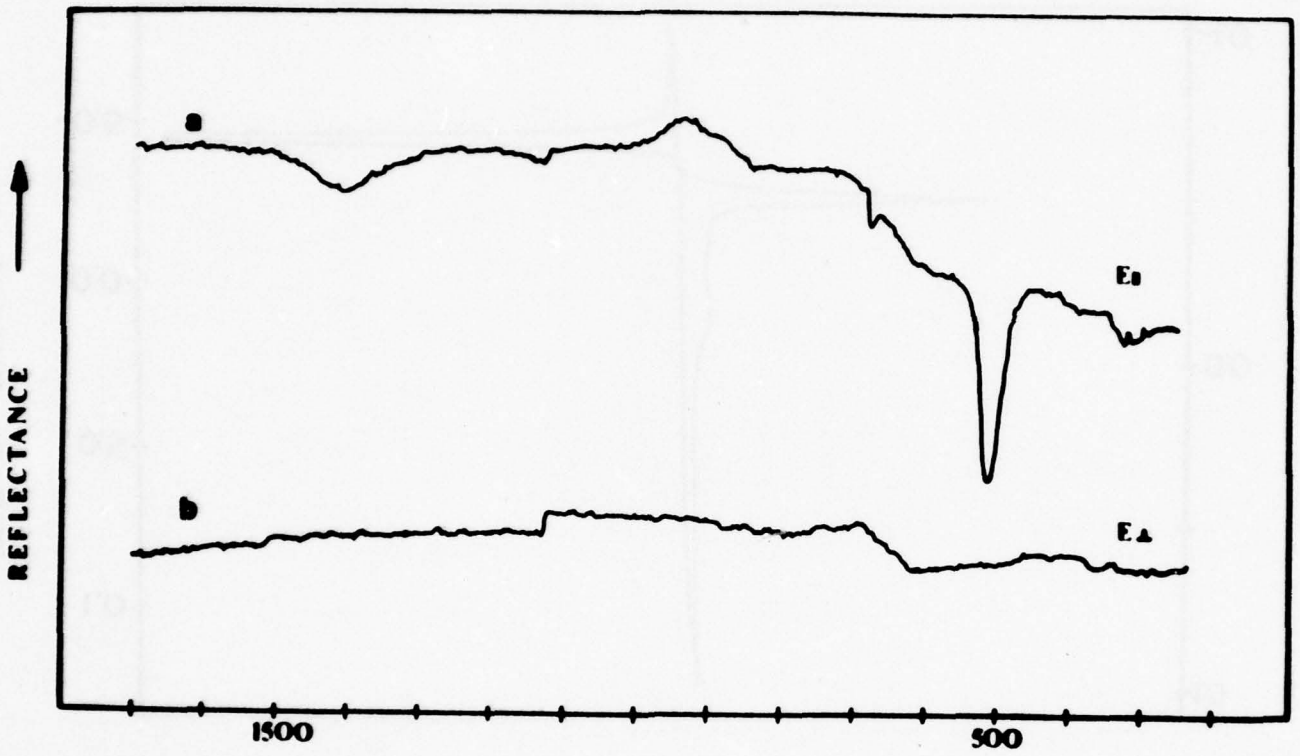

Figure 67. Infrared reflection spectra from lead exposed in 0.1M K_2SO_4, pH=5.75, at -.62 V NHE for 3 hours. a) Parallel polarization. b) Perpendicular polarization.

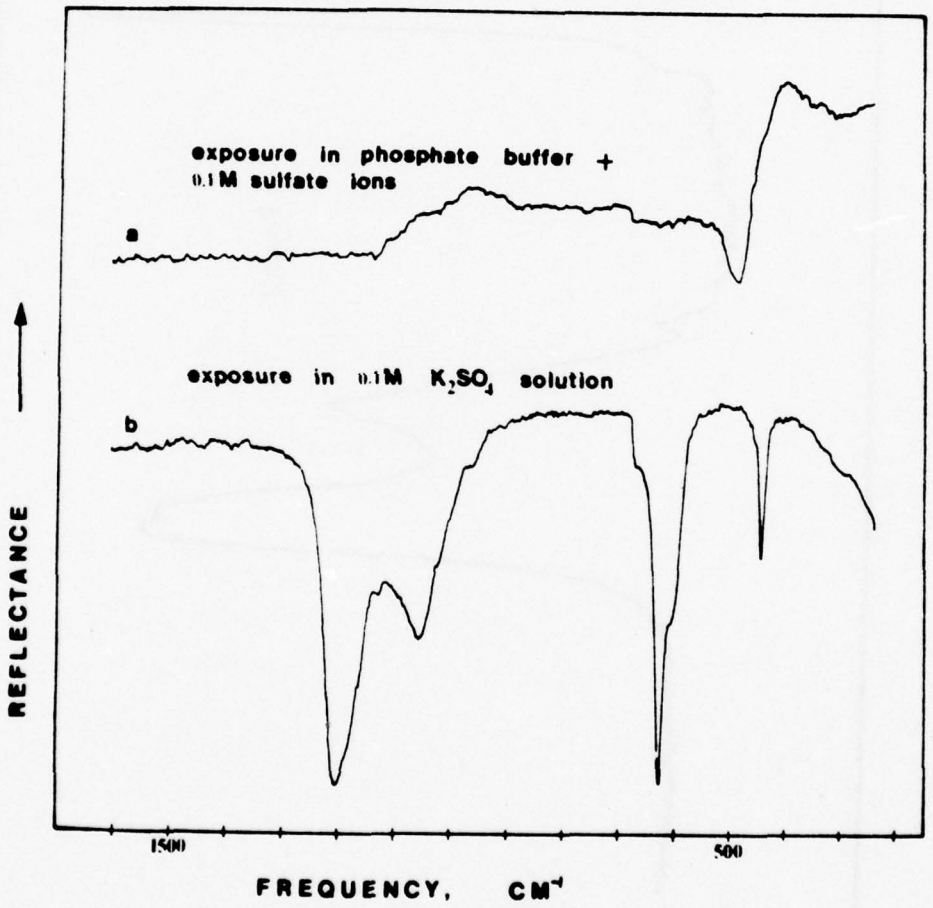

Figure 68. Infrared reflection spectra obtained from lead a) Exposed in phosphate buffer, containing 0.1M sulfate ions, pH=7, at .24 V NHE for 16.75 hours. b) Exposed in 0.1M K_2SO_4 solution, pH=5.75, at .24 V NHE for 1.75 hours.

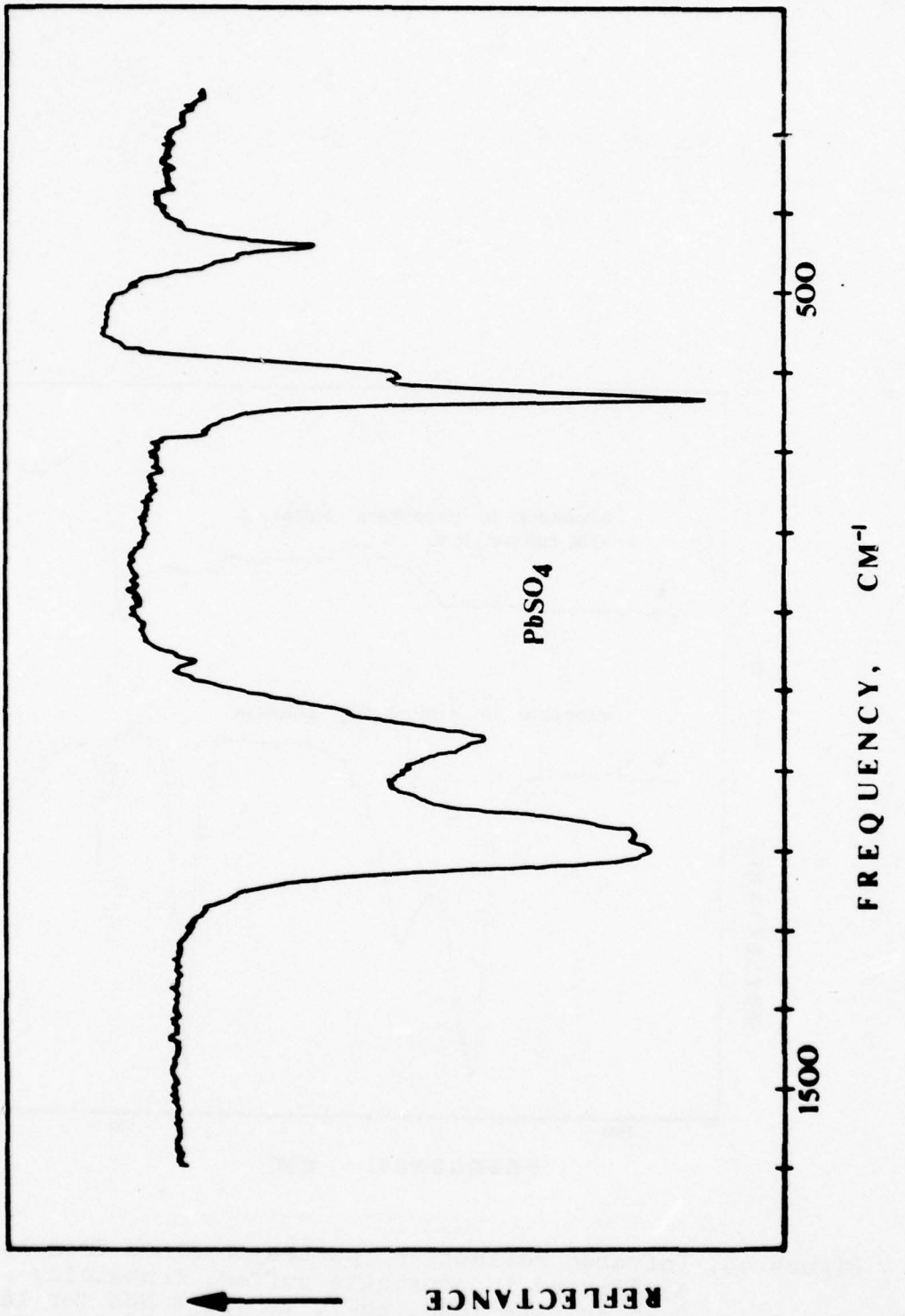

Figure 69. Infrared reflection spectrum from lead exposed in 0.1M K_2SO_4 solution, pH=5.75, at 1.08 V NHE for 3.5 hours.

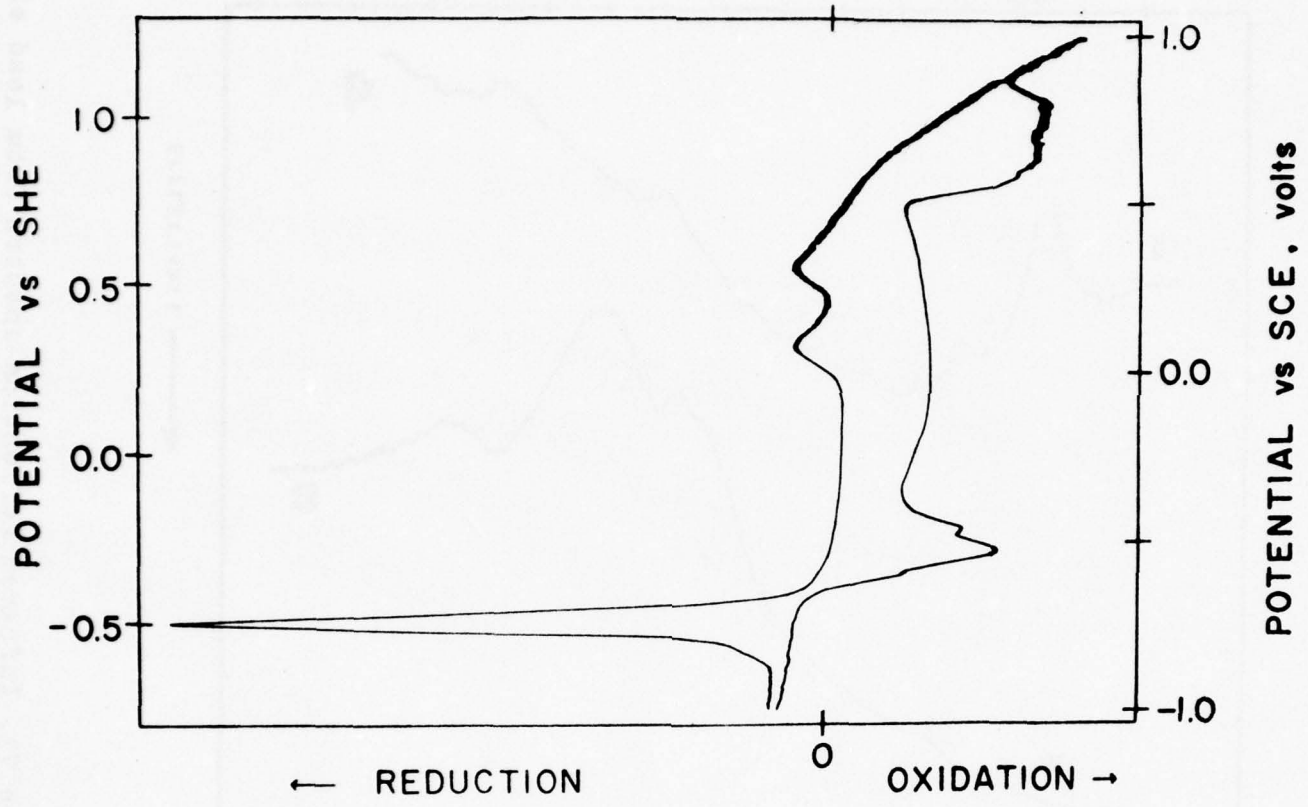

Figure 70. Polarization curve of lead in KOH solution containing 0.1M sulfate ions, pH=10.9-11.2. Scan rate 40 mv/minute.

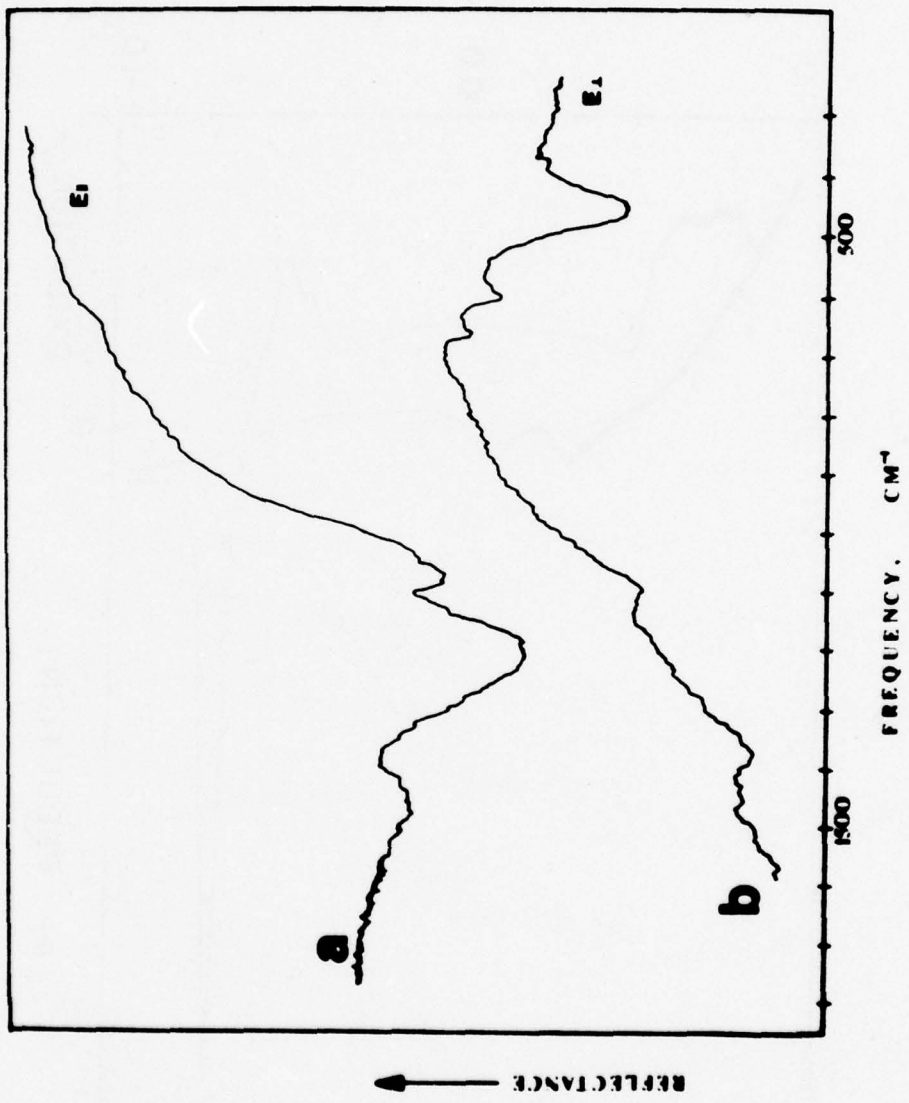

Figure 71. Infrared reflection spectra from lead exposed in KOH solution containing 0.1M sulfate ions, pH=10.9-11.2, at .24 V NHE for 25 minutes. a) Parallel polarization. b) Perpendicular polarization.

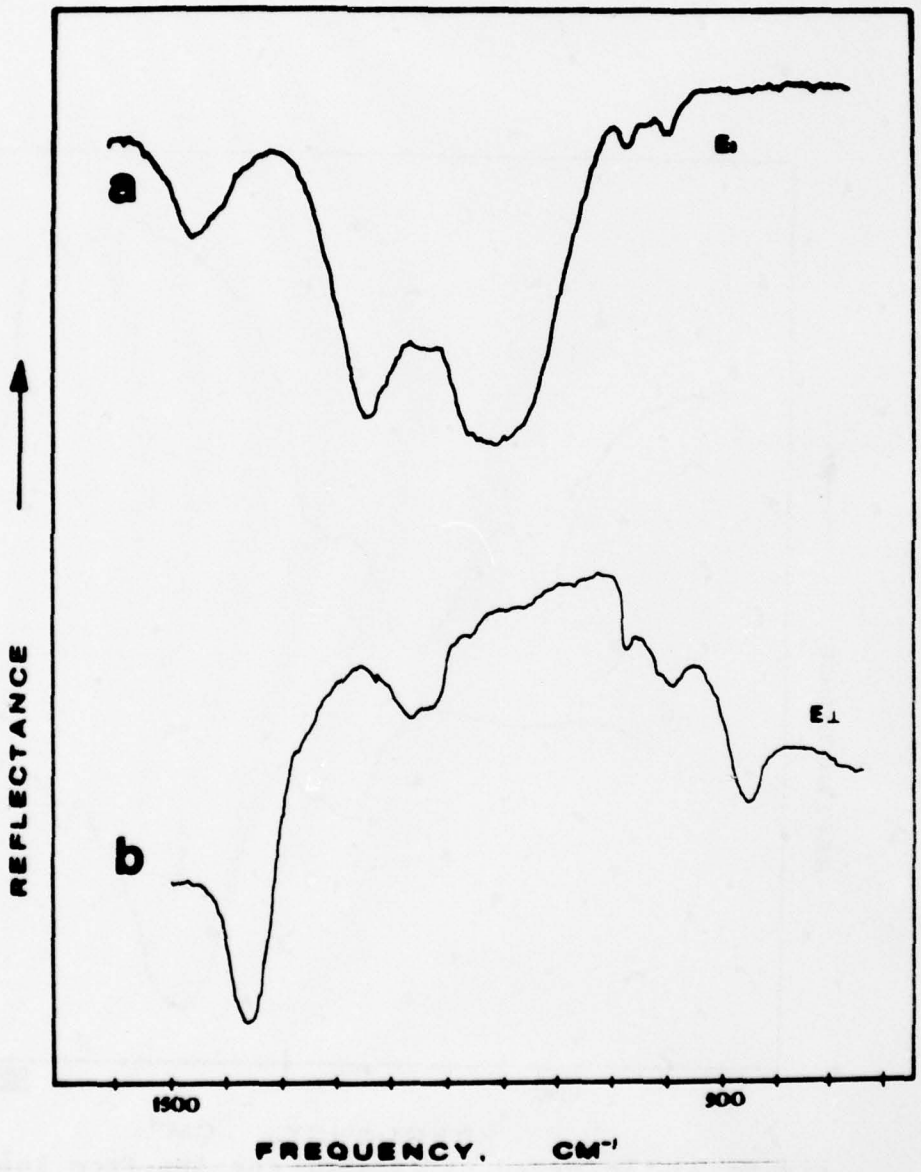

Figure 72. Infrared reflection spectra from lead exposed in KOH solution containing 0.1M sulfate ions, pH=10.9-11.2, especiallyprepared to minimize carbonates content, at .24 V NHE for 2.5 hours. a) Parallel polarization. b) Perpendicular polarization.

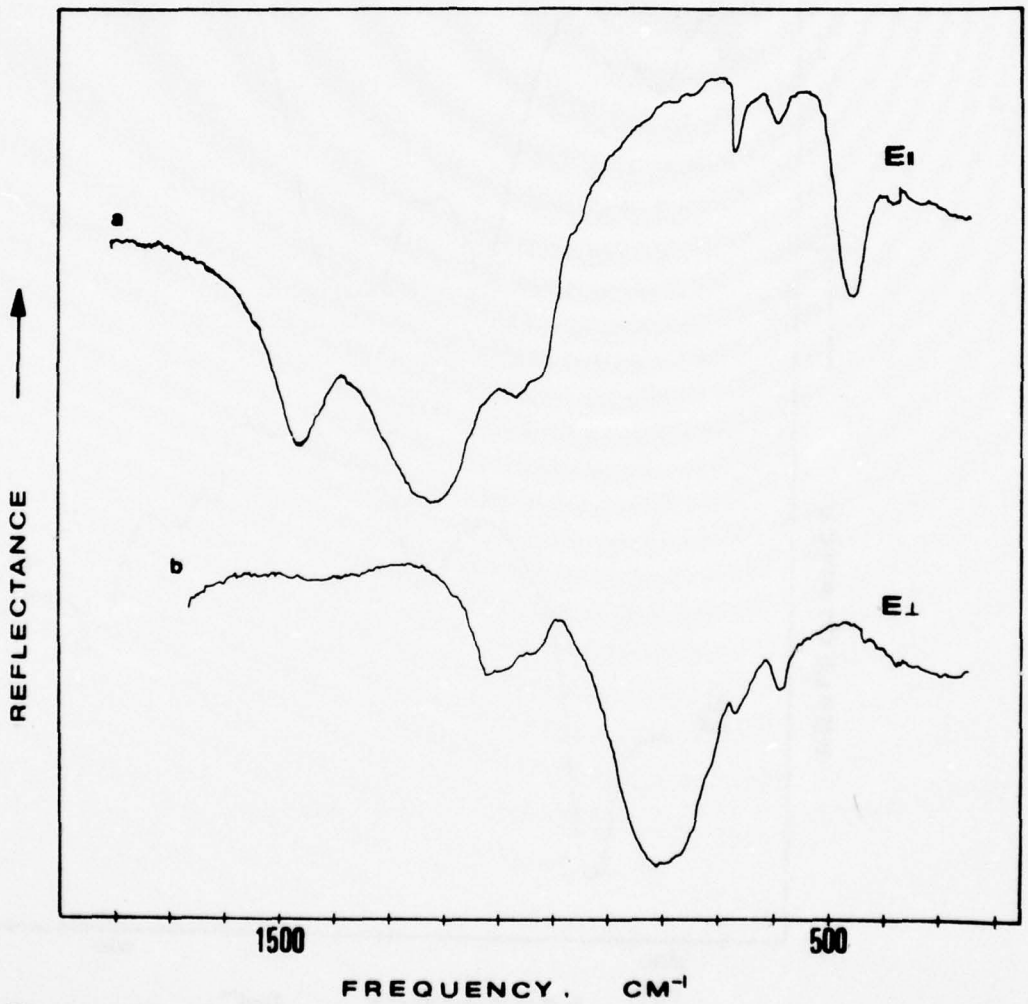

Figure 73. Infrared reflection spectra from lead exposed in KOH solution containing 0.1M sulfate ions, pH=10.9-11.2, at .24 V NHE for 2.75 hours. a) Parallel polarization. b) Perpendicular polarization.

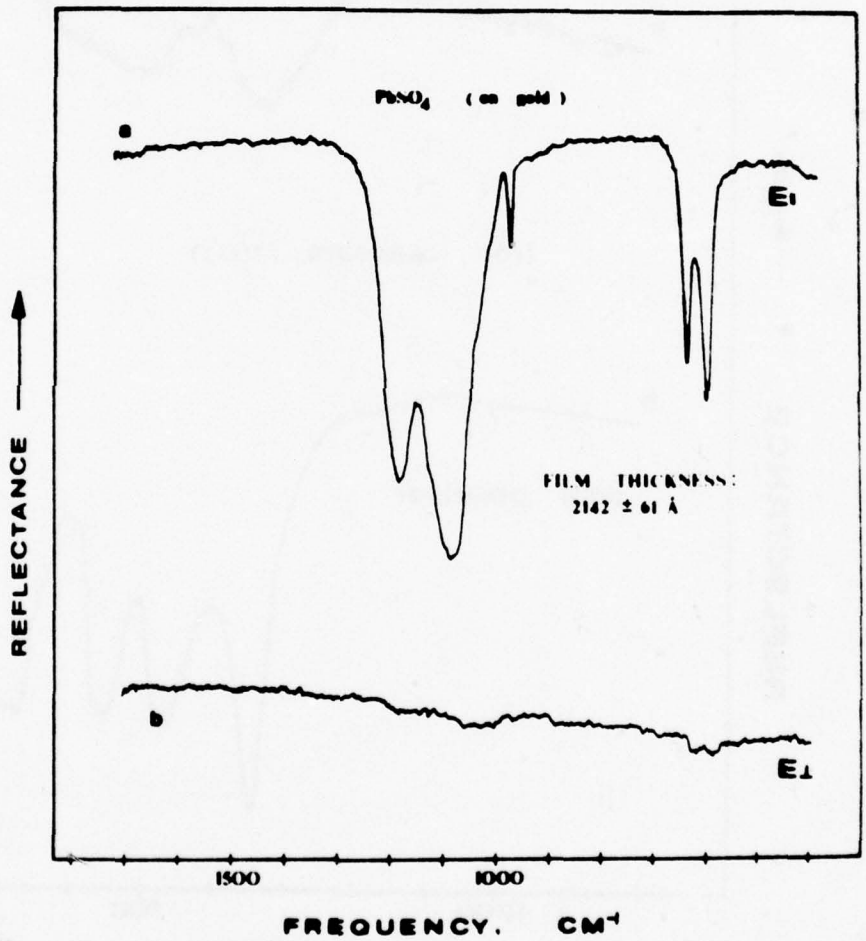

Figure 74. Infrared reflection spectra from lead film, vapor deposited on gold, exposed in 0.1M sulfuric acid, pH=0.9, at .80 V NHE for 20 minutes. Film thickness 2142 angstroms. a) Parallel polarization. b) Perpendicular polarization.

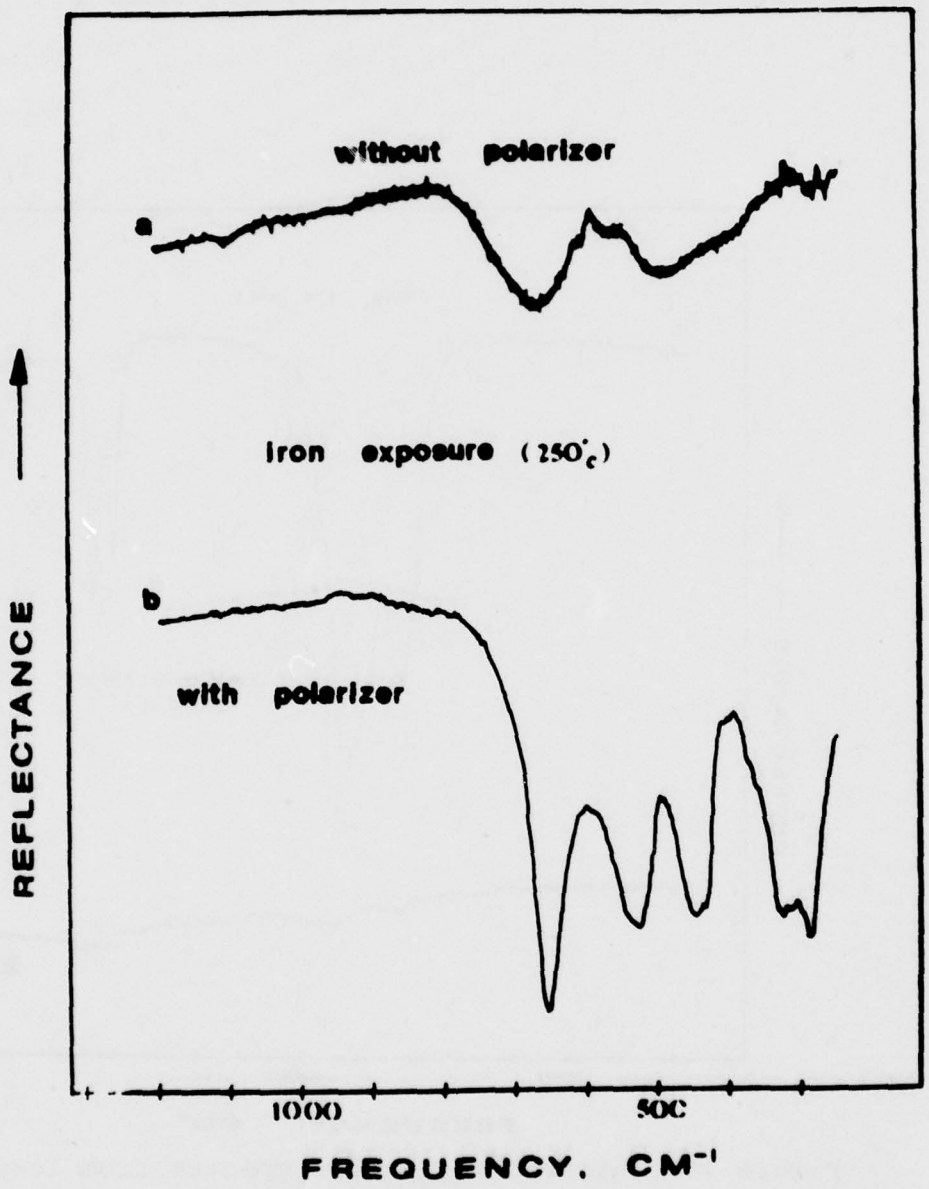

Figure 75. Infrared reflection spectra from Armco iron oxidized at 230°c. a) For 405 hours, no polarizer. b) 288 hours, with parallel polarization.

4. SUMMARY

In the present research infrared reflection spectroscopy was demonstrated to be a sensitive surface analysis technique. The sensitivity of the reflection technique, which is capable of detecting surface films less than 200 angstroms thick, is definitely compound dependent. The sensitivity can either be greater or less than that achieved in this research, depending on the species in the surface layer.

Improvements to enhance the overall sensitivity of the technique can be made by using one or more of the following:

1) Better optics - beam condensers, variable sample position attachment with a better control to balance the reference and sample beams.

2) Signal averaging techniques.

3) Infrared laser spectroscopy - narrow beam, monochromatic radiation, more energy will be available for probing the surface.

One problem area of infrared reflection spectroscopy that requires expansion is the limited availability of reference reflection spectra, thus restricting the use of this technique in routine analytical work.

No thorough matching exists between the results obtained from the electrochemical exposures and the predicted results from the appropriate Pourbaix diagrams. This is not surprising since the information considered in constructing a Pourbaix diagram fixes the information one can obtain from

the diagram. This was demonstrated in the lead-water system where no carbonates were considered in calculating the Pourbaix diagram. Electrochemical exposures, in bicarbonate buffer solution, in the immunity region gave lead carbonate hydroxide (LCH). Thus the region should not be considered an immunity region but rather a passivity region. These results match a published diagram (81) of the lead-water-carbonate system. The theoretical Pourbaix diagrams do not match some of the experimental results because of kinetic effects, which are not taken into account when constructing a Pourbaix diagram, and because of the presence of impurities, which can alter the transformation of one polymorph to another, as was seen in the case of orthorhombic PbO in solutions containing chloride ions.

As expected, infrared reflection spectroscopy could not provide much information on lead-chloride compounds, thus stressing the need for a complementary technique to be used in this research.

On the other hand infrared reflection spectroscopy was demonstrated to be a very sensitive technique for the lead sulfate compounds. It was seen that some evidence on the trapping of water molecules in thick $PbSO_4$+PbO films was obtained. This was not supported by other techniques such as Raman spectroscopy (67), x-ray diffraction and SEM, which either were not sensitive to water or, probably, altered the the film. Some information was obtained about different symmetry of the $PbSO_4$ film in weak acid solution as compared

to the compound film that formed in 0.1N sulfuric acid.

5. BIBLIOGRAPHY

1) M.G. Fontana, N.D. Greene, Corrosion Engineering, McGraw-Hill, N.Y. (1967).

2) R.W. Staehle, "Two Centuries of Passivity and Beyond" Corrosion, 33, 382 (1977).

3) H. Uhlig, Corrosion and Corrosion Control, John Wiley and Sons, N.Y. (1973).

4) V.V. Skorchelletti, Theory of Metal Corrosion, Keter, Jerusalem (1976).

5) E. Gileadi, E. Kirowa-Eisner, J. Penciner, Interfacial Electrochemistry, Addison-Wesley, Reading Mass. (1975).

6) R.P. Frankental, J. of the Electrochemical Society, 116, 580 (1969).

7) M. Pourbaix, Atlas of Electrochemical Equlibrium, Pergamon, N.Y. (1966).

8) R.L. Cusumano, The Establishment of a Three-Dimensional (potential-pH-Composition) Diagram for Binary Fe-Cr alloys in 0.1 Molar Chloride Solutions, MSc. thesis, University of Florida (1971).

9) R. Turcotte, "An Electrochemical Investigation Into The Corrosion of 6351-T6 Aluminum", MSc. Thesis, University of Rhode Island, 1977

10) H. Okada, H. Ogawa, I. Itoh, H. Omata, "Auger Electron Spectroscopic Analysis of the Passive Films on Stainless Steels", in Passivity and Its Breakdownon Iron and Iron Base Alloys, 82, USA-JAPAN seminar (1975).

11) K. Hashimoto, T. Masumoto, S. Shimodaira, "Passivity of Extremly Corrosion Resistive Iron Alloys", 34, ibid.

12) Surface Analysis, Standardization News, ASTM, February 1978.

13) J. Yahalom, L.K. Ives, "Electron-Microscopical Studies of Passive Films on Stainless Steels", in Passivity and Its Breakdown on Iron and Iron Base Alloys, 69, USA-JAPAN seminar (1975).

14) Characterization of Metal and Polymer Surfaces, edited by Lieng-Huang Lee, Academic Press INC. N.Y. (1978).

15) G.W. Simmons, E. Kellerman, H. Leidheiser Jr., "In Situ

Mossbauer Studies of the Passive Film on Cobalt", in Passivity and Its Breakdown on Iron and Iron Base Alloys, 65, USA-JAPAN seminar (1975).

16) J. Demuth, T. Rhodin, "Elastic LEED Intensity - Energy Studies on Clean (001),(110) and (111) Nickel Surfaces", Surface Science, 42, 261 (1974).

17) Ellipsometry in the Measurement of Surfaces and Thin Films, Symposium Proceedings Washington 1963, U.S Department of Commerce, National Bureau of Standards, Miscellaneous Publication 256.

18) R.W. Hannah, "An Optical Accessory for Obtaining the Infrared Spectra of Very Thin Films", Applied Spectroscopy, 17, 23-24 (1963).

19) G.W. Poling, "Reflection Infrared Studies of the Oxidation of Copper and Iron", J. Electrochemical Society, 116, 958-63 (1969).

20) J. Pritchard, M.L. Sims, "Infrared Reflection Spectra of Adsorbed CO on Copper", Transactions of the Faraday Society, 66, 427-33 (1970).

21) D.A. Allara, "The Study of Thin Polymer Films on Metal Surfaces Using Reflection-Absorption Spectroscopy", in Characterization of Metal and Polymer Surfaces, 2, 193-206, Academic Press, N.Y. (1977).

22) L.L. Hench, E.C. Ethridge, "Ceramic Surface Degradation", ONR contract N00014-68-A0175-0006 and Air Force Office of Scientific Research contract 77-3210.

23) L.L. Hench, "Characterization of Glass Corrosion and Durability", J. Non-Crystalline Solids, 19, 27-39 (1975).

24) A.S. Barker, Jr. , "Infrared Lattice Vibrations and Dielectric Dispersion in Corundum", Physical Review, 132, 1474-1481 (1963).

25) R. Marshall, S.S. Mitra, P.J. Gielisse, J.N. Plendl, L.C. Mansur, "Infrared Lattice Spectra of Al_2O_3 and Cr O ", J. of Chemical Physics, 43, 2893-4 (1965).

26) G.W. Poling, R.P. Eischens, "Infrared Study of Adsorbed Corrosion Inhibitors: Butyl Nitrite and Nitric Oxide on Iron-Iron Oxide", J. of the Electrochemical Society, 113, 218-24 (1966).

27) S.A. Francis, A.H. Ellison, "Infrared Spectra of Monolayers on Metal Mirrors", J. of the Optical Society of America, 49, 131-8 (1959).

28) R.G. Greenler, "Infrared Study of Adsorbed Molecules on Metal Surfaces by Reflection Techniques", J. Chemical Physics, 44, 310-5 (1966).

29) R.G. Greenler, "Reflection Method for Obtaining the Infrared Spectrum of Thin Layer on a Metal Surface", ibid, 50, 1963-8 (1969).

30) R.G. Greenler, "Infrared Reflection-Absorption Studies of Molecular Adscrption on Metals", J. Applied Physics, Supp. 2, Pt. 2, 265-8 (1974).

31) R.G. Greenler, "Design of a Reflection-Absorption Experiment for Studying the Infrared Spectrum of Molecules Adsorbed on a Metal Surfaces", J. Vac. Sci. Tech., 12, 1410-17 (1975).

32) G.W. Poling, "Infrared Reflection Spectra of Metal Surfaces", J. Colloid and Interface Science, 34, 365 (1970).

33) H.G. Tompkins, "Some Reflection on Infrared Spectroscopy", Applied Spectroscopy, 30, 377 (1976).

34) N.J. Harrick, "Transmission and Reflection Spectroscopy, Nature of the Spectra", in Characterization of Metal and Polymer Surfaces, 2, 153-92, Academic Press, N.Y. (1977).

35) E.P. Lavin, Specular Reflection, Monographs of Applied Optics No. 2, Elsevier, N.Y. (1971).

36) Lead in Modern Industry, Lead industries Associations (1952).

37) B. Dickens, "The Bonding in the Yellow Form of Lead Monoxide", J. Incrg. Nucl. Chem., 27, 1495-1501 (1965).

38) B. Dickens, "The Bonding in Red PbO", ibid., 27, 1503-7 (1965).

39) B. Dickens, "The Bonding in Pb_3O_4 and Structural Principles in Stoichiometric Lead Oxides", ibid., 27, 1509-15 (1965).

40) T.S. Moss, A.G. Peacock, "Infrared Optical Properties of Lead Halides", Infrared Physics, 1, 104 (1961).

41) H.W. Billhardt, "New Data on Basic Lead Sulfates", J. of the Electrochemical Society, 117, 690 (1970).

42) D.M. Adams, D.C. Stevens, "Single-Crystal Vibrational Spectra of Tetragonal and Orthorhombic Lead Monoxide",

Dalton Trans., 1096-1103 (1977).

43) W.B. White, R. Roy, "Phase Relations in the System Lead-Oxygen", J. Amer. Ceramic Soc., 47, 242 (1964).

44) E.M. Otto, "Equilibrium Pressures of Oxygen Over Oxides of Lead at Various Temperatures", J. of the Electrochemical Society, 113, 525 (1966).

45) J. Burbank, "The Anodic Oxides of Lead", ibid., 106, 369 (1959).

46) R.A. Baker, "Conditions for the Formation of or Lead Dioxide During the Anodic Oxidation of Lead ", ibid., 109, 337 (1962).

47) T.F. Sharp, Encyclopedia of the Electrochemistry of the Elements, 1, A.J. Bard ed., 235, M. Dekker, N.Y. (1973).

48) P. Ruetschi, R.T. Angstadt, "Anodic Oxidation of Lead at Constant Potential", J. of the Electrochemical Society, 111, 1323 (1964).

49) H. Vaidyanathan, R.A. Narasagoudor, T.F. O'Keefe, W.J. James, J.W. Johnson, "Film Formation on Anodically Polarized Lead", ibid., 121, 876 (1974).

50) D. Pavlov, C.N. Paulieff, E. Klaja, N. Iordanov, "Dependence of the Composition of the Anodic Layer on the Oxidation Potential of Lead in Sulfuric Acid", ibid., 116, 316 (1969).

51) J. Burbank, "Anodization of Lead and Lead Alloys in Sulfuric Acid", ibid., 104, 693 (1957).

52) P. Casson, N. Hampson, "The electrochemistry of the $Pb/PbO_2/PbSO_4$ Electrode", ibid., 124, 1655 (1977).

53) D. Pavlov, N. Iordanov, "Growth Processes of Anodic Crystalline Layer on Potentiostatic Oxidation of Lead in Sulfuric Acid", ibid., 117, 1103 (1970).

54) D. Pavlov, S. Zanova, G. Papazov, "Photochemical Properties of the Lead Electrode During Anodic Oxidation in Sulfuric Acid Solution", ibid., 124, 1522 (1977).

55) P. Ruetschi, "Ion Selectivity and Diffusion Potentials in Corrosion Layers", ibid., 120, 331 (1973).

56) R.E. Geisert, N.D. Greene, V.S. Agarwala, "A Versatile Polarization Cell System", Corrosion, 32, 407 (1976).

57) F.P.A. Robinson, D.J. DuPlessis, "Polarization and Corrosion of Ferrosilicon Alloys for Iron Ore Beneficiation Media", ibid., 22, 120 (1966).

58) R.F. Steigerwald, "Effect of Cr Content on Pitting Behavior of Fe-Cr Alloys", ibid., 22, 108 (1966).

59) P. Ruetschi, B.D. Cahan, "Anodic Corrosion and Hydrogen and Oxygen Overvoltage on Lead and Lead Antimony Alloys", J. of the Electrochemical Society, 104, 407 (1957).

60) J.R. Myers, E.G. Greenler, A.L. Smulczenski, "Improved Working Electrode Assembly for Electrochemical Measurements", Corrosion, 24, 352 (1968).

61) W.D. France Jr., "A Specimen Holder for Precise Electrochemical Polarization Measurements on Metal Sheets and Foils", J. of the Electrochemical Society, 114, 818 (1967).

62) D.A. Jones, "Anodic Polarization of Anodized Aluminum", Corrosion, 25, 187 (1969).

63) N.D. Greene, Experimental Electrode Kinetics, Rensselar Polytechnique Institute, Troy N.Y. (1965).

64) K. Appelt, Electrochmica Acta, 13, 1521-32 (1968).

65) D.D. Wagman, W.H. Evans, V.B. Parker, I. Halow, S.M. Bailey, R.H. Schumm, "Selected Values of Chemical Thermodynamic Properties", NBS technical note 270-3 (1968).

66) R. Nyquist, R.O. Kagel, IR Spectra of Organic Compounds, Academic Press INC, N.Y. (1971).

67) R.J. Thibeau, "Characterization of Oxidation Product Films on Lead in Aqueous Media by in Situ Raman Spectroscopy", Ph.D Dissertation, University of Rhode-Island (1978).

68) K. Nakamoto, Infrared Spectra of Inorganic and Coordination Compounds, Wiley Interscience, N.Y. (1970).

69) Optical Studies in Liquids and Solids, vl. 39, D.V. Skobel'tsyn ed., Consultant Bureau, N.Y. (1969).

70) W. Kwestro, J. DeJonge, P.H.G.M Vromans, "Influence of Impurities on the Formation of Red and Yellow PbO", J. Inorg. Nuc. Chem., 29, 39 (1967).

71) W. Kwestro, A. Huizing, "The Preparation of Ultrapure Lead Oxide", ibid., 27, 1951-4 (1965).

72) W.B. White, R. Roy, Amer. Mineralogist, 49, 1670 (1967).

73) Kammori, OHiko, "Application of IR Spectra to Studies on Iron and Steel", Bunseki Kagaku, 16, 1050 (1967).

74) F. Vranty, M. Dilling, F. Gugliotta, C.N.R. Rao, "Infrared Spectra of Metallic Oxides, Phosphates and Chromates", J. Sci. and Indus. Res., 20b, 590 (1961).

75) J. Van den Broek, "Optical Lattice Vibrations and Dielectric Constant of Tetragonal Lead Monoxide", Philips Res. Repts., 24, 119-30 (1969).

76) N.T. McDevitt, W.L. Baun, Electrochimica Acta., 20, 799-808 (1964).

77) S.S. Mitra, P.J. Gielisse, T.J. Rockett, "Window Materials for CO_2 Gas Laser, A Review", Prepared for Air Force Cambridge Research Lab. L.G. Hanscom Field, Bedford Mass.

78) P.J. Gielisse, S.S. Mitra, "Infrared Spectra of Crystals", Air Force Cambridge Research Lab., AFCRL-65-395 (1965).

79) "Infrared Spectra and Characteristic Frequencies of Inorganic Ions", Analytical Chemistry, 24, 1253 (1952).

80) R.A. Schroeder, E.R. Lippincott, C.E. Weir, "Low Temperature Infrared Spectra of Crystalline Inorganic Compounds Containing Tetrahedral Anions", J. Inorg. Nuc. Chem., 28, 1397 (1966).

81) P. Delahay, M. Pourbaix, P. Van Rysselberghe, "Potential-pH Diagram of Lead and its Applications to the Study of Lead Corrosion and to the Lead Storage Battery", J. of the Electrochemical Society, 98, 57 (1951).

APPENDIX I

Calculation of The Pourbaix Diagram of The Lead-Water System

ΔG° - Free Energy of Formation (65), cal/Mole

Pb^{++}..... -5830

PbO (Y)..... -44910

PbO (R)..... -45160

PbO_2..... -51950

Pb_3O_4..... -143700

Equlibrium Reactions:

1) $Pb + H_2O = PbO(R) + 2H^+ + 2e^-$

$E = 0.25 - 0.059pH$

2) $3PbO + H_2O = Pb_3O_4 + 2H^+ + 2e^-$

$E = 1.051 - 0.059pH$

3) $2Pb_3O_4 + H_2O = 3Pb_2O_3 + 2H^+ + 2e^-$

$E = 1.059 - 0.059pH$

4) $Pb_3O_4 + 2H_2O = 3PbO_2 + 4H^+ + 4e^-$

$E = 1.097 - 0.059pH$

5) $Pb_2O_3 + H_2O = 2PbO_2 + 2H^+ + 2e^-$

$E = 1.110 - 0.059pH$

6) $Pb^{++} + H_2O = PbO\ (R) + 2H^+$

$\log K = -12.74$

$a_{Pb^{++}} = 10^{-6}$

$pH = 9.37$

7) $Pb = Pb^{++} + 2e^-$

$E = -0.126 + 0.0295\log(a_{Pb^{++}})$

8) $3Pb^{++} + 4H_2O = Pb_3O_4 + 8H^+ + 2e^-$

$E = 2.18 - 0.236pH - 0.089\log(a_{Pb^{++}})$

9) $2Pb^{++} + 3H_2O = Pb_2O_3 + 6H^+ + 2e^-$

$E = 1.806 - 0.177pH - 0.059\log(a_{Pb^{++}})$

10) $Pb^{++} + 2H_2O = PbO_2 + 4H^+ + 2e^-$

$E = 1.458 - 0.118pH - 0.0295\log(a_{Pb^{++}})$

* Free energies of formation (ΔG^o) that were used in the calculation of this appendix but were not written in the above table, are no different from those used by M. Pourbaix (7).

APPENDIX II

Calculation of The Pourbaix Diagram of The Lead-Water-Chloride System

ΔG° - Free Energy of Formation (65), cal/mole

OH^-		-37594
Cl^-		-31372
$PbCl_2$		-75080
$3PbO \cdot PbCl_2$	(R)	-224686
	(Y)	-224246

a) $4PbO + 2Cl^- + H_2O = 3PbO \cdot PbCl_2 + 2OH^-$

b) $4PbO + 2Cl^- + 2H^+ = 3PbO \cdot PbCl_2 + H_2O$

Caculation of ΔG° of $3PbO \cdot PbCl_2$:

$$\Delta G^\circ (3PbO \cdot PbCl_2) = -1.364K - 2\Delta G^\circ (OH^-) + 4\Delta G^\circ (PbO) + 2\Delta G^\circ (Cl^-) + \Delta G^\circ (H_2O)$$

K can be calculated using Appellet's thermodynamic values (64) : -147 cal/mole

Equilibrium Reactions:

1) $Pb^{++} + H_2O = PbO + 2H^+$

(R) pH = 7.75

(Y) pH = 7.80

2) $4Pb^{++} + 2Cl^- + 3H_2O = 3PbO \cdot PbCl_2 + 6H^+$

(R) pH = 6.026

(Y) pH = 6.079

3) $Pb^{++} + 2Cl^- = PbCl_2$

$a_{Cl^-} = 0.1$

$\log(a_{Pb^{++}}) = -2.769$

4) $Pb = Pb^{++} + 2e^-$

$E = - 0.208$

5) $4PbCl_2 + 3H_2O = 3PbO \cdot PbCl_2 + 6Cl^- + 6H^+$

(R) pH = 6.021

(Y) pH = 6.075

6) $Pb + H_2O = PbO + 2H^+ + 2e^-$

(R) $E = 0.250 - 0.059pH$

(Y) $E = 0.252 - 0.059pH$

7) $4Pb + 2Cl^- + 3H_2O = 3PbO \cdot PbCl_2 + 6H^+ + 8e^-$

(R) $E = 0.059 - 0.044pH$

(Y) $E = 0.061 - 0.044pH$

8) $Pb + 2Cl^- = PbCl_2 + 2e^-$

$E = - 0.208$

9) $3Pb + PbCl_2 + 3H_2O = 3PbO \cdot PbCl_2 + 6H^+ + 6e^-$

(R) $E = 0.148 - 0.059pH$

(Y) $E = 0.151 - 0.059pH$

10) $Pb + 3PbO + 2Cl^- = 3PbO \cdot PbCl_2 + 2e^-$

(R) $E = - 0.515$

(Y) $E = - 0.512$

11) $3PbO \cdot PbCl_2 + H_2O = 4PbO + 2Cl^- + 2H^+$

(R) & (Y) pH = 12.92

12) $3PbO + H_2O = Pb_3O_4 + 2H^+ + 2e^-$

$E = 1.051 - 0.059pH$

13) $Pb_3O_4 + 2H_2O = 3PbO_2 + 4H^+ + 4e^-$

$E = 1.097 - 0.059pH$

14) $3Pb^{++} + 4H_2O = Pb_3O_4 + 8H^+ + 2e^-$

$E = 2.18 - 0.236pH - 0.089\log(a_{Pb^{++}}) = 2.426 - 0.236pH$

15) $Pb^{++} + 2H_2O = PbO_2 + 4H^+ + 2e^-$

$E = 1.458 - 0.118pH - 0.0295\log(a_{Pb^{++}}) = 1.540 - 0.118pH$

16) $PbCl_2 + 2H_2O = PbO_2 + 4H^+ + 2Cl^- + 2e^-$

$E = 1.541 - 0.118pH$

17) $3PbCl_2 + 4H_2O = Pb_3O_4 + 8H^+ + 6Cl^- + 2e^-$

$E = 2.426 - 0.236pH$

18) $3(3PbO \cdot PbCl_2) + 7H_2O = 4Pb_3O_4 + 14H^+ + 6Cl^- + 8e^-$

$E = 1.625 - 0.103pH$

19) $3PbO \cdot PbCl_2 + 5H_2O = 4PbO_2 + 10H^+ + 2Cl^- + 8e^-$

$E = 1.273 - 0.074pH$

* $PbCl_4$ was not considered due to lack of thermodynamic data.

** Pb_2O_3 was considered but the results obtained for its potential-pH relations did not fit into the diagram, probably due to the lack of modern thermodynamic data.

APPENDIX III

Calculation of The Pourbaix Diagram of The Lead-Water-Sulfate System

ΔG^{o} - Free Energy of Formation (65), cal/mole

SO_4^{--}..... -177970

HSO_4^{-}..... -180690

$PbSO_4$..... -194320

$PbO \cdot PbSO_4$..... -246700

$3PbO \cdot PbSO_4 \cdot H_2O$..... -397300

$5PbO \cdot 2H_2O$..... -336350

Equlibrium Reactions:

1) $Pb + HSO_4^{-} = PbSO_4 + H^{+} + 2e^{-}$

$E = -0.296 - 0.0295pH - 0.0295\log(a_{HSO_4^{-}})$

$a_{SO_4^{--}} + a_{HSO_4^{-}} = 0.1$

$E = -0.3255 - 0.0295pH$

2) $Pb + SO_4^{--} = PbSO_4 + 2e^{-}$

$E = -0.3245$

3) $2Pb + SO_4^{--} + H_2O = PbO \cdot PbSO_4 + 2H^{+} + 4e^{-}$

$E = -0.116 - 0.0295pH$

4) $4Pb + SO_4^{--} + 4H_2O = 3PbO \cdot PbSO_4 \cdot H_2O + 6H^{+} + 8e^{-}$

$E = 0.047 - 0.0443pH$

5) $5Pb + 2H_2O = 5PbO \cdot 2H_2O + 10H^{+} + 10e^{-}$

$E = 0.260 - 0.059pH$

6) $PbSO_4 + 2H_2O = PbO_2 + HSO_4^{-} + 3H^{+} + 2e^{-}$

$E = 1.598 - 0.0885pH$

7) $PbSO_4 + 2H_2O = PbO_2 + SO_4^{--} + 4H^{+} + 2e^{-}$

$E = 1.657 - 0.118pH$

8) $PbO \cdot PbSO_4 + 3H_2O = 2PbO_2 + 6H^+ + SO_4^{--} + 4e^-$

$E = 1.447 - 0.885pH$

9) $3PbO \cdot PbSO_4 \cdot H_2O + 4H_2O = 4PbO_2 + 10H^+ + SO_4^{--} + 8e^-$

$E = 1.285 - 0.0738pH$

10) $5PbO \cdot 2H_2O + 3H_2O = 5PbO_2 + 10H^+ + 10e^-$

$E = 1.070 - 0.059pH$

11) $Pb_3O_4 + 2H_2O = 3PbO_2 + 4H^+ + 4e^-$

$E = 1.097 - 0.059pH$

12) $Pb_2O_3 + H_2O = 2PbO_2 + 2H^+ + 2e^-$

$E = 1.110 - 0.059pH$

13) $2PbSO_4 + 3H_2O = Pb_2O_3 + 2SO_4^{--} + 6H^+ + 2e^-$

$E = 2.203 - 0.177pH$

14) $PbO \cdot PbSO_4 + 2H_2O = Pb_2O_3 + SO_4^{--} + 4H^+ + 2e^-$

$E = 1.785 - 0.118pH$

15) $3PbO \cdot PbSO_4 \cdot H_2O + 2H_2O = 2Pb_2O_3 + SO_4^{--} + 6H^+ + 4e^-$

$E = 1.458 - 0.0885pH$

16) $2Pb_3O_4 + H_2O = 3Pb_2O_3 + 2H^+ + 2e^-$

$E = 1.059 - 0.059pH$

17) $3PbSO_4 + 4H_2O = Pb_3O_4 + 3SO_4^{--} + 8H^+ + 2e^-$

$E = 2.776 - 0.236pH$

18) $3(PbO \cdot PbSO_4) + 5H_2O = 2Pb_3O_4 + 3SO_4^{--} + 10H^+ + 4e^-$

$E = 2.148 - 0.148pH$

19) $3(3PbO \cdot PbSO_4 \cdot H_2O) + 4H_2O = 4Pb_3O_4 + 3SO_4^{--} + 14H^+ + 8e^-$

$E = 1.658 - 0.103pH$

20) $3(5PbO \cdot 2H_2O) = 5Pb_3O_4 + 10H^+ + H_2O + 10e^-$

$E = 1.014 - 0.059pH$

BASIC DISTRIBUTION LIST

Technical and Summary Reports April 1978

Organization	Copies
Defense Documentation Center Cameron Station Alexandria, VA 22314	12
Office of Naval Research Department of the Navy 800 N. Quincy Street Arlington, VA 22217	
ATTN: Code 471	1
Code 102	1
Code 470	1
Commanding Officer Office of Naval Research Branch Office Building 114, Section D 666 Summer Street Boston, MA 02210	1
Commanding Officer Office of Naval Research Branch Office 536 South Clark Street Chicago, IL 60605	1
Office of Naval Research San Francisco Area Office 760 Market Street, Room 447 San Francisco, CA 94102	1
Naval Research Laboratory Washington, DC 20375	
ATTN: Codes 6000	1
6100	1
6300	1
6400	1
2627	1
Naval Air Development Center Code 302 Warminster, PA 18964 ATTN: Mr. F. S. Williams	1

Organization	Copies
Naval Air Propulsion Test Center Trenton, NJ 08628 ATTN: Library	1
Naval Construction Batallion Civil Engineering Laboratory Port Hueneme, CA 93043 ATTN: Materials Division	1
Naval Electronics Laboratory San Diego, CA 92152 ATTN: Electron Materials Sciences Division	1
Naval Missile Center Materials Consultant Code 3312-1 Point Mugu, CA 92041	1
Commanding Officer Naval Surface Weapons Center White Oak Laboratory Silver Spring, MD 20910 ATTN: Library	1
David W. Taylor Naval Ship Research and Development Center Materials Department Annapolis, MD 21402	1
Naval Undersea Center San Diego, CA 92132 ATTN: Library	1
Naval Underwater System Center Newport, RI 02840 ATTN: Library	1
Naval Weapons Center China Lake, CA 93555 ATTN: Library	1
Naval Postgraduate School Monterey, CA 93940 ATTN: Mechanical Engineering Department	1

BASIC DISTRIBUTION LIST (cont'd)

Organization	Copies
Naval Air Systems Command Washington, DC 20360 ATTN: Codes 52031 52032	1
Naval Sea System Command Washington, DC 20362 ATTN: Code 035	1
Naval Facilities Engineering Command Alexandria, VA 22331 ATTN: Code 03	1
Scientific Advisor Commandant of the Marine Corps Washington, DC 20380 ATTN: Code AX	1
Naval Ship Engineering Center Department of the Navy Washington, DC 20360 ATTN: Code 6101	1
Army Research Office P.O. Box 12211 Triangle Park, NC 27709 ATTN: Metallurgy & Ceramics Program	1
Army Materials and Mechanics Research Center Watertown, MA 02172 ATTN: Research Programs Office	1
Air Force Office of Scientific Research Bldg. 410 Bolling Air Force Base Washington, DC 20332 ATTN: Chemical Science Directorate Electronics & Solid State Sciences Directorate	1 1
Air Force Materials Laboratory Wright-Patterson AFB Dayton, OH 45433	1
Library Building 50, Rm 134 Lawrence Radiation Laboratory Berkeley, CA	1

Organization	Copies
NASA Headquarters Washington, DC 20546 ATTN: Code RRM	1
NASA Lewis Research Center 21000 Brookpark Road Cleveland, OH 44135 ATTN: Library	1
National Bureau of Standards Washington, DC 20234 ATTN: Metallurgy Division Inorganic Materials Div.	1 1
Director Applied Physics Laboratory University of Washington 1013 Northeast Forthieth Street Seattle, WA 98105	1
Defense Metals and Ceramics Information Center Battelle Memorial Institute 505 King Avenue Columbus, OH 43201	1
Metals and Ceramics Division Oak Ridge National Laboratory P.O. Box X Oak Ridge, TN 37380	1
Los Alamos Scientific Laboratory P.O. Box 1663 Los Alamos, NM 87544 ATTN: Report Librarian	1
Argonne National Laboratory Metallurgy Division P.O. Box 229 Lemont, IL 60439	1
Brookhaven National Laboratory Technical Information Division Upton, Long Island New York 11973 ATTN: Research Library	1
Office of Naval Research Branch Office 1030 East Green Street Pasadena, CA 91106	1

C
April 1978

SUPPLEMENTARY DISTRIBUTION LIST

Technical and Summary Reports

Dr. T. R. Beck
Electrochemical Technology Corporation
10035 31st Avenue, NE
Seattle, Washington 98125

Professor I. M. Bernstein
Carnegie-Mellon University
Schenley Park
Pittsburgh, Pennsylvania 15213

Professor H. K. Birnbaum
University of Illinois
Department of Metallurgy
Urbana, Illinois 61801

Dr. Otto Buck
Rockwell International
1049 Camino Dos Rios
P.O. Box 1085
Thousand Oaks, California 91360

Dr. David L. Davidson
Southwest Research Institute
8500 Culebra Road
P.O. Drawer 28510
San Antonio, Texas 78284

Dr. D. J. Duquette
Department of Metallurgical Engineering
Rensselaer Polytechnic Institute
Troy, New York 12181

Professor R. T. Foley
The American University
Department of Chemistry
Washington, D.C. 20016

Mr. G. A. Gehring
Ocean City Research Corporation
Tennessee Avenue & Beach Thorofare
Ocean City, New Jersey 08226

Dr. J. A. S. Green
Martin Marietta Corporation
1450 South Rolling Road
Baltimore, Maryland 21227

Professor R. H. Heidersbach
University of Rhode Island
Department of Ocean Engineering
Kingston, Rhode Island 02881

Professor H. Herman
State University of New York
Material Sciences Division
Stony Brook, New York 11794

Professor J. P. Hirth
Ohio State University
Metallurgical Engineering
Columbus, Ohio 43210

Dr. D. W. Hoeppner
University of Missouri
College of Engineering
Columbia, Missouri 65201

Dr. E. W. Johnson
Westinghouse Electric Corporation
Research and Development Center
1310 Beulah Road
Pittsburgh, Pennsylvania 15235

Professor R. M. Latanision
Massachusetts Institute of Technology
77 Massachusetts Avenue
Room E19-702
Cambridge, Massachusetts 02139

Dr. F. Mansfeld
Rockwell International Science Center
1049 Camino Dos Rios
P.O. Box 1085
Thousand Oaks, California 91360

Professor A. E. Miller
University of Notre Dame
College of Engineering
Notre Dame, Indiana 46556

C
April 1978

SUPPLEMENTARY DISTRIBUTION LIST
(Continued)

Professor H. W. Pickering
Pennsylvania State University
Department of Material Sciences
University Park, Pennsylvania 16802

Professor R. W. Staehle
Ohio State University
Department of Metallurgical Engineering
Columbus, Ohio 43210

Dr. E. A. Starke, Jr.
Georgia Institute of Technology
School of Chemical Engineering
Atlanta, Georgia 30332

Dr. Barry C. Syrett
Stanford Research Institute
333 Ravenswood Avenue
Menlo Park, California 94025

Dr. R. P. Wei
Lehigh University
Institute for Fracture and
Solid Mechanics
Bethlehem, Pennsylvania 18015

Professor H. G. F. Wilsdorf
University of Virginia
Department of Materials Science
Charlottesville, Virginia 22903

August 1978

SUPPLEMENTARY DISTRIBUTION LIST

Technical and Summary Reports

People and organizations who have requested copies of reports on this research.

Dr. F.P. Mertlas
Department of Energy and Environment
Building 815
Upton, NY 11973

Dr. B. Vyas
Brookhaven National Laboratory
Building 703
Upton, NY 11973

Dr. Henry White
Physics Department
University of Missouri - Columbia
Columbia, MO 65211

Dr. M.J. Graham
National Research Council of Canada
Division of Chemistry
Ottawa, Ontario
Canada K1A OR9

Dr. B.J. Berkowitz
Corporate Research Laboratories
Exxon Research and Engineering Company
P.O. Box 45
Linden, NJ 07036

Dr. S. Gottesfeld
Bell Laboratories
600 Mountain Avenue
Murray Hill, NJ 07974

Dr. Jeff Perkins
Liason Scientist, Metallurgy
Office of Naval Research
Branch Office, London
Box 39
FPO New York 09510

T.E. Evans
Inco Europe, Ltd.
European R & D Centre
Wiggin Street, Birmingham
B160AJ
England

Dr. N. Sato
Faculty of Engineering
Hokkaido University
Kita-Ku, Sapporo, 060
Japan

Dr. K. Sugimoto
Department of Metallurgy
Tohoku University

Distribution List - ONR

Martin W. Kendig
Corrosion Science Group
Department of Nuclear Energy
Brookhaven National Laboratory
Upton, NY 11973

A.S. (Bert) Krisher
Engineering Fellow
Materials Technology
Monsanto
Corporate Engineering Department
Monsanto Company
800 N. Lindbergh Boulevard
St. Louis, Missouri 63166

Tom E. Furtak
Leader, Electrochemistry Group
Solid State Physics Division
Ames Laboratory
U.S. Department of Energy
Iowa State University
Ames, Iowa 50011

Alan G. Miller, Ph.D.
Analytical Specialist Engineer
Boeing Materials Technology
Boeing Commercial Airplane Co.
P.O. Box 3707
MS 73-43
Seattle, WA 98124